

DTIC FILE COPY

2

# NAVAL POSTGRADUATE SCHOOL Monterey, California

DTIC  
ELECTE  
JUN 21 1990  
S D D  
CQ



AD-A223 028

## THESIS

EFFECTS OF 2 HZ IMPOSED BULK FLOW  
UNSTEADINESS ON  
LAMINAR/TURBULENT TRANSITION IN A  
STRAIGHT CHANNEL

by

Francis J. Greco

December 1989

Thesis Advisor  
Co-Advisor

Phillip M. Ligrani  
Chelakara S. Subramanian

Approved for public release; distribution is unlimited.

90 06 21 012

Unclassified

security classification of this page

## REPORT DOCUMENTATION PAGE

1a Report Security Classification <b>Unclassified</b>			1b Restrictive Markings		
2a Security Classification Authority			3 Distribution Availability of Report		
2b Declassification Downgrading Schedule			Approved for public release; distribution is unlimited.		
4 Performing Organization Report Number(s)			5 Monitoring Organization Report Number(s)		
6a Name of Performing Organization <b>Naval Postgraduate School</b>		6b Office Symbol (if applicable) <b>34</b>	7a Name of Monitoring Organization <b>Naval Postgraduate School</b>		
6c Address (city, state, and ZIP code) <b>Monterey, CA 93943-5000</b>		7b Address (city, state, and ZIP code) <b>Monterey, CA 93943-5000</b>			
8a Name of Funding Sponsoring Organization <b>NPS Direct Funding</b>		8b Office Symbol (if applicable)	9 Procurement Instrument Identification Number <b>NPS Direct Fund- ing (ONR Review)</b>		
8c Address (city, state, and ZIP code) <b>Monterey, CA 93943-5000</b>		10 Source of Funding Numbers			
		Program Element No	Project No	Task No	Work Unit Accession No
11 Title (include security classification) <b>EFFECTS OF 2 HZ IMPOSED BULK FLOW UNSTEADINESS ON LAMINAR TURBULENT TRANSITION IN A STRAIGHT CHANNEL</b>					
12 Personal Author(s) <b>Francis J. Greco</b>					
13a Type of Report <b>Master's Thesis</b>		13b Time Covered From To		14 Date of Report (year, month, day) <b>December 1989</b>	
15 Page Count <b>134</b>					
16 Supplementary Notation The views expressed in this thesis are those of the author and do not reflect the official policy or po- sition of the Department of Defense or the U.S. Government.					
17 Cosati Codes			18 Subject Terms (continue on reverse if necessary and identify by block number)		
Field	Group	Subgroup	Plane Channel Flow; Imposed Unsteadiness; Transition Events; Tollmien-Schlichting Waves; Vortical Ribbon/Like Structures. <i>These are the</i>		
19 Abstract (continue on reverse if necessary and identify by block number)					
<p>Laminar turbulent transition is studied in a straight channel with 2 Hz imposed bulk flow unsteadiness for Reynolds numbers of 1100 to 3800 and Strouhal numbers of 0.121 to 0.035. Channel aspect ratio is 40 to 1 with 1.27 cm height, 50.8 cm width and 4.27 m length. Observations, videos, and photographs of smoke patterns show different subcritical transition events including Tollmien-Schlichting waves, vortex-array type motion evidenced by smoke swirls, ribbon-like patterns, turbulent spots, and fully turbulent flow. Fluctuating intensity magnitudes relative to velocities from imposed unsteadiness are determined from phase-averaged velocity traces. With 2 Hz unsteadiness, transition events begin to occur at lower Reynolds numbers and extend over a wider range of Reynolds numbers compared to flows with no imposed unsteadiness.</p>					
20 Distribution Availability of Abstract			21 Abstract Security Classification		
<input checked="" type="checkbox"/> unclassified unlimited <input type="checkbox"/> same as report <input type="checkbox"/> DTIC users			<b>Unclassified</b>		
22a Name of Responsible Individual <b>Phillip M. Igrani</b>			22b Telephone (include Area code) <b>(408) 646-3382</b>		22c Office Symbol <b>6913</b>

DD FORM 147-3, MAR

83 APR edition may be used until exhausted  
All other editions are obsolete

security classification of this page

Unclassified

Approved for public release; distribution is unlimited.

Effects of 2 Hz Imposed Bulk Flow  
Unsteadiness on  
Laminar/Turbulent Transition in a Straight Channel

by

Francis J. Greco  
Lieutenant Commander, United States Navy  
B.S., United States Naval Academy, 1977

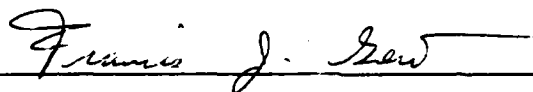
Submitted in partial fulfillment of the  
requirements for the degree of

MASTER OF SCIENCE IN MECHANICAL ENGINEERING

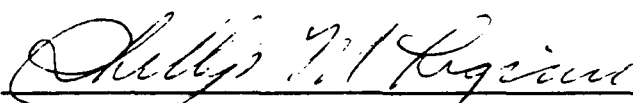
from the

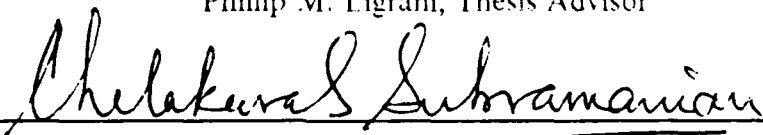
NAVAL POSTGRADUATE SCHOOL  
December 1989

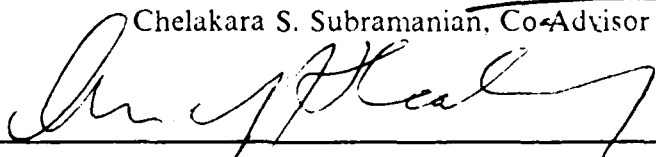
Author:

  
Francis J. Greco

Approved by:

  
Phillip M. Eigrani, Thesis Advisor

  
Chelakara S. Subramanian, Co-Advisor

  
Anthony J. Healey, Chairman,  
Department of Mechanical Engineering

## ABSTRACT

Laminar / turbulent transition is studied in a straight channel with 2 Hz imposed bulk flow unsteadiness for Reynolds numbers of 1100 to 3800 and Strouhal numbers of 0.121 to 0.035. Channel aspect ratio is 40 to 1 with 1.27 cm height, 50.8 cm width and 4.27 m length. Observations, videos, and photographs of smoke patterns show different subcritical transition events including Tollmien-Schlichting waves, vortex-array type motion evidenced by smoke swirls, ribbon-like patterns, turbulent spots, and fully turbulent flow. Fluctuating intensity magnitudes relative to velocities from imposed unsteadiness are determined from phase-averaged velocity traces. With 2 Hz unsteadiness, transition events begin to occur at lower Reynolds numbers and extend over a wider range of Reynolds numbers compared to flows with no imposed unsteadiness.



Accession For	
NTIS - CRA&I	<input checked="" type="checkbox"/>
DTIC - TAB	<input type="checkbox"/>
Unannounced	<input type="checkbox"/>
Justification	
By	
Distribution /	
Availability Codes	
Dist	Avail and/or Special
A-1	

## TABLE OF CONTENTS

I. INTRODUCTION .....	1
A. BACKGROUND .....	1
B. OBJECTIVES .....	4
C. ORGANIZATION .....	5
II. EXPERIMENTAL FACILITIES .....	6
A. CHANNEL .....	6
B. UNSTEADY DEVICE .....	7
C. FLOW MEASUREMENTS .....	8
1. Bulk Velocity .....	8
2. Instantaneous Velocity .....	9
a. Hot-wire Probe and Probe Positioning .....	9
b. Hot-wire Bridge .....	10
c. Signal Conditioner .....	10
d. High Speed Data Acquisition System .....	10
e. Data Storage .....	11
f. Data Processing .....	11
D. FLOW VISUALIZATION .....	13
1. Smoke Wire System .....	13
2. Video Equipment .....	14
III. EXPERIMENTAL PROCEDURES .....	15
A. ORIFICE DP CALIBRATION .....	15
B. HOT-WIRE CALIBRATION .....	15

C. CHANNEL VALIDATION .....	15
1. Channel Flow Tests .....	15
2. Laminar Average Velocity Profile Calibration .....	16
D. FLOW MEASUREMENT .....	16
1. Reynolds Number Survey .....	16
2. Multi-run Averaging .....	17
3. Velocity Profiles .....	17
E. FLOW VISUALIZATION .....	17
IV. RESULTS AND DISCUSSION .....	18
A. CHANNEL FLOW QUALIFICATION .....	18
B. EFFECT OF 2.0 HZ IMPOSED UNSTEADINESS ON LOCAL MEAN VELOCITY AT $y/d=0.88$ .....	19
C. EFFECT OF 2.0 HZ IMPOSED UNSTEADINESS ON RMS VELOCITY AT $y/d=0.88$ .....	19
D. EFFECT OF REYNOLDS NUMBER ON PHASE-AVERAGED VELOCITY .....	20
E. MEAN VELOCITY PROFILES .....	21
F. RMS VELOCITY PROFILES .....	21
G. VARIATION OF PHASE-AVERAGED QUANTITIES WITH REYNOLDS NUMBER AND $y/d$ .....	22
H. FLOW VISUALIZATION .....	24
V. CONCLUSIONS .....	26
APPENDIX A. (SOFTWARE DIRECTORY) .....	28
APPENDIX B. (FIGURES) .....	30

LIST OF REFERENCES .....	125
INITIAL DISTRIBUTION LIST .....	127

## **I. INTRODUCTION**

### **A. BACKGROUND**

Many typical flows found in nature and in aerodynamic applications and almost all flows associated with turbomachinery involve freestream unsteadiness. Most of these flows, especially those of technological interest undergo transition from a laminar state to a turbulent condition. The accurate prediction of the location and extent of transition and the accompanying changes of important flow properties is vital to the design of aircraft and most energy transformation machines involving fluid flow.

Laminar-turbulent transition results in significant increases in local wall shear stress and convective heat transfer rates. This becomes evident by first considering laminar flows, where transport of heat and momentum normal to streamlines occurs only as a result of molecular diffusion. This is usually an advantage since tangential forces at solid surfaces (drag) and heat flux normal to surfaces are relatively low. Occasionally, laminar flows are undesirable since they tend to separate from surfaces more easily than turbulent flows. In most applications, laminar flows are unstable and transitional or fully turbulent flows exist. In the latter, higher rates of diffusion across mean streamlines due to turbulent transport cause significantly higher drag and heat flux at surfaces.

The parameter generally used to describe the onset of transition is the Reynolds number. In channel flows, linear stability theory predicts that the laminar flow becomes unstable to small amplitude disturbances at a critical Reynolds number of 5772. Here the Reynolds number is based on mean centerline velocity and channel



half-width. With large amplitude disturbances, however, the transitional Reynolds number for channel flow may be as low as 1000-1500. The value of Reynolds number at the onset of transition depends strongly on the disturbances existing in the flow and conditions which prevail in the entry region of the channel.

Also, the sequence of events which occur during transition are strongly dependent on upstream history, especially laminar boundary layer character and development. There is a growing collection of evidence which also suggests that turbulent shear layer development is more strongly dependent on its upstream history than previously believed. This would mean: (1) that transition affects turbulent boundary layer structure downstream, and (2) that turbulent boundary layer results obtained under equilibrium conditions (i.e. streamwise self-similarity) may not adequately represent flow behavior near surfaces of operating turbines and airfoils. Non-equilibrium shear layer development near turbine passage surfaces and near airfoils is due to varying surface curvature, varying pressure gradients, and freestream unsteadiness. Unsteadiness is particularly important in this regard since it affects shear properties at a given location in two ways: (1) by its local direct influence and (2) from its affect on shear layers upstream, whose history affects downstream development. The computational work of Singer, Ferziger and Reed [Ref. 1] indicates that moderately low frequency oscillations in the channel can initiate nonlinear effects which trigger transition on flow regimes where the steady flow remains laminar. These happen even though linear theory indicates that the flow is stable. Experimental clarification of these points is needed, along with the verification of the sequence of events occurring during the transition process at different Strouhal numbers. The view of the overall transition process is especially valuable to the gas turbine research community.

Unsteadiness is additionally important since boundary layers which exist near turbulent blades are significantly different from equilibrium boundary studied in many laboratories. A number of recent studies indicate the inadequacy of results obtained from equilibrium boundary layers. Gillis and Johnston's [Ref. 2] measurements in boundary layers downstream of a convex curved surface and Ligrani's [Ref. 3] results in boundary layers downstream of artificial thickening devices showed that many structural changes persist long distances downstream of perturbations. This indicates that boundary layer behavior may depend on upstream history to a greater extent than previously believed. This is important regarding unsteadiness since it alters boundary layers locally as well as the history of boundary layers upstream.

Few experiments have been performed to study the stability or transition of oscillating flow in a plane channel. Most known information is from a handful of analytic studies and the full Navier-Stokes simulation undertaken at Stanford.

Regarding the latter, the work by Singer, Reed and Ferziger [Ref. 1] provides fascinating information as to the effects of unsteadiness on transition. For plane channel flow linear theory has been verified at a Reynolds number of 5000. With mean flow frequency in the range of the non-dimensional frequency of the least stable TS wave (Tollmien-Schlichting), they find that the mechanisms driving the transition are similar to those described by Herbert's secondary instability theory [Ref. 4 and 5] and observed experimentally by Nishioka et. al. [Ref. 6 and 7], and Kozlow and Ramazanov [Ref. 8]. In the plane channel flow these mechanisms have been studied extensively in previous computational investigations. The addition of mean flow modulation causes significant variations in the amplitude of the TS wave during the period, hence the dominant flow structures depend on the Strouhal number and the magnitude of the modulation.

In a straight channel without imposed unsteadiness the process of transition begins with TS waves experiencing mild growth at sufficiently high Reynolds numbers. When these waves grow to an amplitude of about 0.3 percent of the free stream velocity, three-dimensional waves become unstable. Transition often occurs at Reynolds numbers below that at which TS waves become unstable. These waves cause Lambda shaped vortices to lift from the near wall region and "burst" ejecting low speed fluid from close to the wall into the faster moving fluid away from the wall. These events then lead to a rapid breakdown of the laminar boundary layer into a turbulent one. The process can be modified by a number of different factors. Freestream turbulence can lead to non-sinusoidal oscillations in the nominally laminar boundary layer. Local disturbances, such as roughness elements, may lead to structures known as turbulent spots. These patches of turbulent-like flow form a characteristic arrowhead shape and spread in the downstream direction. Distributed roughness, acoustic disturbances, surface waviness and other factors all serve to complicate the basic process. There also exist equilibrium states where two dimensional waves (which are similar in form to TS waves) with a given amplitude will neither grow nor decay. The initial disturbances in the inlet of the channel can evolve into these or similar structures, after which the strong secondary instability of three-dimensional waves can take place.

## **B. OBJECTIVES**

This research is a follow-on to the work undertaken by Longest [Ref. 9], and is believed to be the first experimental (quantitative) study, known to the author, on the effects of imposed mean flow unsteadiness on transition in straight channel flow. The objective is to investigate the effects of imposed, periodic, and deterministic

unsteadiness on the transition process from laminar to turbulent flow. Answers to the following questions are sought:

- 1.) What parameters govern the unsteady flow?
- 2.) What events occur in the flow during the onset and development of transition?
- 3.) What is the interaction between the organized induced unsteadiness and transition (e.g., development of two-dimensional Tollmien-Schlichting waves into three-dimensional instabilities)?
- 4.) At what range of frequencies can one expect interactions between the organized imposed unsteadiness and transition phenomena?

Flow measurements (using hot-wire anemometry) and flow visualization are used to analyze the effect of oscillating the bulk flow in otherwise steady plane Poiseuille flow. An attempt is made to determine whether the type of unsteadiness studied (sinusoidal at two hertz) contributes to the early onset of transition, delay of transition, or has no effect. Sinusoidal oscillation was chosen to induce a deterministic periodic variation of velocity. The results are compared with the results of Singer's [Ref. 1] numerical simulation, which suggests that such oscillations provide a stabilizing effect at all but very low frequencies.

### **C. ORGANIZATION**

Section II follows this introduction and describes the experimental facilities. In section III experimental procedures are discussed, including calibrations, channel validation, flow measurements and flow visualization. The phase averaging technique is also detailed here. A discussion of the results follows in section IV. Conclusions are presented in section V.

## II. EXPERIMENTAL FACILITIES

### A. CHANNEL

The 40 to 1 aspect ratio straight channel, shown schematically in Figure 1, is located in the laboratories of the Department of Mechanical Engineering. The details of the design and construction are discussed by Ligrani and Subramanian [Ref 10]. Briefly, the channel is made of 6.35 mm thick plexiglass with a straight test section 4.27 m in length, with inside dimensions of 1.27 cm in height and 50.8 cm in width. The top and bottom walls of the channel are supported by ribs and cross beams along its length. The side walls are removable in order to gain access to the inside of the channel. The inlet section consists of a honeycomb assembly, 3 frames with screens and a 20:1 contraction ratio nozzle. Two layers of cheesecloth are placed at the inlet lip for filtering the air entering the channel. At the exit of the 4.27 m long test section are three 10.16 cm long frames with screens for housing the unsteady device (the device used to create unsteadiness in the flow) and a second honeycomb. A two dimensional diffuser 45.72 cm long with a 3 degree total angle is located just upstream of the plenum chamber. The exit plenum chamber has inside dimensions of 60.96 cm by 60.96 cm. A 3.81 cm orifice plate assembly between the plenum chamber and the blower is provided to meter the flow through the channel. The exit of the plenum chamber is connected to the suction side of a 5 H.P. blower with a long 50.8 cm diameter pipe. A valve is provided between the plenum and the blower to regulate the flow. Bulk flow velocities up to 15 m/s are achieved in the channel. In our experiments, bulk flow velocities in the range 1.0-4.5 m/s are used.

The channel is designed with a sufficient length such that transition occurs after the laminar velocity profile (parabolic) is fully developed (self similar). The initial flow development length is estimated [Ref. 11:p. 186] to be within about 25 per cent of the test section length for the range of speeds used in the present tests.

## **B. UNSTEADY DEVICE**

The most important aspect in the design of any unsteady device for a transition study is to ensure that the device produces a deterministic and periodic unsteadiness without adding other disturbances. To achieve this in an open circuit induction tunnel, the unsteady device is best located at the exit of the channel. This way, problems caused from the wakes and the flow disturbances resulting when the unsteady device is upstream of the test section are avoided.

The design is based on the design used by Miller and Fejer [Ref. 12] and is shown in Figure 2. Since the depth of the channel is only 12.7 mm, a single rotating vane driven through a spur gear train by a DC stepper motor is adequate to introduce the required unsteadiness in the flow. The rotating vane causes varying resistances to the flow in the test section. The frequency of the imposed unsteadiness is controlled by changing the vane rpm and the amplitude is controlled by using different vane widths. It is also important to match the flow speed with the vane speed. A vane 8.7 mm wide was used in this study.

The vane in Figure 2 is made of a 3.2 mm thick brass strip with rounded edges, and spans the entire width of the channel. The vane is supported at the ends by a 3.2 mm diameter shaft and bushings that are fitted to the side walls of the frame. Three additional intermediate spanwise struts are provided to increase the rigidity of the vane. One end of the shaft is extended to accommodate a 48 TPI (Threads Per Inch) spur

gear. The driver spur gear has 12 TPI and is mounted on the Superior Electric, M092-FD310 Stepper Motor. To achieve a fine step control, a Modulynx MITAS PMS085-D050 Drive with Modulynx MITAS PMS085-C2AR Drive Controller is used. This combination facilitates motor shaft speeds up to 100 revolutions per second, with a constant 200 steps per motor shaft revolution. Note that, with a 1:4 gearing ratio and two cycles of imposed flow oscillations per vane rotation, one motor revolution corresponds to one half cycle of the imposed flow oscillation by the vane. The Drive Controller is programmed for the required motor speed (rps). The Modulynx MITAS PMS085-D050 Drive was also used to provide a trigger signal to initiate data acquisition. This trigger also enabled the correlation of data taken with the position of the vane at the time that the data was recorded.

### **C. FLOW MEASUREMENTS**

The equipment used for flow measurement includes a digital manometer, hot-wire probe, hot-wire bridge, signal conditioner, digital multimeter, high speed data acquisition system, oscilloscope and a microcomputer. These are described in detail below

#### **1. Bulk Velocity**

The bulk flow velocity through the channel is determined from the pressure drop across the 3.81 cm orifice plate which is installed in the piping between the blower and the exit plenum chamber. This pressure drop is measured and displayed by a Validyne Model PS 309 digital manometer (inches of water).

## **2. Instantaneous Velocity**

A constant temperature hot-wire anemometer is used to measure instantaneous velocities of the flow. Briefly, the principles of hot-wire anemometry (constant temperature mode) are as follows.

The flow sensing element (hot-wire probe) consists of a short length of wire, connected to two supports, which forms the leg of a wheatstone bridge. This bridge maintains the wire at elevated temperature and is initially balanced prior to exposing the probe to the flow. This balancing resistance, referred to as "cold" resistance is multiplied by an "overheat ratio". Once the bridge is set to this value, and as the probe is exposed to the flow, the bridge is placed in operation and a small current (60 mA) passes through the circuit. Wire temperature increases because of resistive heating and the wire resistance increases until the bridge is rebalanced. The governing relationship is:

$$R = R_o(1 + \alpha(T - T_o))$$

where  $R$  is the resistance at temperature  $T$ ,  $R_o$  is the resistance at the reference temperature  $T_o$ , and  $\alpha$  is the temperature coefficient of resistance.

Flow past the probe causes the wire to cool (by convection) and the bridge becomes unbalanced as the resistance decreases. The bridge is rebalanced by a feedback loop and amplifier. Response is rapid enough to maintain wire temperature and resistance nearly constant. As such, the variations in the bridge voltage are directly proportional to the current variations, and flow velocity can be calculated as a function of the bridge voltage.

Now the different components used to measure instantaneous velocity are described.

### ***a. Hot-wire Probe and Probe Positioning***

A Dantec Electronics Inc. P51 probe, mounted such that the wire is horizontal and normal to the streamwise flow direction, is used. The wire sensor is 5.0 microns in



diameter and approximately 1.25 mm long. The probe is mounted through the side wall of the channel and is held fixed by a rotatable lever arm which allows placing of the probe at various  $y/d$  positions ranging from 0.2 to 0.9. A scale graduated in terms of  $y/d$  is mounted adjacent to the lever arm for probe positioning to an accuracy of approximately 0.5 mm. Longitudinal and transverse position of the probe for this study were 46.12 cm and 15.64 cm, measured from the near flange at the end of the test section, and from the inside of the left channel wall (looking downstream), respectively. By rearranging the sidewalls the probe can be positioned at other streamwise locations for future studies.

#### ***b. Hot-wire Bridge***

The hot-wire is operated with a DISA 55 M10 constant temperature bridge. A five meter coaxial cable is used to connect the hot-wire to the bridge. For the purposes of this study the cold resistance was multiplied by an overheat ratio of 1.8. The DC voltage from the bridge is measured with a Hewlett-Packard 3466A digital multimeter.

#### ***c. Signal Conditioner***

The hot-wire signal is filtered and amplified by a DISA 56W20 signal conditioner. The high-pass filter is set to 0.1 Hz in all cases to remove the DC signal. This however, did not alter the effects of 2.0 Hz imposed flow unsteadiness. The low-pass filter is set at 10 KHz to filter out noise existing above this frequency. The hot-wire signal is amplified using a gain of 10 to achieve an acceptable signal to noise ratio. Output from the signal conditioner is sent to the high speed data acquisition system and to a B & K Precision 10 MHz Oscilloscope used to signal monitor the signal.

#### ***d. High Speed Data Acquisition System***

A Hewlett-Packard 6944A Multiprogrammer is used in conjunction with a Hewlett-Packard series 9000, Model 310 microcomputer to acquire data. A buffered

69759A A/D card configuration is used with the Multiprogrammer to allow continuous data acquisition. The A/D card is externally triggered using 2-3 volt TTL type signals from the unsteady device motor drive. When the unsteady device is not in operation, triggering is provided by a Hewlett-Packard 3311A Function Generator set to the same frequency as that used with the unsteady device in operation. Sampling occurs as square wave voltage changes from high to low.

The storage capacity of the A/D buffer is 64,000 bytes. The number of imposed unsteadiness cycles which can be sampled depends on the desired number of data points per cycle. For example, if 100 points per cycle are desired, then 640 cycles can be sampled. In this study, sampling was done at 100 points per cycle for all cases, where cycle refers to the cycle of flow blockage caused by the vane rotation of the unsteady device. 100 points per cycle were chosen so that there would be sufficient resolution to determine the effect of unsteadiness over the complete phase of each unsteadiness cycle.

#### *e. Data Storage*

The Hewlett-Packard microcomputer is used to acquire the data from the A/D buffer, using a data acquisition program HOTWIREPAV, described in the software directory (APPENDIX A). Raw instantaneous voltage data is acquired and stored on standard 3.5 inch micro diskettes for further processing. Manual inputs to the program include bulk flow velocity, flow blockage frequency, and date and time.

#### *f. Data Processing*

Processing of the data is done using a Hewlett-Packard microcomputer using the programs MAX\_MIN and AVG\_PLOT. This software is described in detail in the software directory (APPENDIX A). Many of the curves used to graphically display the results were generated using a Macintosh SE personal computer and the graphics program

CRICKETGRAPH. The phase averaging technique employed by the program MAX\_MIN is described below.

In the case of an unsteady flow the instantaneous velocity can be split into three components.

$$U = \bar{U} + \tilde{U} + U'$$

where  $\bar{U}$  is the time averaged velocity,  $\tilde{U}$  is the imposed phase averaged velocity and  $U'$  is the instantaneous fluctuating component.  $\tilde{U}$  is the component due to the unsteadiness, and is zero for steady bulk flow. In the present study  $\tilde{U}$  and  $\bar{U}$  are combined to represent the phase averaged velocity ( $\hat{U}$ ). Thus,

$$U = \hat{U} + U'$$

$\hat{U}$  is determined by phase averaging  $U$  over, say 640 cycles (ncycl), at different positions of the phase of each oscillation.

$$\hat{U}(n) \Big|_{n=1}^{100} = \frac{1}{ncycl} \sum_{m=1}^{ncycl} U(m, n) \Big|_{n=1}^{100}$$

When  $U'$  is a large percentage of  $\hat{U}$  then a larger number of cycles, sometimes up to 4640 cycles, are used to determine  $\hat{U}$ . For this, multi-run data acquisition is made, with the vane at the same starting position for each run. Only the last 580 data points (due to sampling procedure) of each run are used in the cumulative phase averaging. Once  $\hat{U}$  is determined,  $U'$  is calculated from  $U' = U - \hat{U}$ , and  $(U')^2 = (U - \hat{U})^2$ . Therefore, the phase averaged root mean squared velocity is,

$$\hat{U}'(n) \Big|_{n=1}^{100} = \sqrt{\frac{1}{ncycl} \sum_{m=1}^{ncycl} (U(m, n) - \hat{U}(n))^2 \Big|_{n=1}^{100}}$$

Time averaged velocity,  $\bar{U}$ , and rms velocity  $\sqrt{(u')^2}$  are calculated by averaging over all the points (100 x ncycl) per run and in the case of multi-runs, 100 x ncycl x no. of multi-runs.

$$\bar{U} = \frac{1}{ncycl} \sum_{m=1}^{ncycl} \frac{1}{100} \sum_{n=1}^{100} U(m,n)$$

$$\sqrt{u'^2} = \sqrt{\frac{1}{ncycl} \sum_{m=1}^{ncycl} \frac{1}{100} \sum_{n=1}^{100} (U(m,n) - \bar{U})^2}$$

#### D. FLOW VISUALIZATION

The equipment utilized for flow visualization studies includes a smoke wire for generating smoke in the channel and video equipment to photograph the flow in the channel. These are described in detail below.

##### 1. Smoke Wire System

The smoke wire system is a modified Vertical Smoke Wire Instrument made by Flow Visualization Systems of Bolingbrook, IL. The system in its present configuration consists of a 0.127 mm diameter nichrome wire that is stretched across the width of the channel through access ports in the channel side walls. The wire is passed through these access ports through a thin stainless steel tube (hypodermic needle) which allows the wire to move freely. The smoke wire is connected to an A/C-D/C converter and this in turn has voltage supplied by a Calrad 45-740 (0-130 VAC) variac set at 45 VAC. The wire is energized by pulsing the "Momentary On" switch of the A/C-D/C converter. Since the wire acts as a resistor and heats up when a current is passed it becomes more elastic and has a tendency to sag in the channel. To prevent this from affecting the flow

visualization, a tensioning device has been installed on one end of the wire to ensure that the wire is held taut in the channel when it is energized. This tension device consists of two pulleys which support the wire and a third pulley with a weight attached between the two support pulleys. The wire is coated with a paraffin based oil which is applied by means of a thin rod with an absorbent piece of felt at the tip. When applied in this manner, the wire is coated evenly with small droplets of oil. Energizing the wire produces a thin even sheet of smoke until all the oil on the wire burns. The smoke from the wire lasts for about 4-8 seconds depending on the flow rate in the channel.

The wire is placed horizontally normal to the flow 76.8 cm upstream from the end of the test section. For the purposes of this study, the wire was located at a  $y/d$  value of 0.84 ( $d$  being the width of the channel and  $y$  the height from the bottom of the channel).

## **2. Video Equipment**

The video equipment used for flow visualization is the same as that described by Longest [Ref. 9]. Briefly, a high speed video camera is mounted on a tripod above the channel and focused on the area of interest. The focal plane from the camera lens to the channel is surrounded by an enclosure to exclude all extraneous light and thus decreasing the reflections which interfere with the flow visualization. The bottom of the channel was blacked out and lighting was provided by two 600 Watt floodlights placed 1 m from the sidewall on either side of the channel at the same height as the channel.

Still photographs were made by taking pictures of the aforementioned video when viewed on a monitor. A Nikon F-3 SLR and Kodak Tri-Xpan film were used to take the pictures. The shutter speed was one-eighth of a second and the focal aperture was set at  $f 5.6$ .

### **III. EXPERIMENTAL PROCEDURES**

#### **A. ORIFICE DP CALIBRATION**

The orifice differential pressure calibration for bulk velocity flow measurements was performed by Longest [Ref. 9]. Results of the calibration are shown in Figure 4.

#### **B. HOT-WIRE CALIBRATION**

The hot-wire was calibrated in the freestream of the wind tunnel, also located in the laboratories of the Mechanical Engineering Department of the Naval Postgraduate School.

The hot-wire probe is mounted normal to the flow in the center of the channel so that it is in the freestream. The hot-wire is connected to the same hot-wire bridge previously discussed. Output from the hot-wire bridge is read on a digital multimeter. Freestream velocity in the wind tunnel is measured utilizing a Kiel pressure probe, a wall static pressure tap, and a Validyne digital manometer. Voltage and differential pressure readings are taken for a range of pressure drops corresponding to velocities of 1.0 to 4.0 m/s. The computer program HWCAL is run on the Naval Postgraduate School's IBM main frame computer to calculate all calibration constants. Following the calibration, the hot-wire is installed in the straight channel.

#### **C. CHANNEL VALIDATION**

##### **1. Channel Flow Tests**

Assembly and installation of the straight channel in the Mechanical Engineering Laboratory of the Naval Postgraduate School, along with the initial flow visualization

and measurement results are detailed by Longest [Ref. 9]. Prior to commencing flow measurements for this study a check of the channel flow quality is performed as follows. Smoke is generated using the smoke generator described by Longest [Ref. 9] and then drawn into the channel at a speed of approximately 2.0 m/s. The first few times this was performed, numerous leaks from the sidewalls of the channel were observed. These leaks are eliminated using removable spring clamps on both sides of the channel, along its entire length. The clamps are left in position while the channel is in operation.

## **2. Laminar Average Velocity Profile Verification**

Velocity profile verification is performed at a Reynolds number of 1103 (bulk velocity of 1.32 m/s) when the flow is laminar. Instantaneous velocity measurements were taken at eight  $y/d$  positions ranging from 0.2 to 0.9, at an  $x/d$  of 300.0. This data was taken using the HOTWIREPAV program, with no imposed unsteadiness. MAX\_MIN was used to process the data, and the time-averaged local velocities were normalized with respect to the maximum value which occurred at the mid-channel location ( $y/d = 0.5$ ). A second order polynomial curve was fit to the data and is shown in Figure 5. The curve demonstrates that the flow is fully developed at this location and follows the expected parabolic behavior.

## **D. FLOW MEASUREMENT**

### **1. Reynolds Number Survey**

Velocity surveys are conducted for Reynolds numbers ranging from 1100 to 3800 with the hot-wire probe at a  $y/d$  position of 0.88, and a  $z/d$  of -7.7. This survey is done to determine how the imposed unsteadiness affects the transition process as Reynolds number varies. Data at each Reynolds number are taken by recording results with no

imposed unsteadiness followed by results with imposed unsteadiness. Data sets of 64,000 points are taken using only the last 58,000 for data processing, as previously described. Average velocity and RMS velocity values from such survey are used to generate Figures 6 and 7. These experiments were repeated at several Reynolds numbers to ensure consistent and repeatable data trends.

## **2. Multi-run Averaging**

Multi-run phase averaging using up to 4640 cycles of flow unsteadiness were conducted at several Reynolds numbers. The purpose of this multi-run averaging is to show that the survey data is statistically stable for higher Reynolds numbers where fluctuation levels are significant with respect to the local mean velocity. Results are presented in Figures 8-35.

## **3. Velocity Profiles**

Velocity profiles with and without imposed unsteadiness are taken at the same Reynolds numbers as used for the multi-run averaging. The purpose of these profiles is to record flow development as the Reynolds number is changed and to study the effect of imposed unsteadiness on average and RMS velocities as a function of the Reynolds number and  $y/d$ . Data acquisition and processing is performed as described in the Reynolds number survey. Results are provided in Figures 36-82.

## **E. FLOW VISUALIZATION**

Smoke patterns were recorded on film using the video camera at Reynolds numbers ranging from 1140 to 2240 with no imposed unsteadiness. Video sequences are taken at different Reynolds numbers spaced apart by approximately 50 units. The purpose of this flow visualization is to record transition events with no imposed unsteadiness. Still photographs are shown in Figures 83-94.



#### IV. RESULTS AND DISCUSSIONS

The coordinate system is right handed.  $x$  is the streamwise distance measured from the exit end of the nozzle,  $y$  is the vertical distance measured from the bottom wall of the channel, and  $z$  is the spanwise distance measured from the channel centerline.

The positive  $z$  distances are to the right of the channel centerline (looking downstream).

The Reynolds number,  $Re$ , is based on the bulk flow velocity,  $v_{bulk}$ , and the channel height  $d$ , and is given as:

$$Re = v_{bulk} * d / \nu$$

Where  $\nu$  is the kinematic viscosity. The Strouhal number,  $Str$ , is based on the imposed unsteadiness frequency,  $f_{osc}$ , bulk flow velocity, and channel height. The Strouhal number is given as:

$$Str = 2\pi * f_{osc} * d / v_{bulk}$$

Reynolds numbers ranged from 1100 to 3800 in the present study. The imposed oscillation frequency is 2.0 Hz. Strouhal numbers varied from 0.0351 to 0.121.

##### A. CHANNEL FLOW QUALIFICATION

For fully developed laminar channel flow, the mean velocity is given by as:

$$\bar{u} / \bar{u}_{max} = 4.0[y/d - (y/d)^2]$$

Where  $u$  is the local mean velocity and  $\bar{u}_{max}$  is centerline velocity [Ref 11:p. 280-281].

Figure 5 shows the velocity profile taken at  $x/d = 300$  at a  $Re$  of 1103 ( $v_{bulk} = 1.32$  m/s)

The velocity profile (normalized with respect to  $\bar{u}_{max}$ ) is parabolic and is in good agreement with the above equation. For this situation, the maximum centerline velocity is 1.774 m/s giving a ratio of  $v_{bulk} / \bar{u}_{max}$  of 0.774.

**B. EFFECT OF 2.0 HZ IMPOSED UNSTEADINESS ON LOCAL MEAN  
VELOCITY AT  $y/d = 0.88$**

Figure 6 shows variation of the mean velocity at  $y/d = 0.88$  with and without the imposed unsteadiness for varying  $Re$ . The variation of the bulk mean velocity is also shown in the plot. The mean velocity shows somewhat non-linear behaviour for Reynolds numbers from 2000 to 2100. The mean velocity distribution is not changed by imposed bulk flow unsteadiness.

**C. EFFECT OF 2.0 HZ IMPOSED UNSTEADINESS ON RMS VELOCITY AT  $y/d = 0.88$**

Figure 7 shows the variation of the time-averaged RMS velocity  $\sqrt{u'^2}$  normalized with respect to the time averaged velocity,  $\bar{u}$  at  $y/d$  of 0.88 and over Reynolds numbers from 1100 to 3800. Data are given with and without unsteadiness at 2.0 Hz at twenty one different Reynolds numbers.

For Reynolds numbers below 1400, no effect of the imposed unsteadiness is observed in the normalized RMS values. With the 2.0 Hz unsteadiness, significant increases in the RMS velocity values occur for Reynolds numbers from 1400 to 2005. The maximum increase in the normalized RMS velocity is about 31.5% over that without the unsteadiness. At higher Reynolds numbers, greater than 2210, however, the plot shows that normalized RMS values decrease with 2.0 Hz unsteadiness. This reduction is observed for Reynolds numbers up to 2400. Here, the maximum decrease in normalized RMS velocity with the imposed unsteadiness is about 5.4% and occurs at a Reynolds number of 2302. For Reynolds numbers greater than 2400, the values of normalized RMS are nearly the same with and without the imposed unsteadiness.

#### D. EFFECT OF REYNOLDS NUMBER ON PHASE-AVERAGED VELOCITY

Figures 8 through 35 show phase-averaged velocity traces at five different Reynolds numbers. The phase-averaged quantities are plotted against the phase angle of the imposed unsteadiness for Re of 1103, 1579, 2005, 2548, and 3660.

Figures 8 through 17 are the phase-averaged quantities with no imposed unsteadiness. Figures 8,10,12,14, and 16 show phase-averaged velocity  $\bar{U}$  (which equals  $\tilde{U}$  in these cases), and Figures 9,11,13,15, and 17 show the plots of phase-averaged RMS velocity normalized with respect to the temporal mean  $\bar{U}$ . For these cases phase averaging is done over 580 flow oscillations. The variations with phase angle in Figures 8 through 17 are quite small and due to data scatter.

Figures 18 through 35 show phase-averaged velocity traces when 2.0 Hz unsteadiness is imposed on the flow. With imposed unsteadiness at this frequency, statistically stable phase-averaged results are obtained after 580 cycles for Reynolds numbers of 1200 and below, after 2320 cycles for Reynolds numbers up to 1600, and after 4640 cycles for higher Reynolds numbers where the fluctuation levels are significant with respect to the local mean velocity. The effect of multi-run averaging is demonstrated in Figures 20 through 35. For example, Figures 24 and 25 show phase-averaged quantities after 580 flow oscillations, and Figures 26 and 27 show the same quantities after 4640 flow oscillations for Re 2005. The curves in figures 26 and 27 are smoother indicating improved averages of  $\bar{U}$  and normalized RMS values at particular phase angles. Figures 20 through 23 are the corresponding plots for Re 1579, Figures 28 through 31 for Re 2548, and Figures 32 through 35 for Re 3660.

Normalized RMS values remain relatively constant with phase angle for all of the cases surveyed with the exception of Re of 2005. Here, as shown in Figure 27, an increase in the normalized RMS velocity is seen between phase angles of 108 and 252

degrees. The maximum value is approximately 17% greater than the temporal RMS velocity and occurs at a phase angle of about 200 degrees. The maximum value of  $\theta$  for this case is seen in figure 26 at about 235 degrees. This behavior occurs at the same Reynolds number where the time-averaged RMS velocity shows the largest increase due to imposed bulk unsteadiness.

#### **E. MEAN VELOCITY PROFILES**

Figures 36 through 42 show mean velocity profiles taken at  $x/d = 300$ .  $y/d$  ranges from 0.2 to 0.9 in these plots. No measurements are given for a  $y/d$  of 0.1 because of the geometry of the hot-wire probe. For all of the profiles, mean velocity is plotted versus  $y/d$  and normalized with respect to the maximum mean velocity.

Figure 36 shows the profile development with Reynolds number with no imposed unsteadiness. Profiles are shown for  $Re = 1103, 1579, 2005, 2548$ , and  $3660$ . The profile is parabolic at low  $Re$  when the flow is fully laminar. At the highest two  $Re$ , the profiles show fully turbulent behavior. The profile is distorted for the transitional Reynolds number of 2005.

Figure 37 shows the profile development with Reynolds number with imposed unsteadiness at 2.0 Hz. The imposed unsteadiness has no observed effect on the mean velocity profiles. This is further evidenced in Figures 38 through 42, where the mean velocity profiles are plotted, both with and without imposed unsteadiness, for each Reynolds number.

## **F. RMS VELOCITY PROFILES**

Figures 43 through 49 show the development of RMS velocity profiles with Reynolds number. In Figures 45 through 49, RMS velocities are normalized with respect to maximum observed mean velocities and plotted against  $y/d$ . Again, the symmetry of the profiles is distorted because data are not given for a  $y/d$  of 0.1.

Figure 43 shows dimensional RMS velocity profiles for the five Reynolds numbers when no bulk unsteadiness is imposed on the flow. Corresponding profiles with imposed unsteadiness at 2.0 Hz. are shown in Figure 44. In Figures 45 through 49 plots both with and without imposed unsteadiness are given for each Reynolds number. For  $Re = 2005$  and lower, the imposed unsteadiness results in significant increases in magnitudes of normalized RMS velocity values. At  $Re = 2005$  values range from 0.04 to 0.11 with imposed unsteadiness compared to 0.03 to 0.08 without, and the relative shapes of the two profiles are nearly the same, as shown in Figure 47. This is not the case for Reynolds numbers 1103 and 1579.

Figures 48 and 49 present profiles for Reynolds numbers 2548 and 3660. At these Reynolds numbers, the imposed unsteadiness seems to have little effect on RMS velocity distributions.

## **G. VARIATION OF PHASE-AVERAGED QUANTITIES WITH REYNOLDS NUMBER AND $y/d$**

Figures 50 through 82 show the variations of phase-averaged quantities  $u$  and  $u'$  as  $y/d$  and Reynolds number are changed.

Figures 50 through 81 show  $\bar{u}$ , and  $\bar{u}'$  (normalized with respect to the temporal mean) plotted versus phase angle at  $Re = 2005$  for  $y/d$  from 0.2 to 0.9. The figures are arranged to show data as  $y/d$  decreases.

Figures 50 through 57 are the plots of  $\bar{u}$  versus phase angle for flow with no imposed unsteadiness. The corresponding  $\bar{u}'$  plots are shown in Figures 58 through 65. Phase-averaged RMS  $\bar{u}'$  decreases from  $y/d$  0.9 to 0.7, and then becomes relatively constant at  $y/d$  of 0.6, 0.5, and 0.4. For flow with no imposed unsteadiness, the  $\bar{u}'$  distributions are relatively constant with phase angle for each  $y/d$  location.

Figures 66 through 73 show  $\bar{u}$  distributions versus phase angle for Re of 2005 with imposed unsteadiness at 2.0 Hz and at  $y/d$  locations 0.9 to 0.2. Maximum values of  $\bar{u}$  are observed at phase angles between about 210 degrees and 240 degrees. Minimum values occur at phase angles between approximately 30 and 75 degrees. Near the wall the curves show considerable fluctuations as shown in Figures 66, 67, and 73. Figures 68 through 72 show smoother curves as the channel centerline is approached. Most  $\bar{u}$  distributions are nearly sinusoidal in shape, as shown in Figure 70.

Figures 74 through 81 show plots of normalized  $\bar{u}'$  versus phase angle with imposed unsteadiness at 2.0 Hz. The previously described increase in phase-averaged RMS velocity at this transitional Reynolds number is again evident between phase angles of 108 and 252 degrees. This increase is less dramatic at  $y/d$  locations near the channel centerline. In fact, the distribution is relatively constant with phase angle at  $y/d$  of 0.5, as shown in Figure 78. The most noticeable increases are observed at  $y/d$  locations of 0.9, 0.8, and 0.2, as shown in Figures 74, 75, and 81, respectively.

In Figure 82, peak to peak phase-averaged velocities  $\bar{u}$  (normalized with respect to the local mean velocity) are shown. Data for 2.0 Hz imposed unsteadiness are given for Re of 1103, 1579, 2005, 2548, and 3660. The  $y/d$  locations vary from 0.5 to 0.9. For the laminar cases, Re of 1103 and 1579, the peak to peak velocity shows a steady increase from 6% at the channel centerline to about 12% near the top wall ( $y/d=0.9$ ). For the intermediate Re of 2005, the variation is greater, 11% at the centerline and 24% near

the wall. For Re 2548, the variation at the centerline of the channel is the same as that for Re 2005. However, at the remaining  $y/d$  locations the respective values are significantly less than those for Re 2005. At  $y/d$  of 0.9 the variation for Re 2548 is 7% less than that for Re 2005 at this location. The shape of the curve for Re 2548 is similar to the curves observed for Reynolds numbers 1103 and 1579. For Re 3660 the distribution is nearly constant at about 12% from  $y/d$  0.5 to 0.8. Then, peak to peak magnitude increases sharply, reaching a maximum value of 25% at  $y/d$  of 0.9.

## **H. FLOW VISUALIZATION**

Figures 83 through 94 show flow visualization results with no imposed unsteadiness at Reynolds numbers ranging from 1136 to 2239. Flow is from the right to the left of the photographs in Figures 83 through 92. In Figures 93 and 94, flow is from the bottom to the top for each photograph.

Figures 83 through 92 show flow structures occurring during the transition process from laminar to turbulent flow. Laminar flow at Re 1136 is shown in Figure 83. Figure 84 shows the presence of Tollmien-Schlichting waves at the higher Reynolds number, Re 1328. The emergence of vortical ribbon-like structures (hereafter referred to as ribbons) at the left side of the channel is seen at Re 1377, in Figure 85. As Re increases, these ribbons are observed to occupy a greater percentage of the width of the channel, from left to right. This is shown in Figures 86 and 87 for Re of 1395 and 1496, respectively. Also noticeable at Re 1496 is the presence of turbulent spots which appear as dark areas in Figure 87. At higher Reynolds numbers, turbulent spots are larger and more abundant. This is shown in Figures 88 through 91, which correspond to Re of 1529, 1713, and 1854, respectively. Figure 92 shows a predominantly turbulent flow at Re 2239. Turbulent ribbons which are hazy and ill-defined compared to those observed

at lower Reynolds numbers are characteristic at this Reynolds number, as shown in the figure.

Figures 93 and 94 show a time sequence which depicts flow behavior at a sub-critical Reynolds number of 1412. The time interval between each of the twelve frames of the sequence (ordered from top to bottom of the page, left to right) is approximately one fifteenth of a second. Therefore, the total time sequence represents flow history of approximately 800 milliseconds. The sequence clearly illustrates the order and duration of transition phenomena with no imposed unsteadiness, as soon as the smoke is released from the wire. The pictures suggest that the ribbons are considerably elongated in the streamwise direction and occupy half of the channel width. Some of these ribbons terminate as dark patches.



## V. CONCLUSIONS

Imposed unsteadiness at 2.0 Hz has no discernible effect on mean velocity profiles for  $Re$  from 1103 to 3660. However, in regard to time-averaged fluctuating velocity magnitudes, the imposed unsteadiness exhibits both a destabilizing effect and a stabilizing effect in the range of Reynolds numbers and Strouhal numbers studied. A destabilizing of the flow is seen for  $Re$  from 1400 to 2200, and  $Str$  from 0.061 to 0.095, whereas a stabilizing of the flow is seen for  $Re$  from 2200 to 2400 and  $Str$  from 0.056 to 0.061.

The imposed unsteadiness affects both time-averaged and phase-averaged RMS values. This is especially evident for the transition Reynolds number of 2005. Here, when the unsteadiness is imposed, the phase-averaged RMS velocity is a maximum at a phase angle slightly ahead of the phase angle where the maximum phase-averaged velocity  $\bar{u}$  is observed. The most significant variations of the phase-averaged velocity across the span of the channel also occurs at this Reynolds number.

The various transition flow structures, which are predicted by numerical simulations and have been observed experimentally during previous flow visualization investigations, are confirmed in this study. Tollmien-Schlichting waves, followed by vortical ribbon-like structures, and then, turbulent spots are the dominant phenomena as Reynolds number is increased with no imposed unsteadiness. Time sequence photography at a sub-critical Reynolds number provides insight into the emergence of the ribbon-like vortical structure in the channel, with subsequent growth in both the spanwise and streamwise directions. Dark patches are sometimes observed following the ribbon structures, suggesting the onset of short duration turbulent spots.

While the above results proved repeatable during this study more investigation is warranted, especially in the range of Reynolds numbers where the imposed unsteadiness seems to stabilize the flow, i.e.,  $Re$  2200 to 2400.

## APPENDIX A

### SOFTWARE DIRECTORY

1. **HWCAL** : This program determines the constants for the King's Law calibration of the hot-wire. The program also provides a polynomial fit of the calibration data.
2. **HOTWIREPAV** : This program is used to read the data stored in the A/D buffer of the high speed data acquisition system and stores the information on micro diskettes. Manual inputs are: triggering frequency, hot-wire DC voltage (ungained), oscillation frequency (flow blockage), bulk velocity and date and time of run.
3. **MAX-MIN** : This program calculates instantaneous and phase averaged velocities. Initially a look up table is created. Here, effective velocities are calculated from the effective voltage values and stored for follow on calculations. The hot-wire calibration constants obtained from HWCAL, and the amplifier gain are incorporated into these calculations. The velocity calibration is given by the equation:
$$U_{eff} = k(E_{eff}^2 - E_0^2)^{1/N}$$
where  $k$  is the proportionality constant,  $E_{eff}$  is the effective voltage, and  $E_0$  is the reference voltage at no flow.  $N$  is a constant value of 0.45 for moderate Reynolds numbers. Once the look up table is created the program reads the instantaneous voltage values from the data file and converts them to instantaneous velocities. At this point a plot of the instantaneous velocity versus time can be generated for any of 580 cycles (The first 60 cycles are discarded to allow for flow stabilization as the unsteady device is started.)

Next the program phase averages the 580 cycles, and velocity versus phase angle (of the flow blockage) plots are available. Two plots are available from the averaged values:  $\bar{u}$  versus phase angle and  $\sqrt{\bar{u'^2}}$  divided by  $\bar{U}$ , versus phase angle, where  $\bar{u}$  is the phase averaged velocity,  $\sqrt{\bar{u'^2}}$  is the phase averaged root mean squared velocity, and  $\bar{U}$  is the average velocity. In the case where there is no imposed unsteadiness, the phase averaged velocity,  $\bar{u}$ , is equal to the time averaged velocity,  $\bar{U}$  since there is no superimposed phase average velocity component,  $\tilde{U}$ .

The program can also be used to process a set of data when multi-run averaging is desired. In this case the averaged values are written to and stored in the computer hard disk memory. Once each of the desired data sets has been averaged and stored in the computer memory, they are copied to micro diskettes.

4. **AVGPLOT** : The program AVGPLOT is used to average any number of data sets. A maximum of eight sets of data (or 4,640 cycles) were averaged for this study. The program AVGPLOT provides the same graphs as those available from MAX\_MIN. Phase averaged data sets are copied to micro diskettes prior to purging them from the computers memory.

## **APPENDIX B**

### **FIGURES**

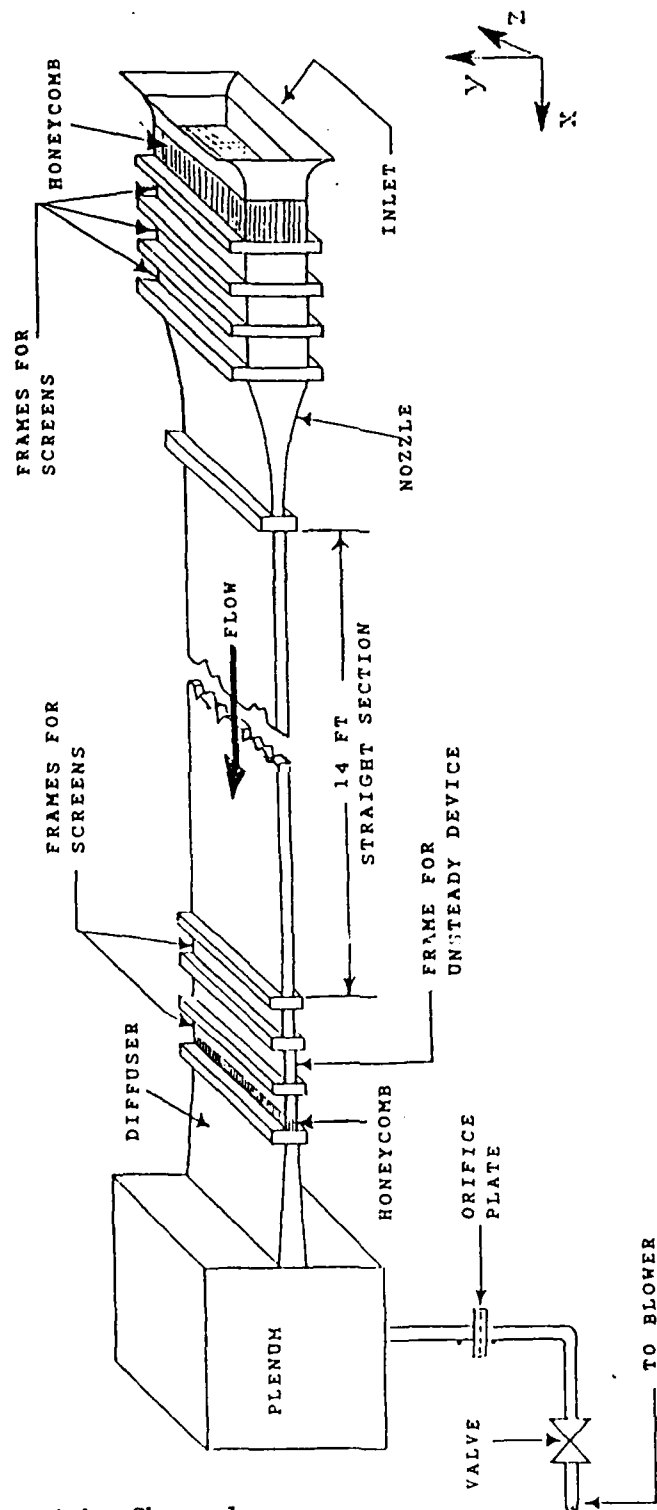


Figure 1. Straight Channel

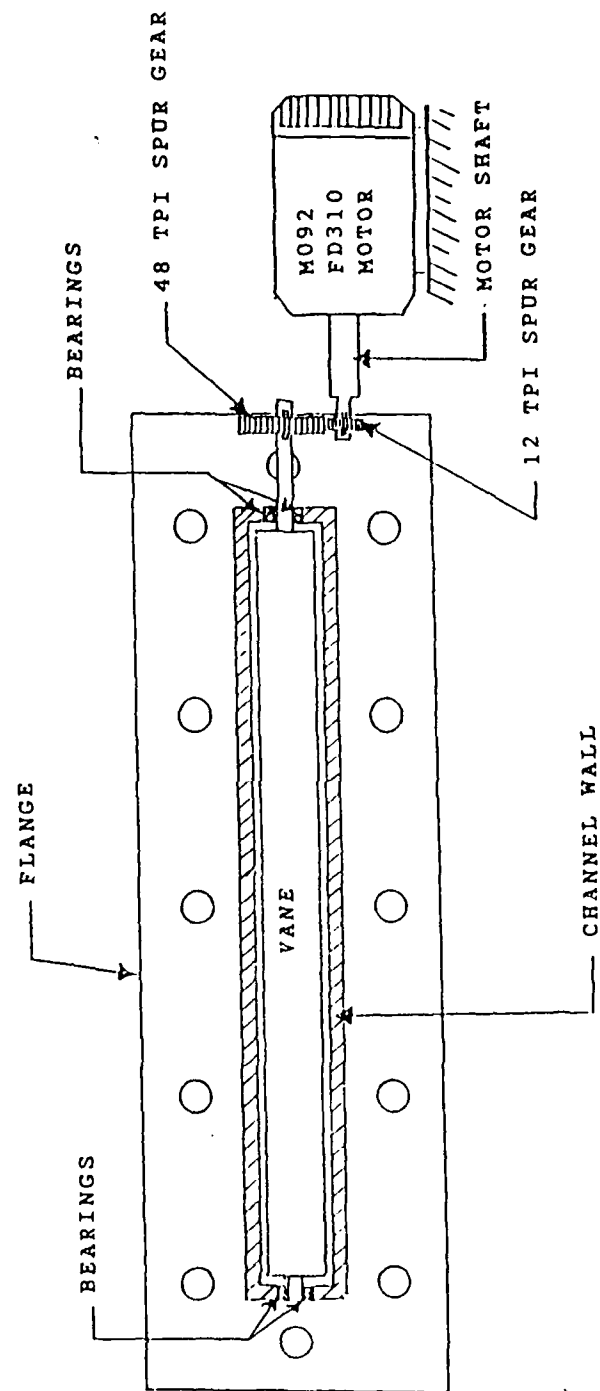


Figure 2. Unsteady Device

### SCHEMATIC OF FLOW MEASUREMENT EQUIPMENT

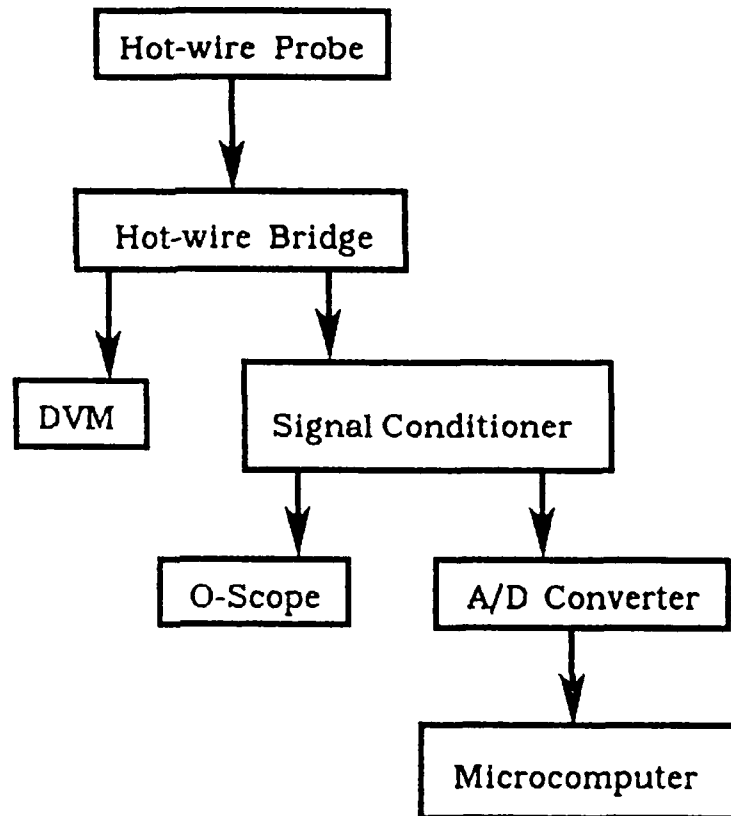


Figure 3.



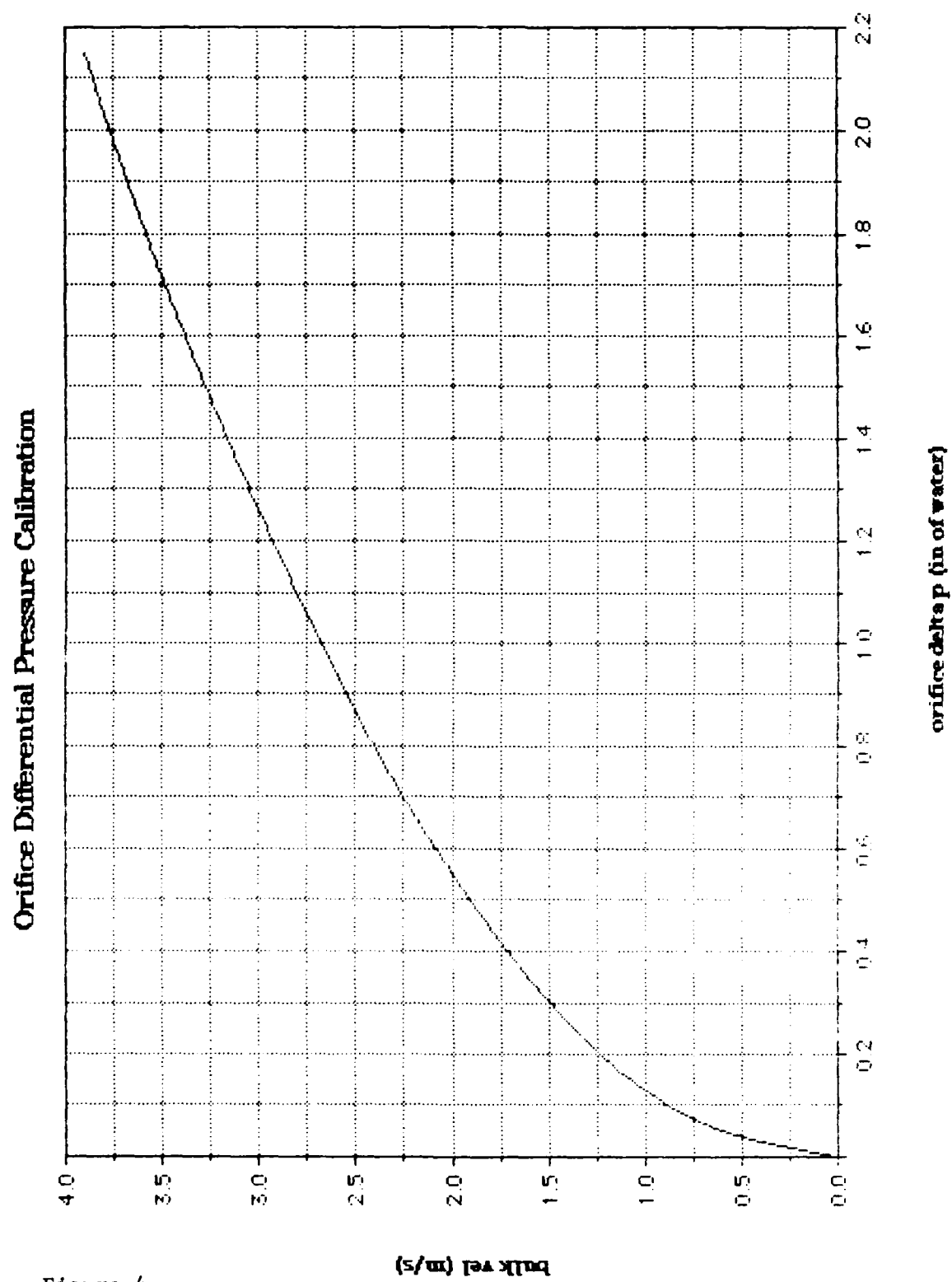


Figure 4.

Fully Developed Flow Validation  
at Re No. = 1103

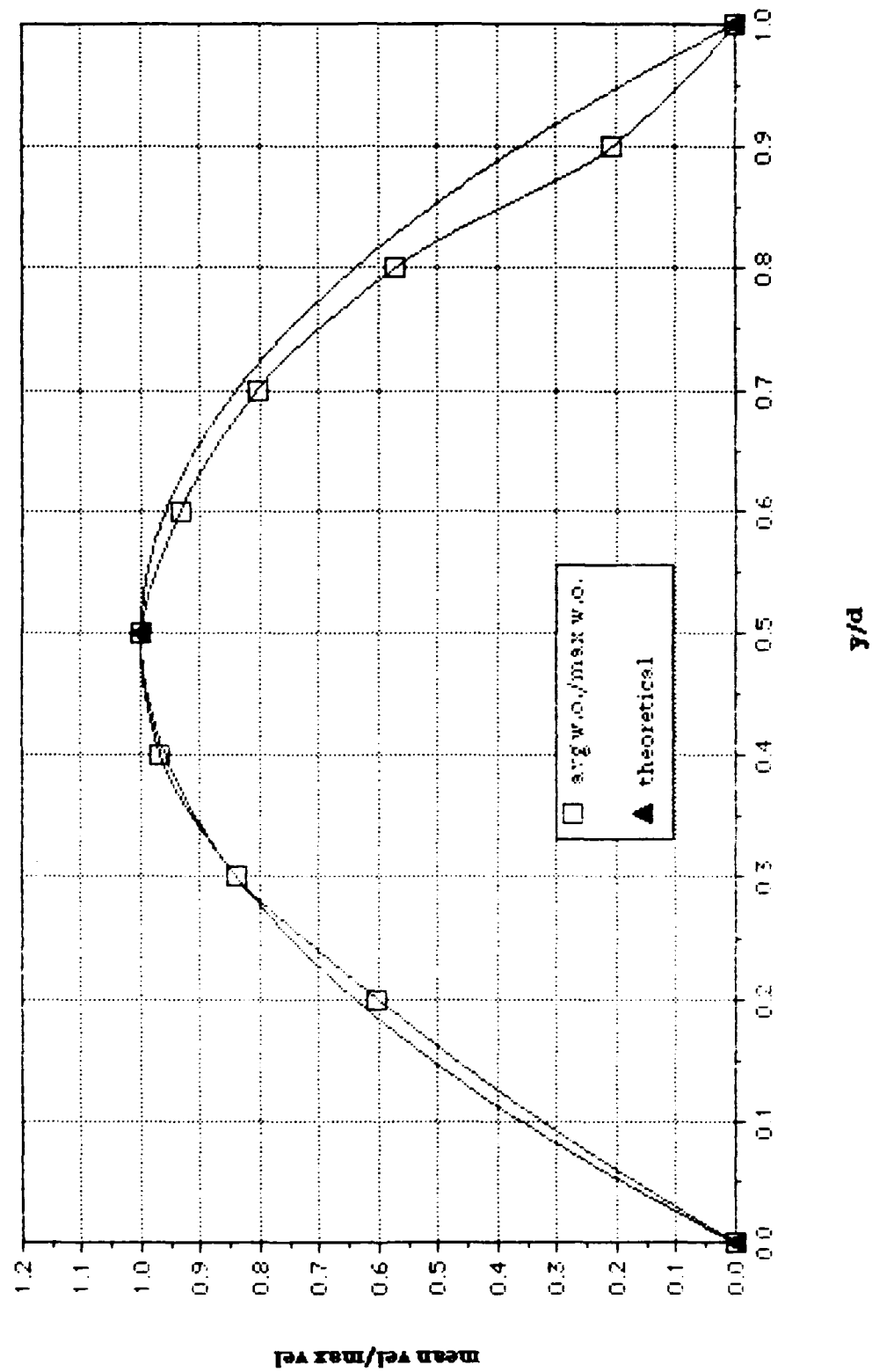


Figure 5.

Effect of Reynolds Number on Local Mean Velocity due to 2 Hz Imposed Unsteadiness

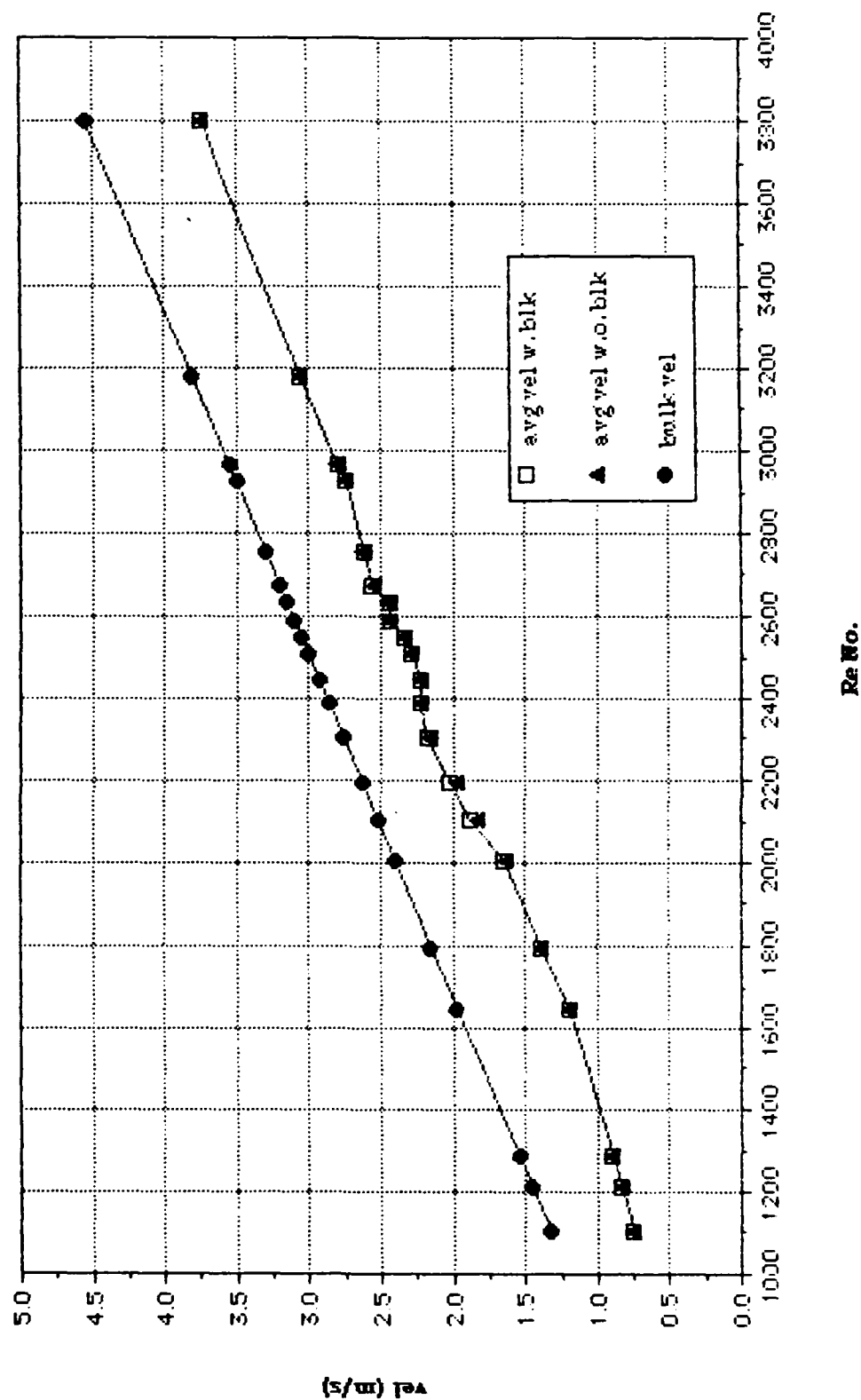


Figure 6.

# Reynolds Number Surveys With and Without 2 Hz Imposed Unsteadiness

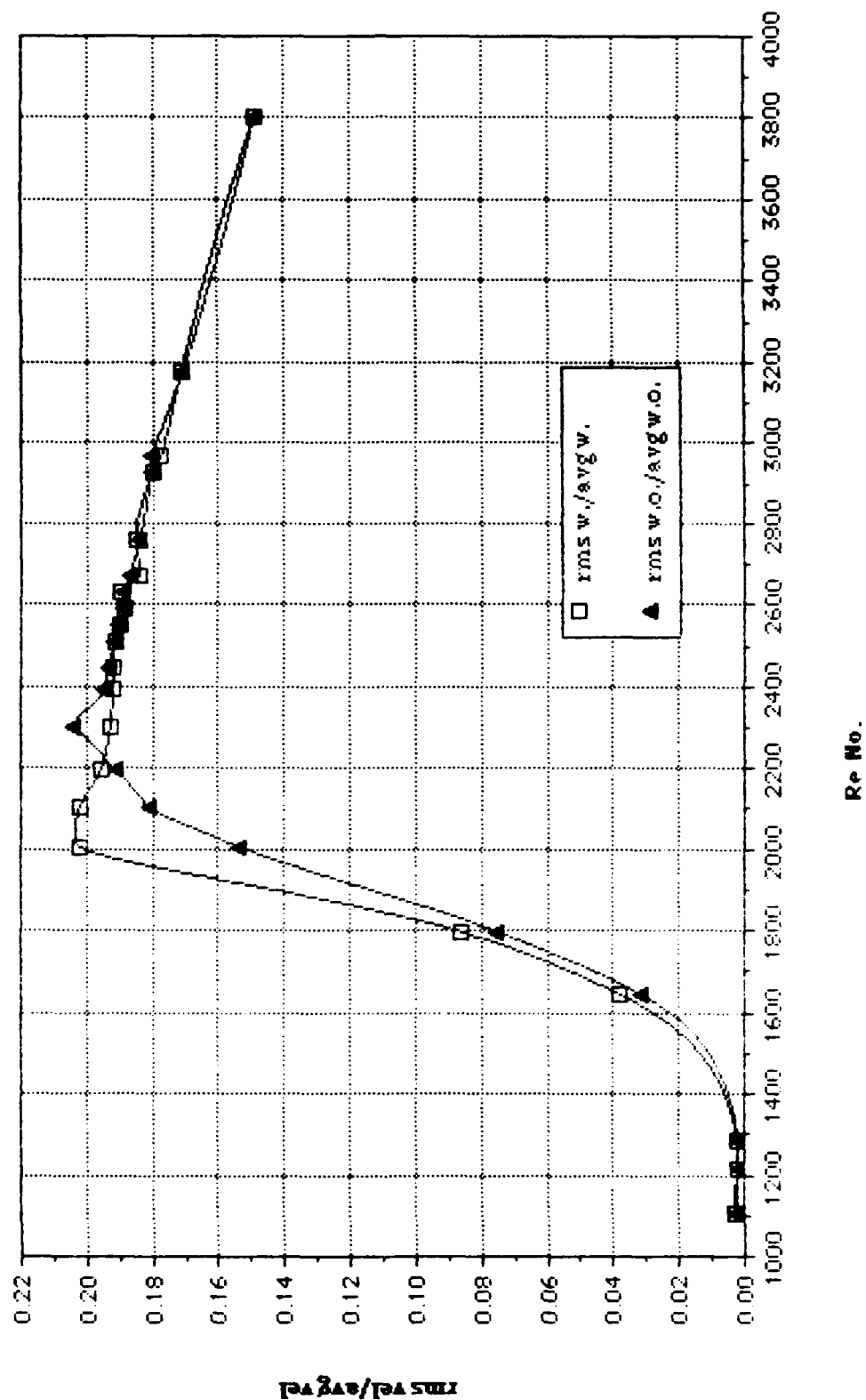


Figure 7.

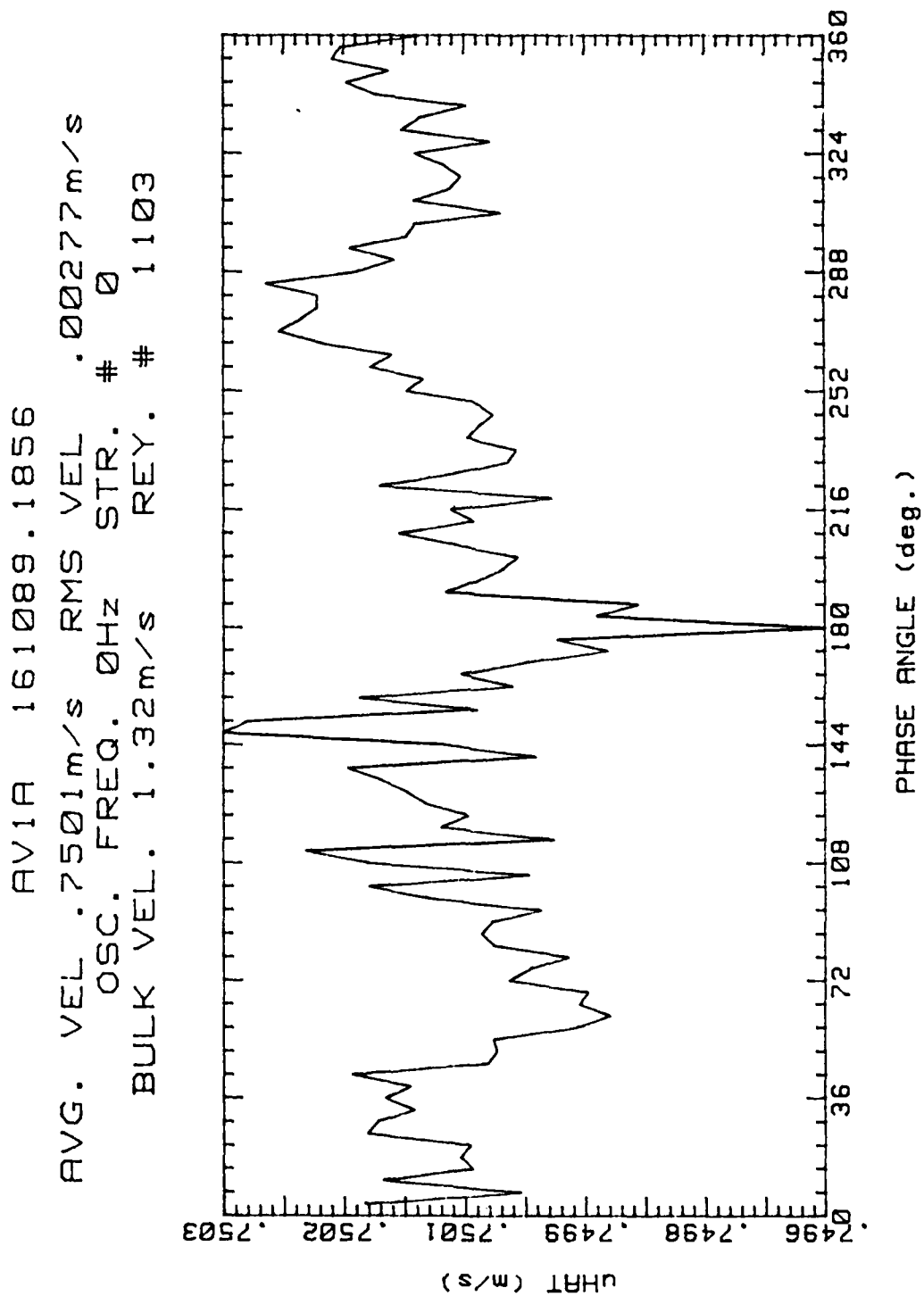


Figure 8.

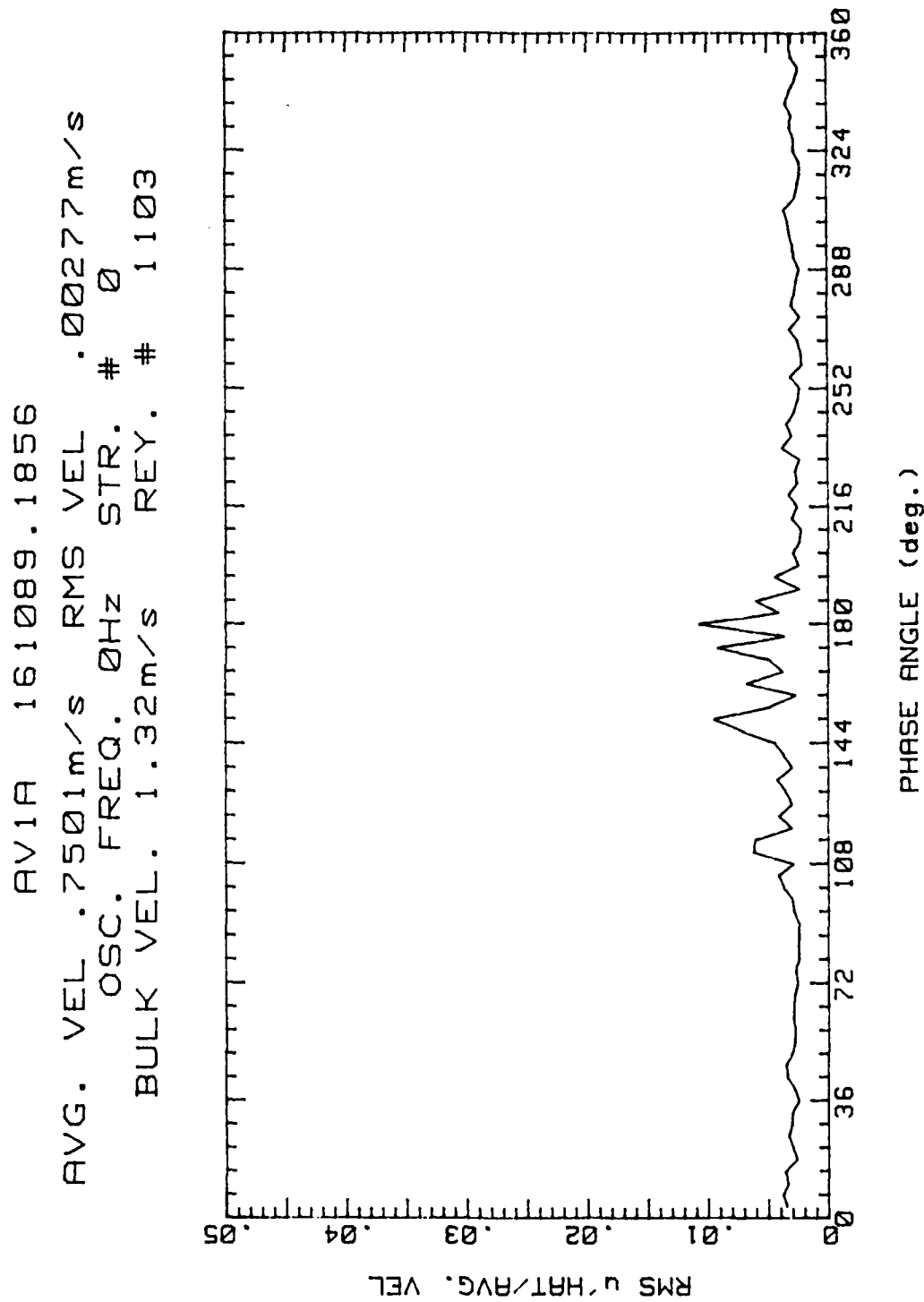


Figure 9.

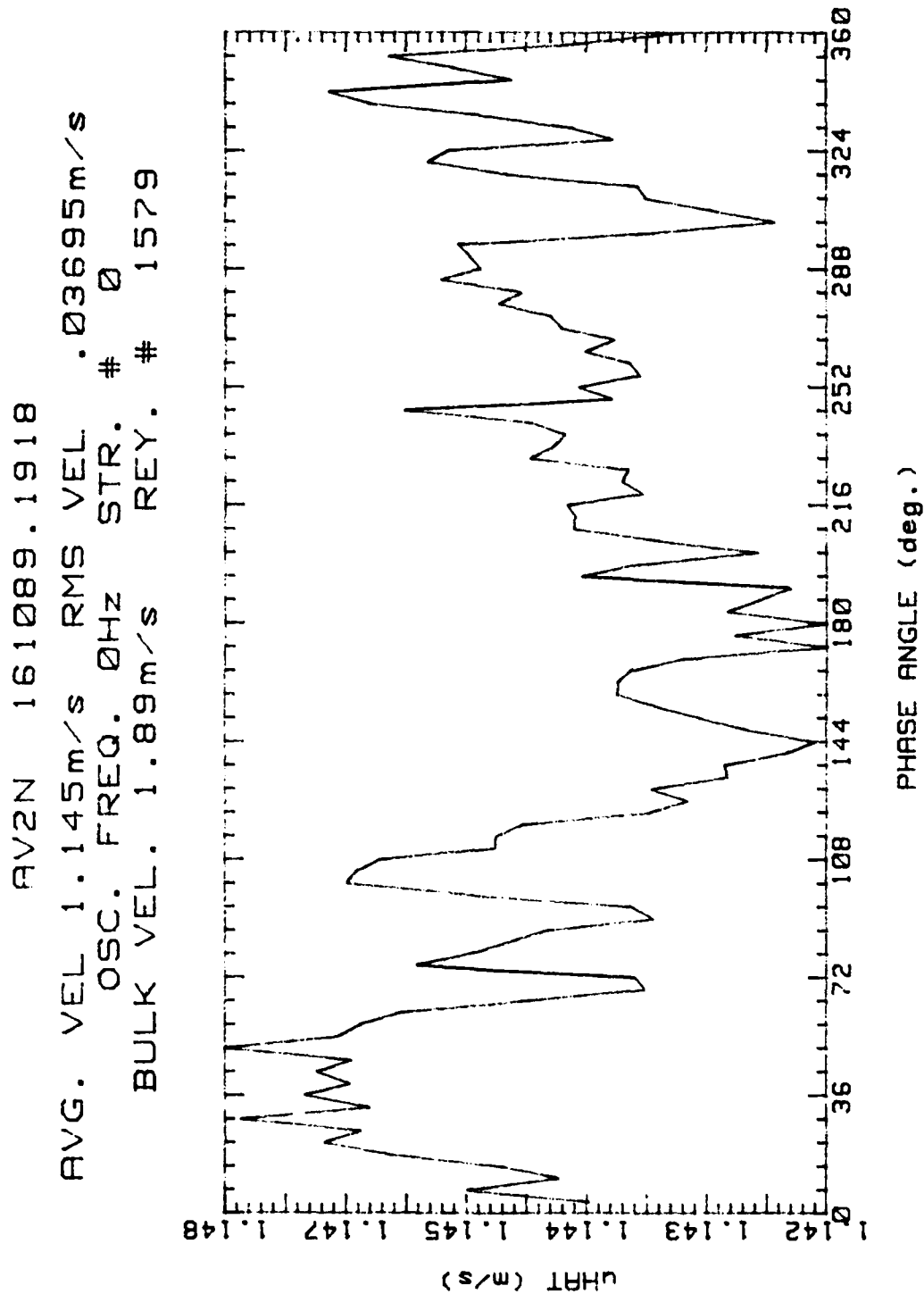


Figure 10.

AV2N 161089.1918  
 AVG. VEL 1.145m/s RMS VEL .03695m/s  
 OSC. FREQ. 0Hz STR. # 0  
 BULK VEL. 1.89m/s REY. # 1579

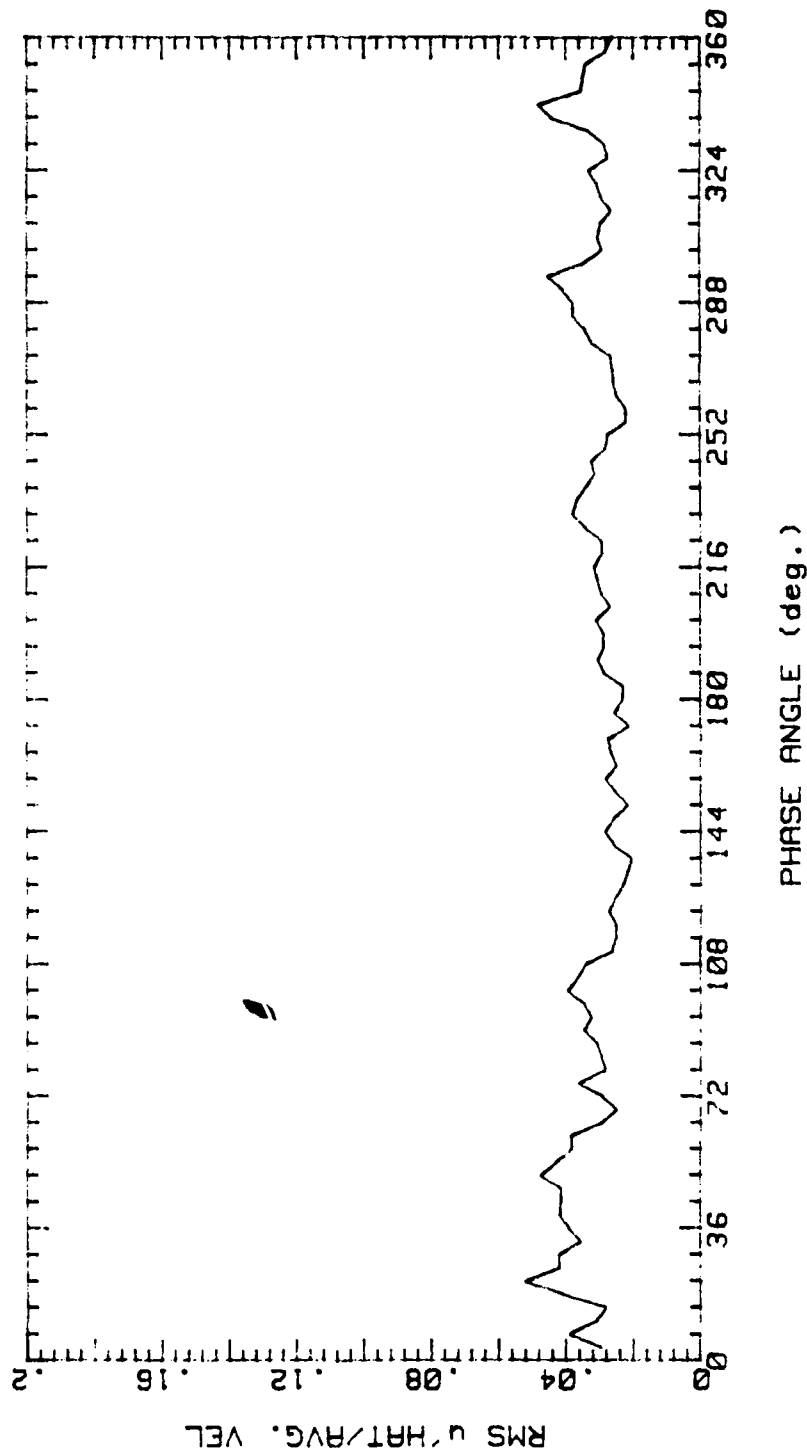


Figure 11.



AV3N 161089.1956  
 AVG. VEL 1.713m/s RMS VEL .2472m/s  
 OSC. FREQ. 0Hz STR. # 0  
 BULK VEL. 2.4m/s REY. # 2005

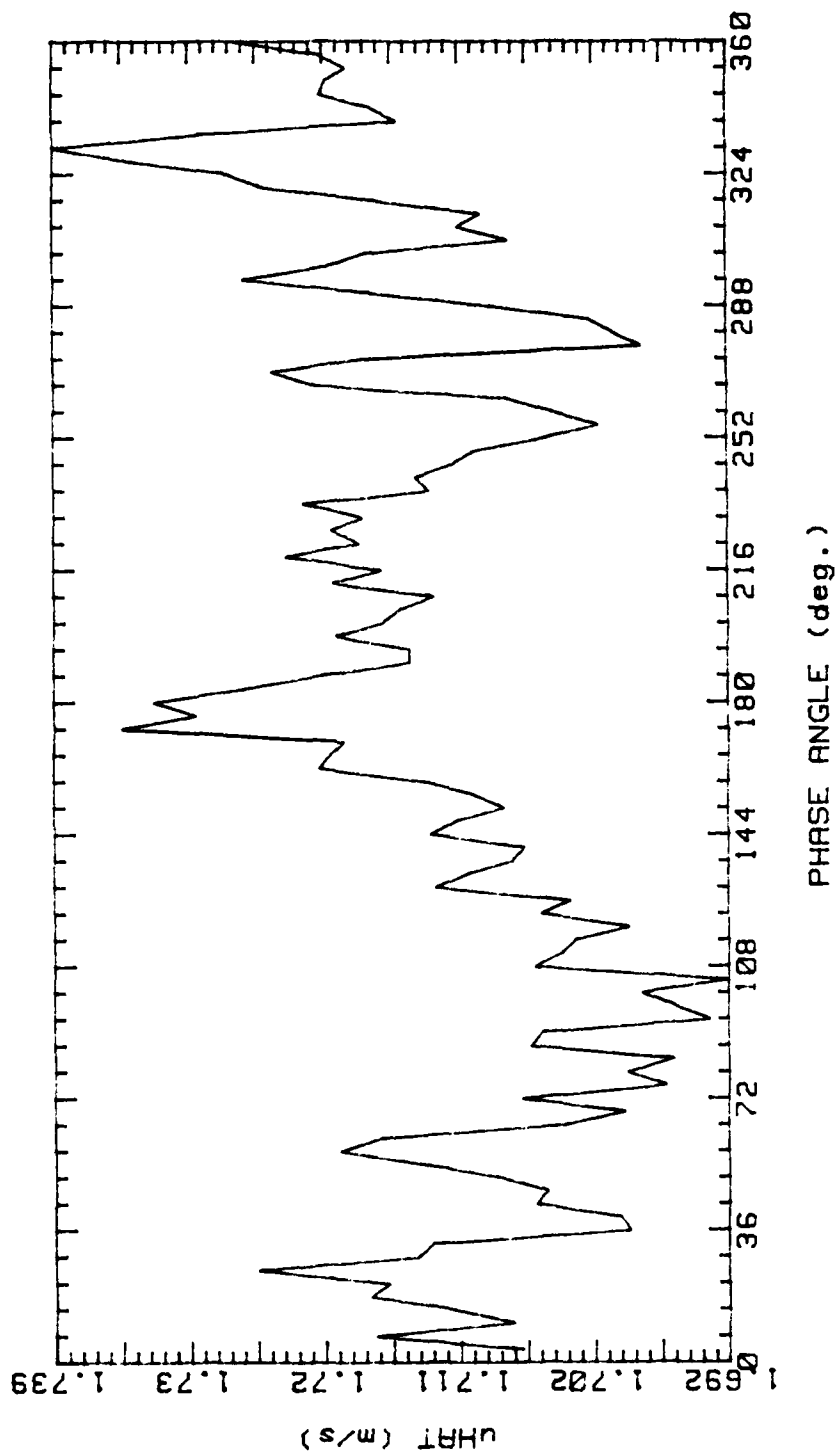


Figure 12.

AV3N 161089.1956

AVG. VEL 1.713m/s RMS VEL .2472m/s  
OSC. FREQ. 0Hz STR. # 0  
BULK VEL. 2.4m/s REY. # 2005

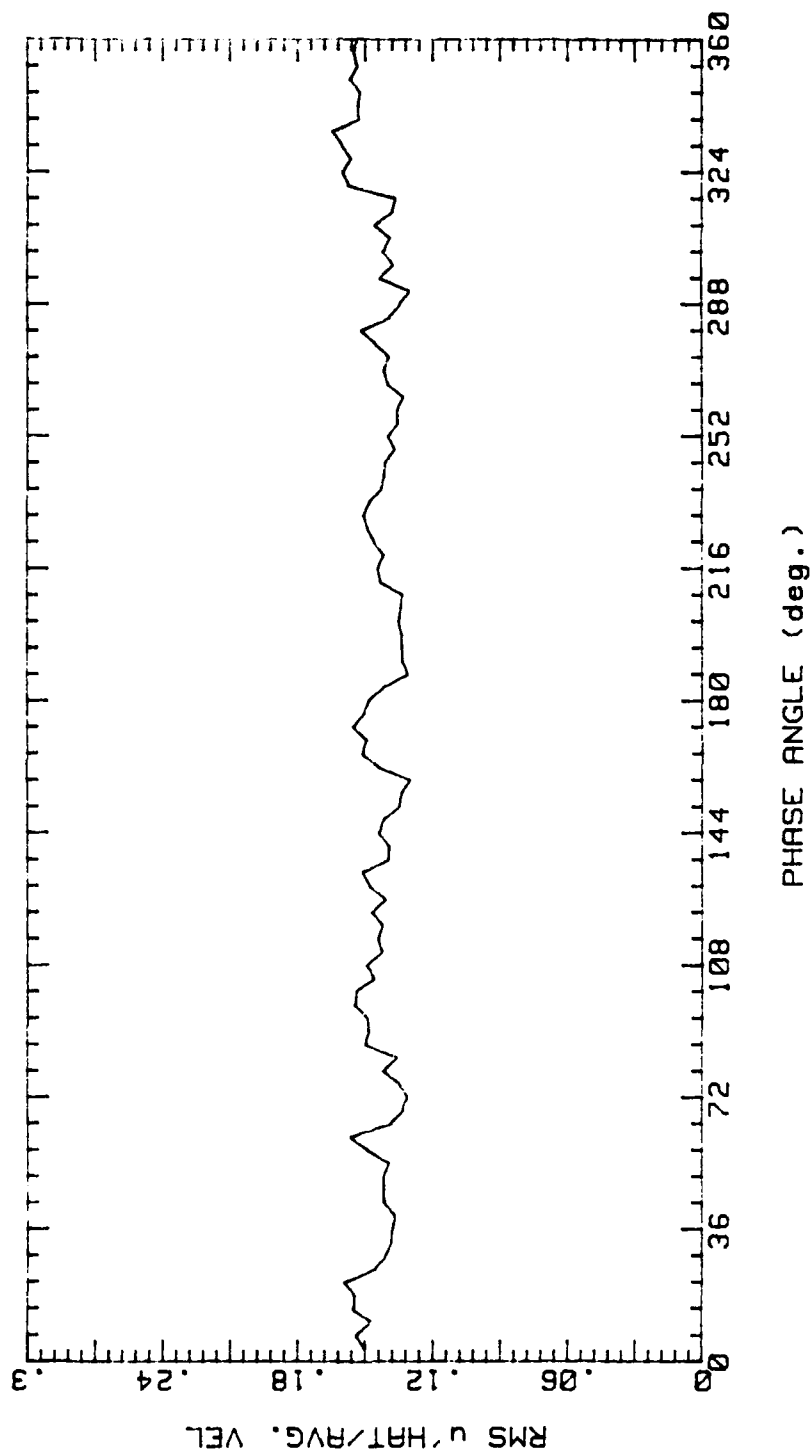


Figure 13.

AV4N 161089.2057  
 AVG. VEL 2.318m/s RMS VEL .4387m/s  
 OSC. FREQ. 0Hz STR. # 0  
 BULK VEL. 3.05m/s REY. # 2548

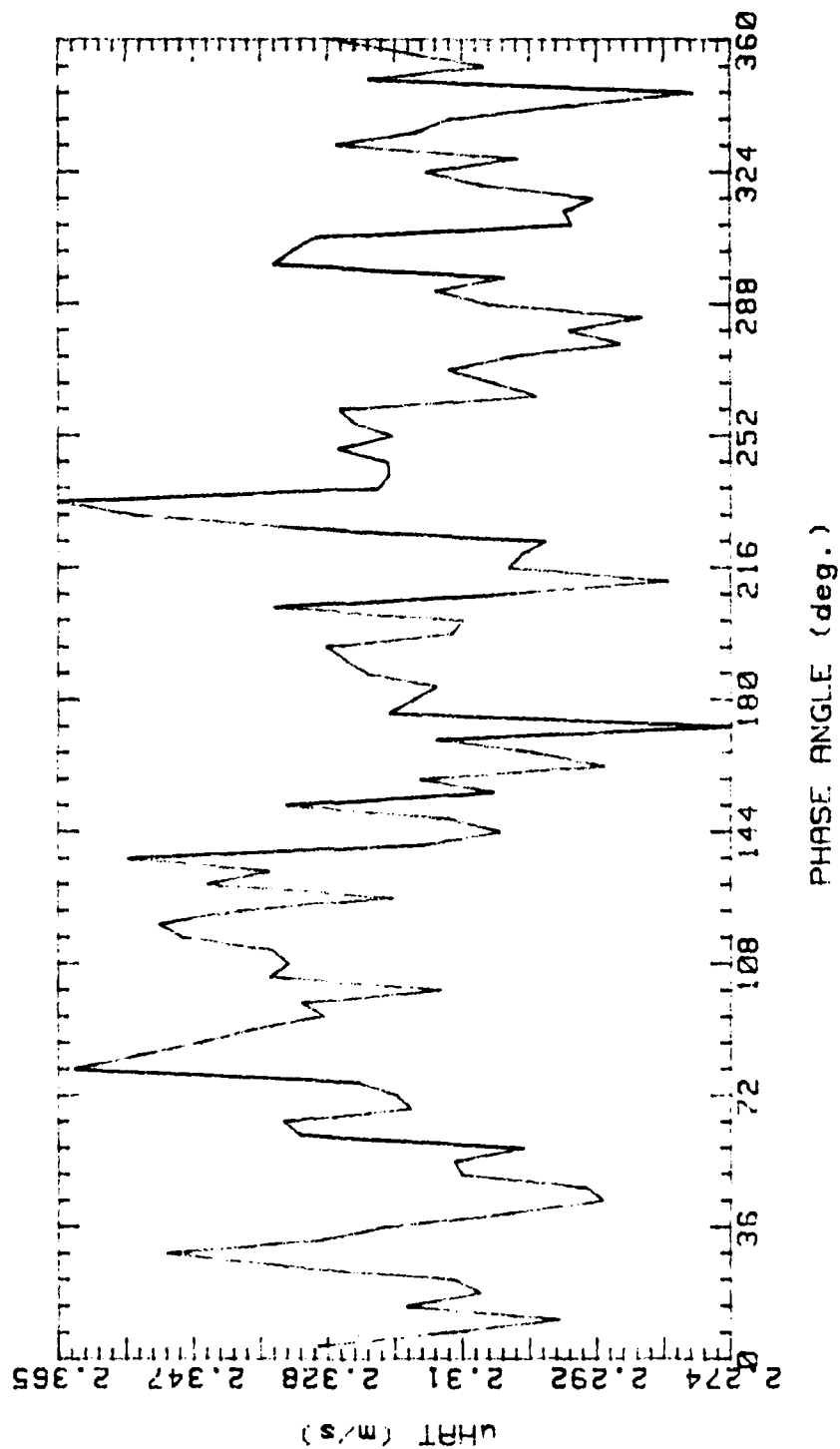


Figure 14.

AV4N 161089.2057  
 AVG. VEL 2.318m/s RMS VEL .4387m/s  
 OSC. FREQ. 0Hz STR. # 0  
 BULK VEL. 3.05m/s REY. # 2548

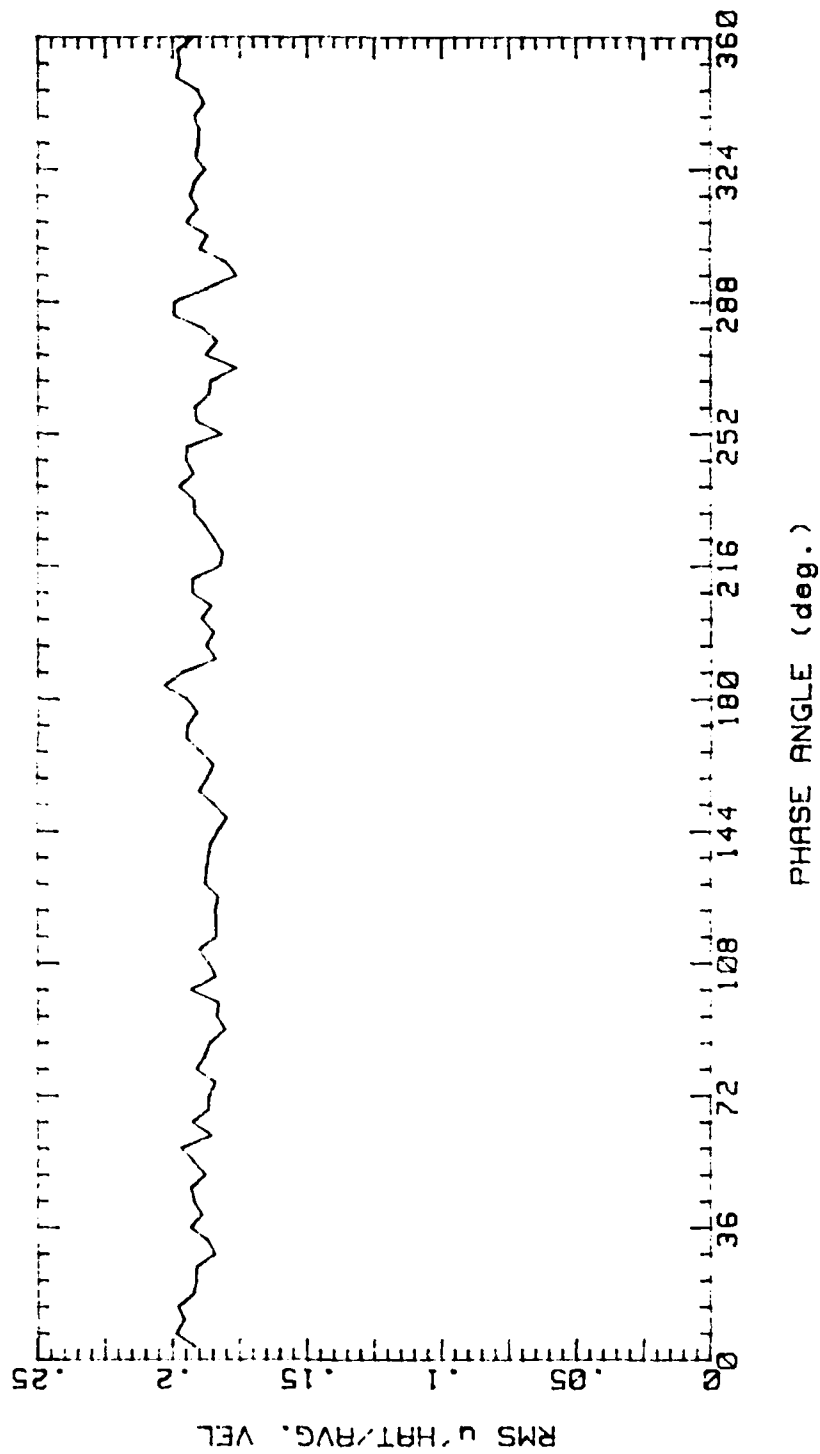


Figure 15.

AV5N 181089.1845  
 AVG. VEL 3.702m/s RMS VEL .5745m/s  
 OSC. FREQ. 0Hz STR. # 0  
 BULK VEL. 4.38m/s REY. # 3660

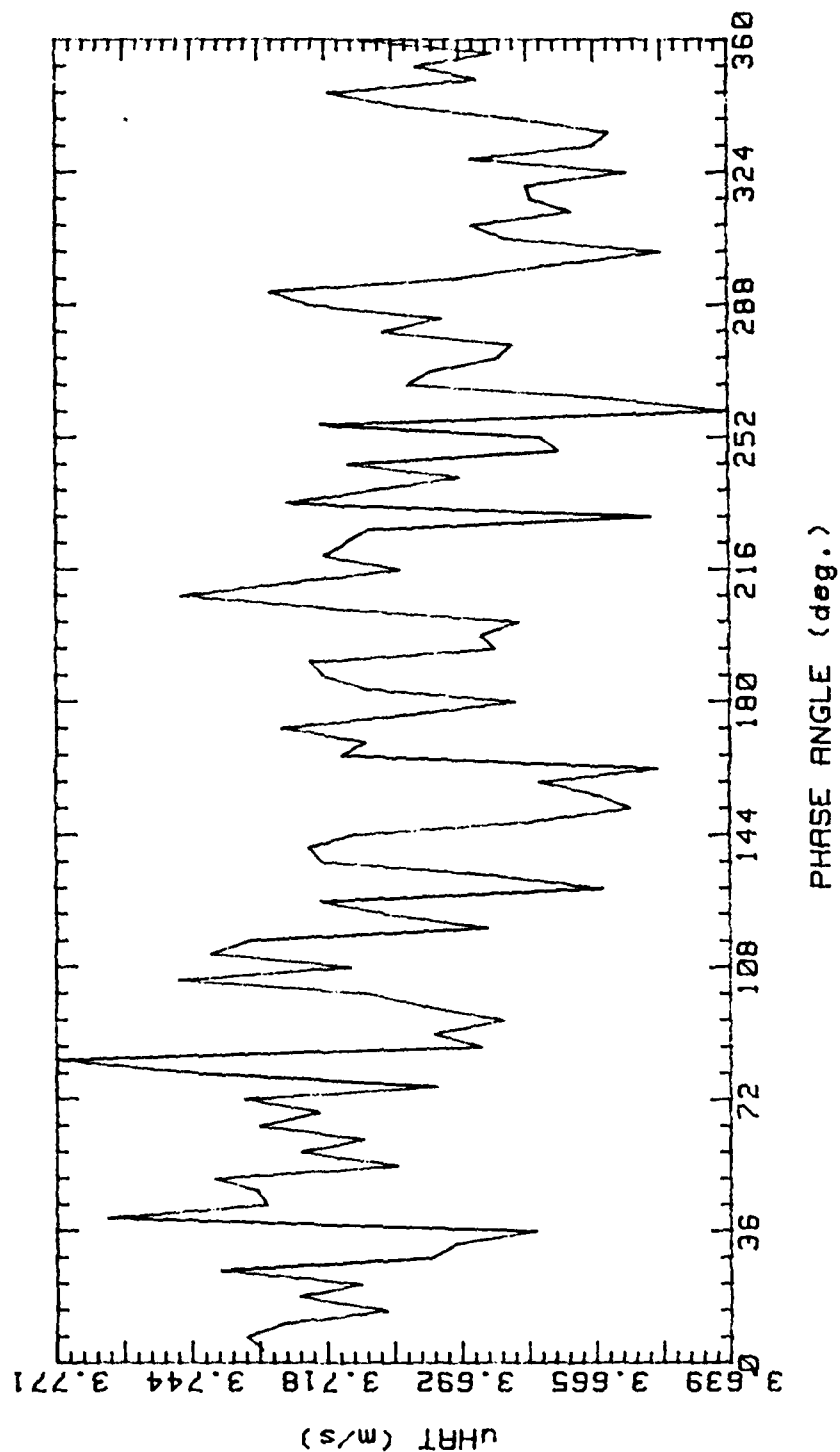


Figure 16.

AV5N 181089.1845  
 AVG. VEL 3.702m/s RMS VEL .5745m/s  
 OSC. FREQ. 0Hz STR. # 0  
 BULK VEL. 4.38m/s REY. # 3660

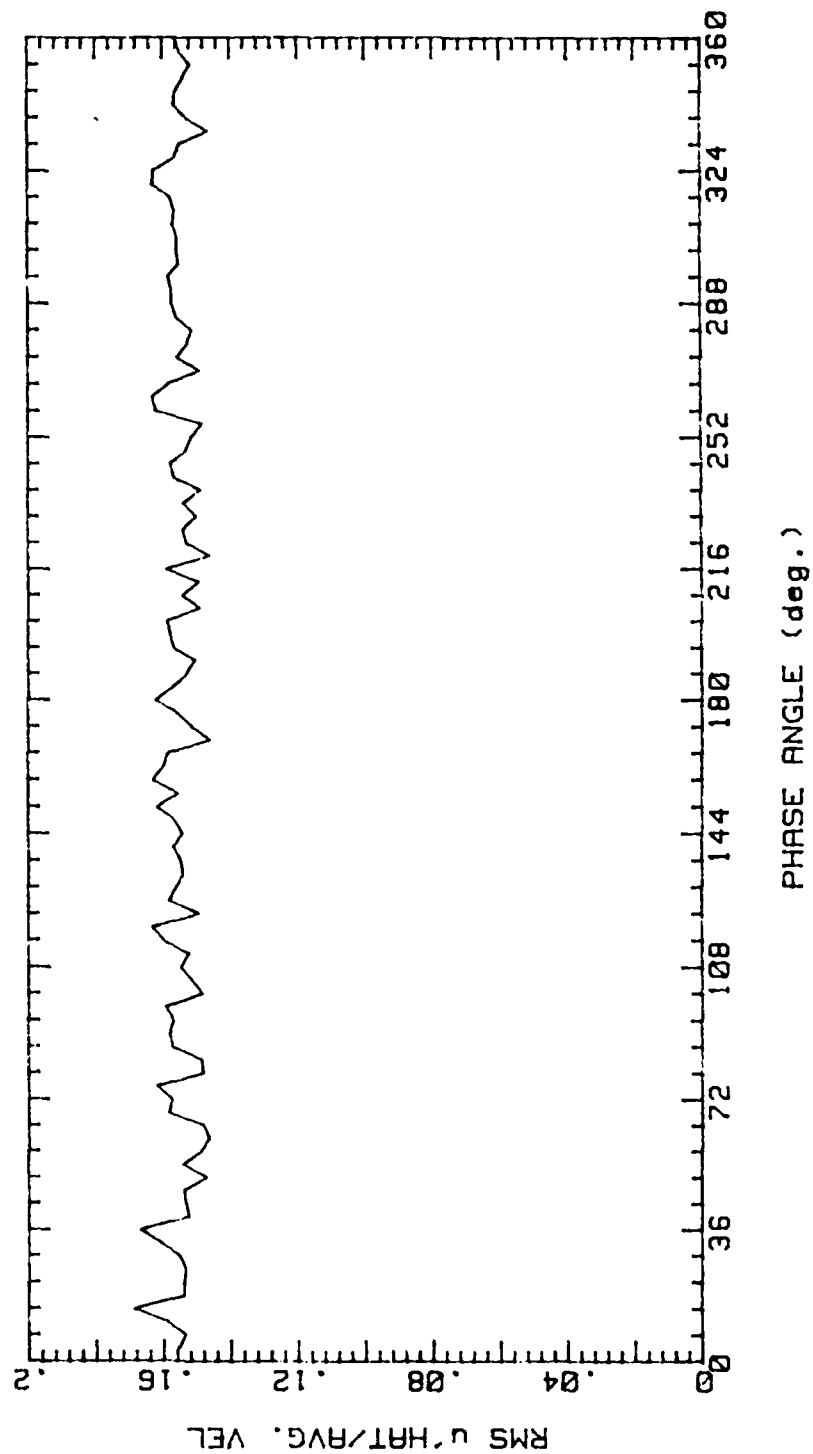


Figure 17.

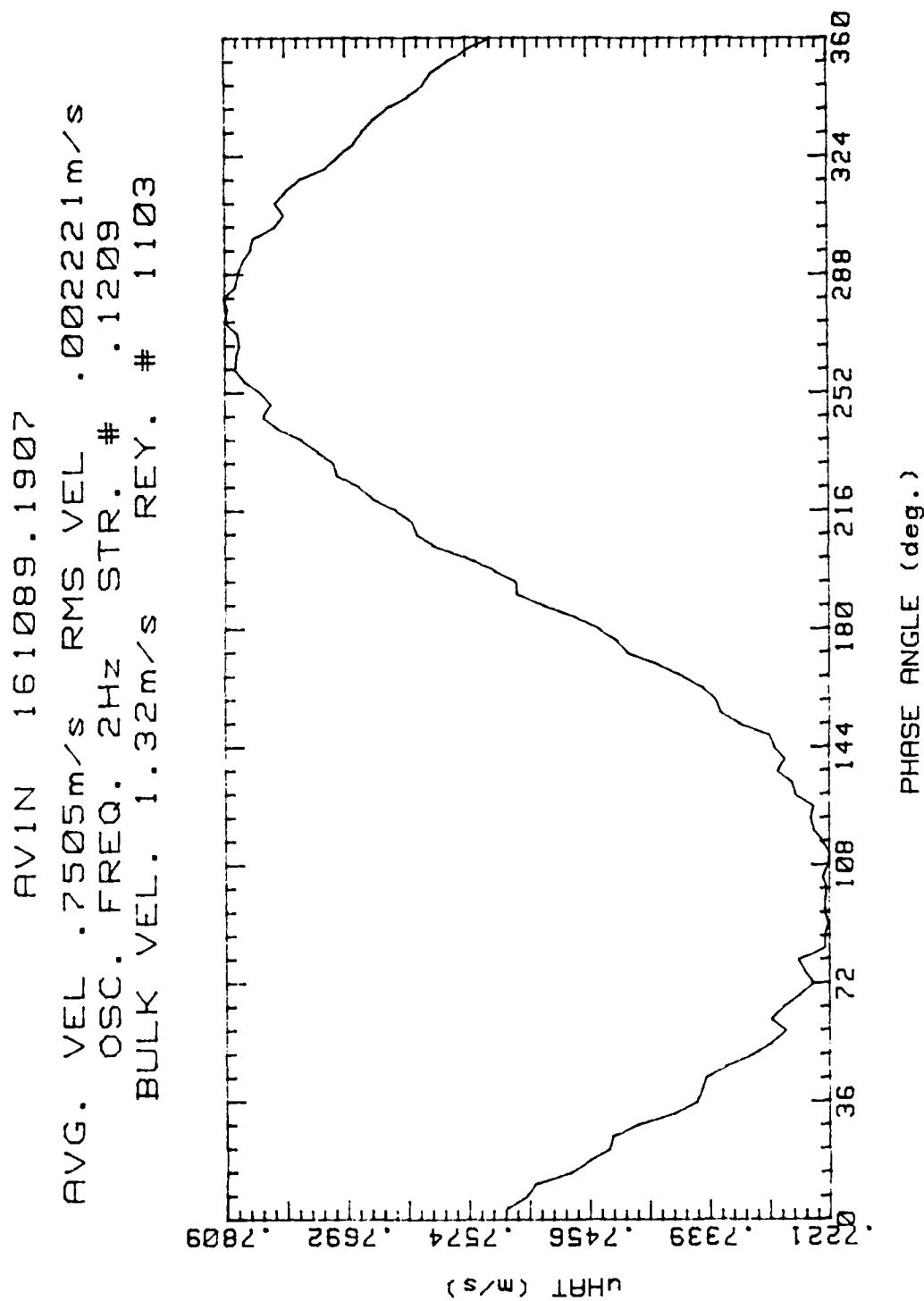


Figure 18.

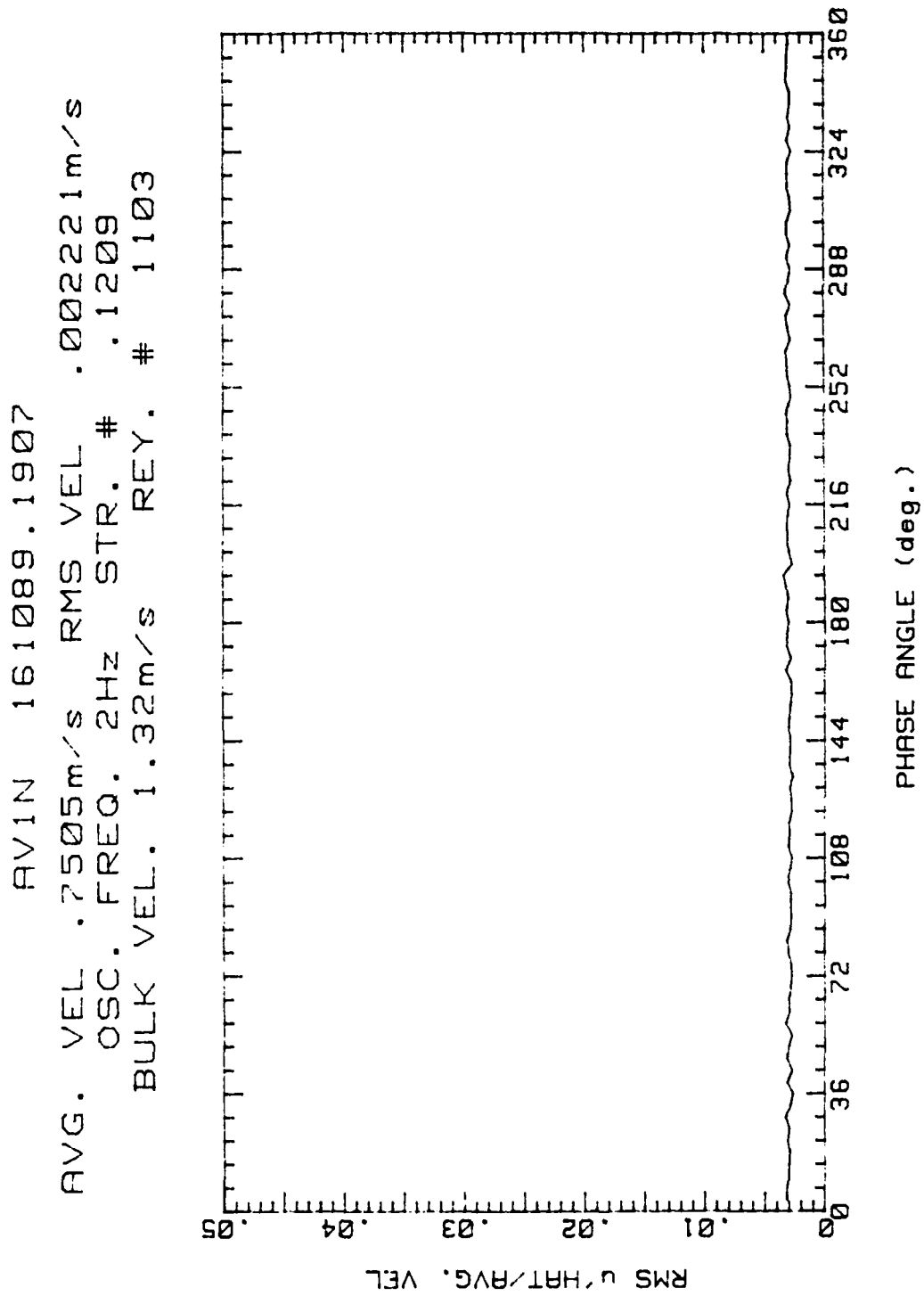


Figure 19.



MULTIRUN (AV2, 1 RUNS) PH. AVE., 161089  
 AVG. VEL 1.144m/s RMS VEL .04558m/s  
 OSC. FREQ. 2Hz STR. # .08444  
 BULK VEL. 1.89m/s REY. # 1579

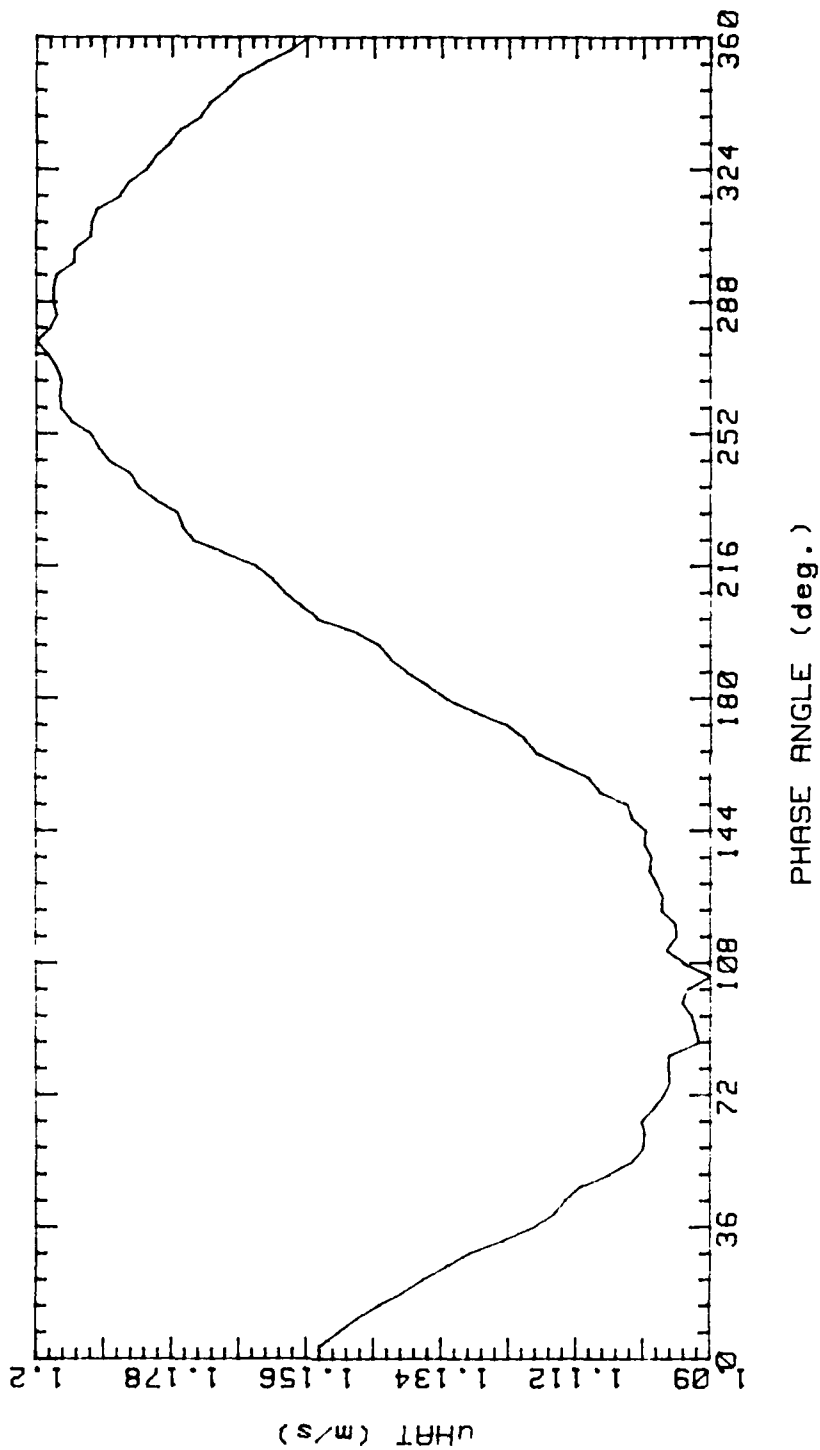


Figure 20.

MULTIRUN (AV2, 1 RUNS) PH. AVE., 161089  
 AVG. VEL 1.144m/s RMS VEL .04558m/s  
 OSC. FREQ. 2Hz STR. # .08444  
 BULK VEL. 1.89m/s REY. # 1579

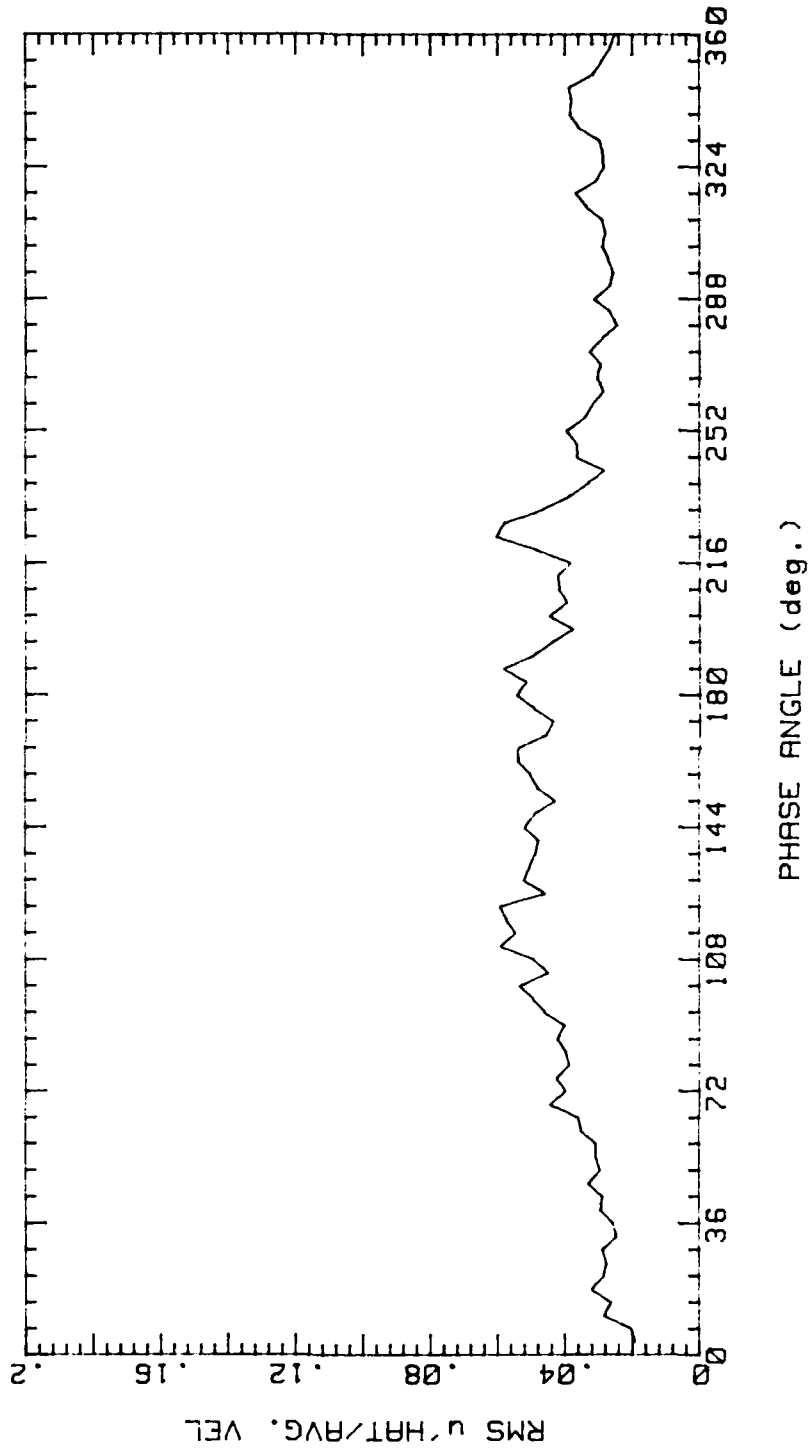


Figure 21.

MULTIRUN (AV2, 4 RUNS) PH. AVE., 161089  
 AVG. VEL 1.145m/s RMS VEL .04265m/s  
 OSC. FREQ. 2Hz STR. # .08444  
 BULK VEL. 1.89m/s REY. # 1579

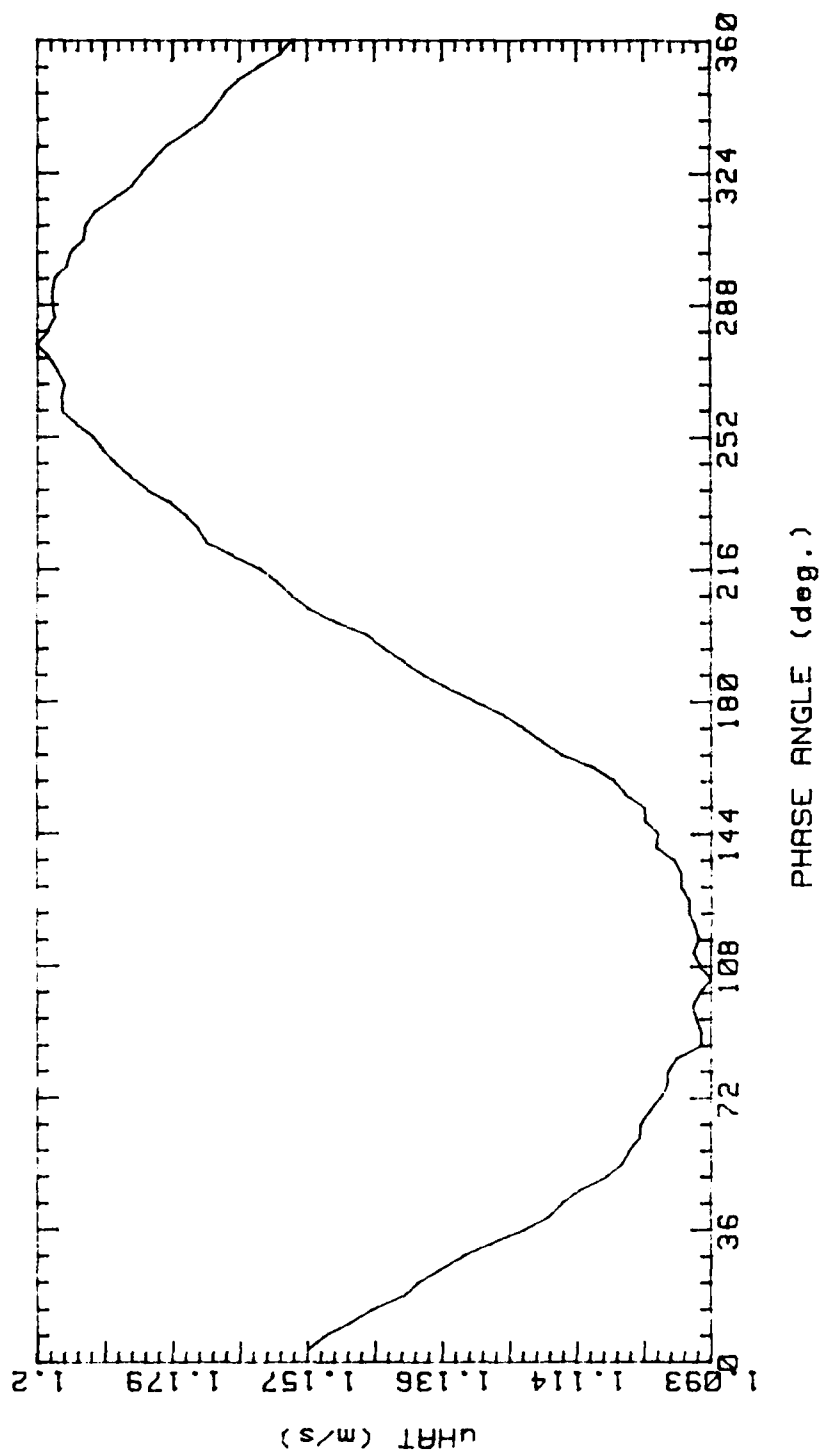


Figure 22.

MULTIRUN (AV2, 4 RUNS) PH. AVE., 161089  
 AVG. VEL 1.145m/s RMS VEL .04265m/s  
 OSC. FREQ. 2Hz STR. # .08444  
 BULK VEL. 1.89m/s REY. # 1579

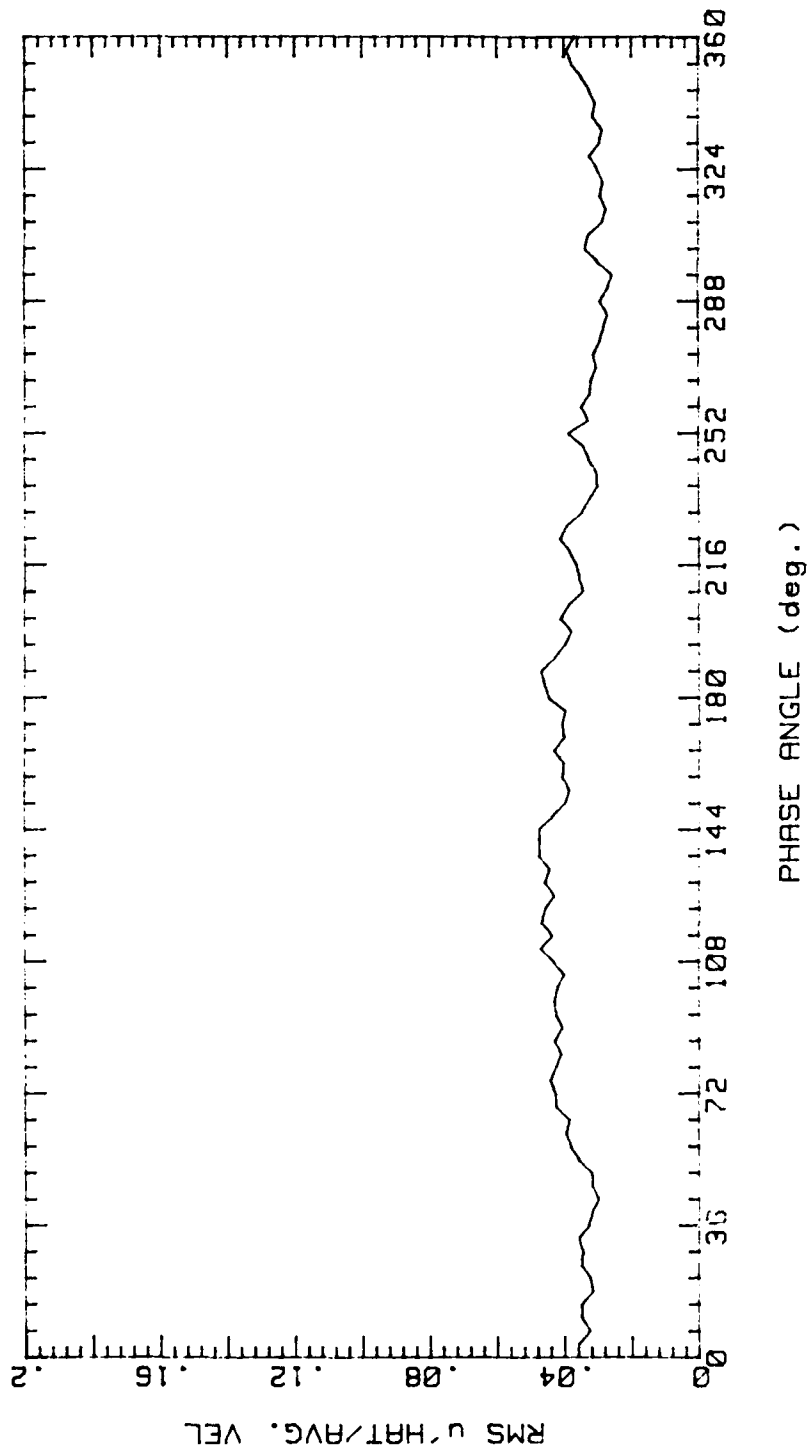


Figure 23.

MULTIRUN (AV3, 1 RUNS) PH. AVE., 161089  
 AVG. VEL 1.719m/s RMS VEL .3271m/s  
 OSC. FREQ. 2Hz STR. # .0665  
 BULK VEL. 2.4m/s REY. # 2005

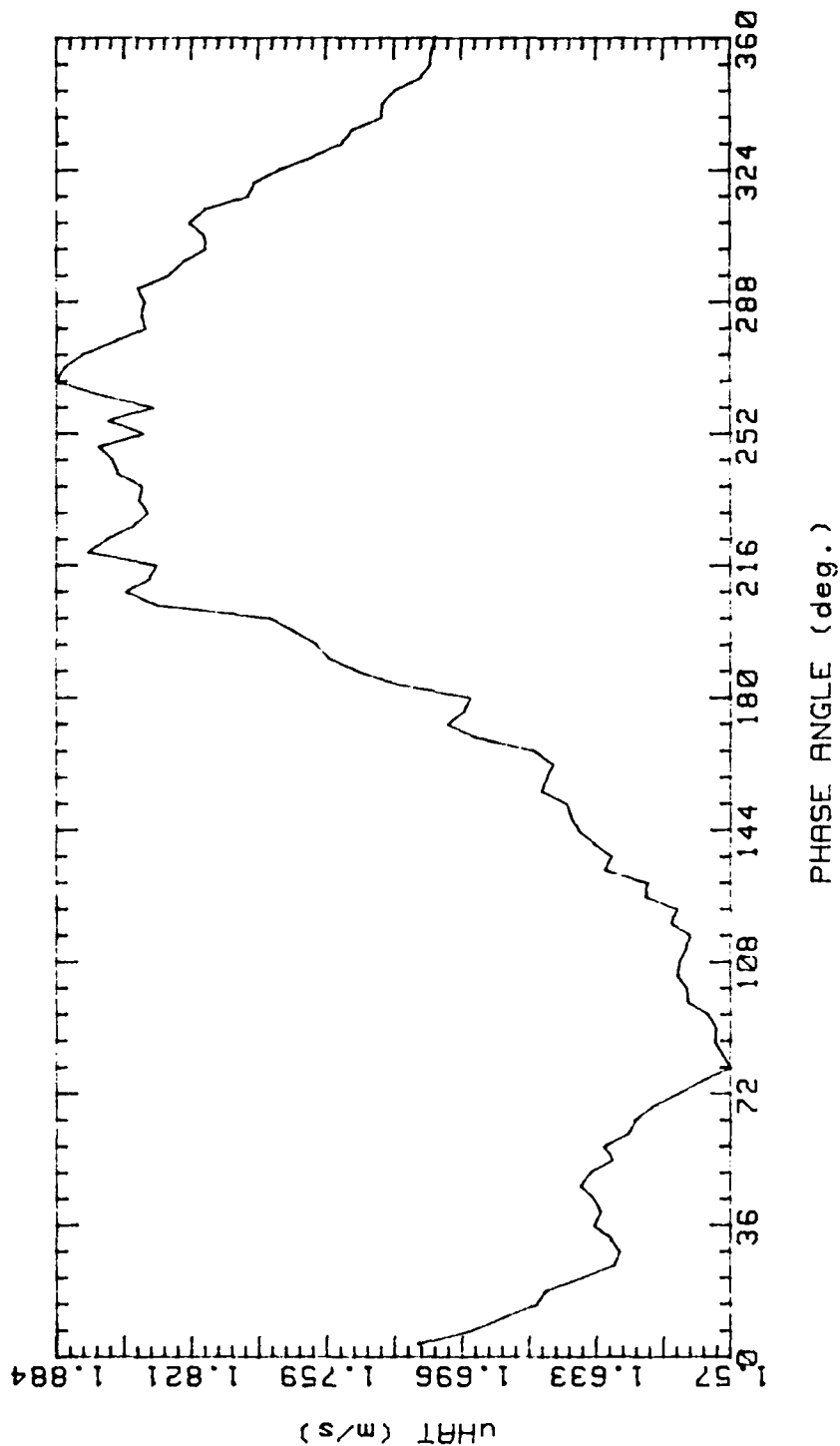


Figure 24.

MULTIRUN (AV3, 1 RUNS) PH. AVE., 161089  
 AVG. VEL 1.719m/s RMS VEL .3271m/s  
 OSC. FREQ. 2Hz STR. # .0665  
 BULK VEL. 2.4m/s REY. # 2005

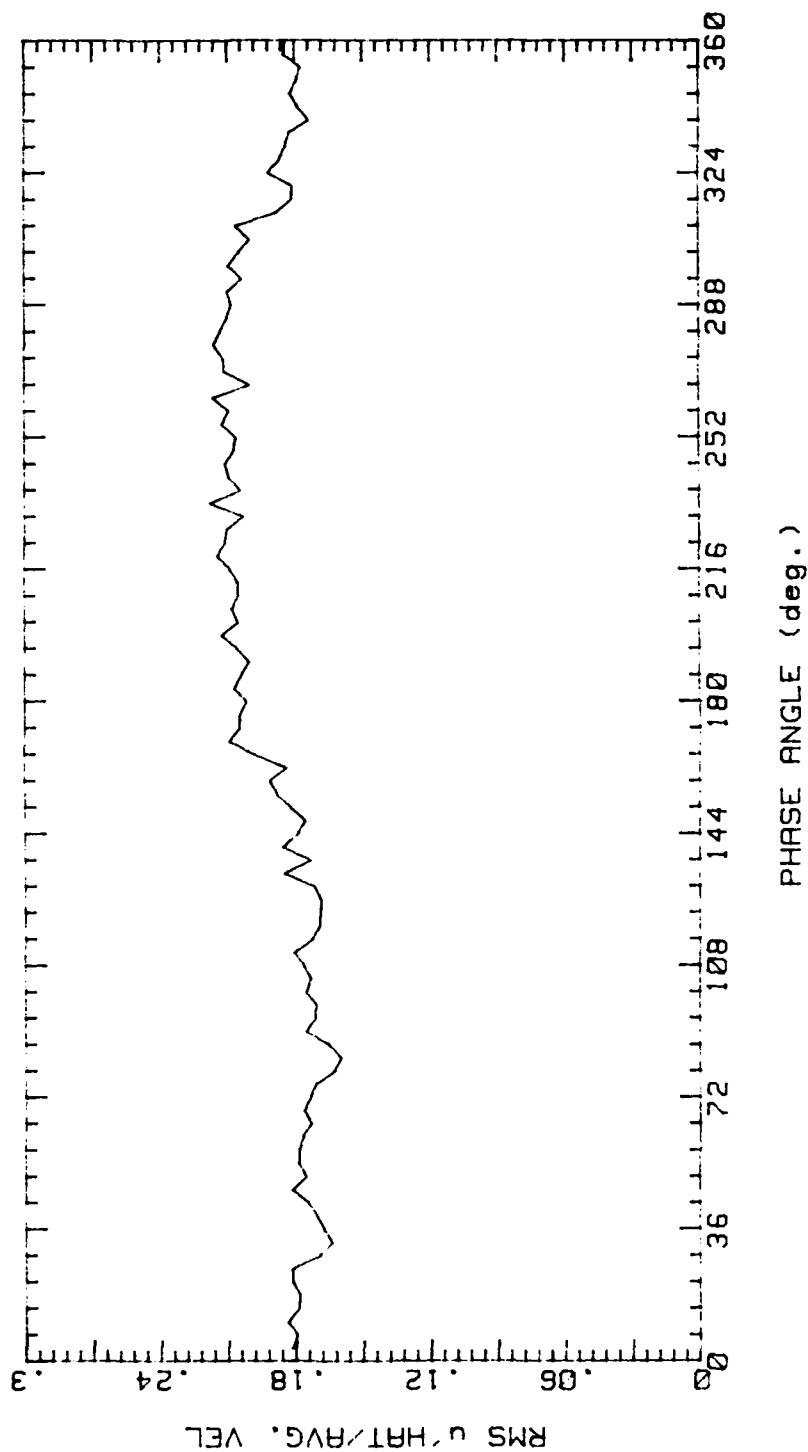


Figure 25.

MULTIRUN (AV3, 8 RUNS) PH. AVE., 161089

AVG. VEL 1.725m/s RMS VEL .337m/s

OSC. FREQ. 2Hz STR. # .0665

BULK VEL. 2.4m/s REY. # 2005

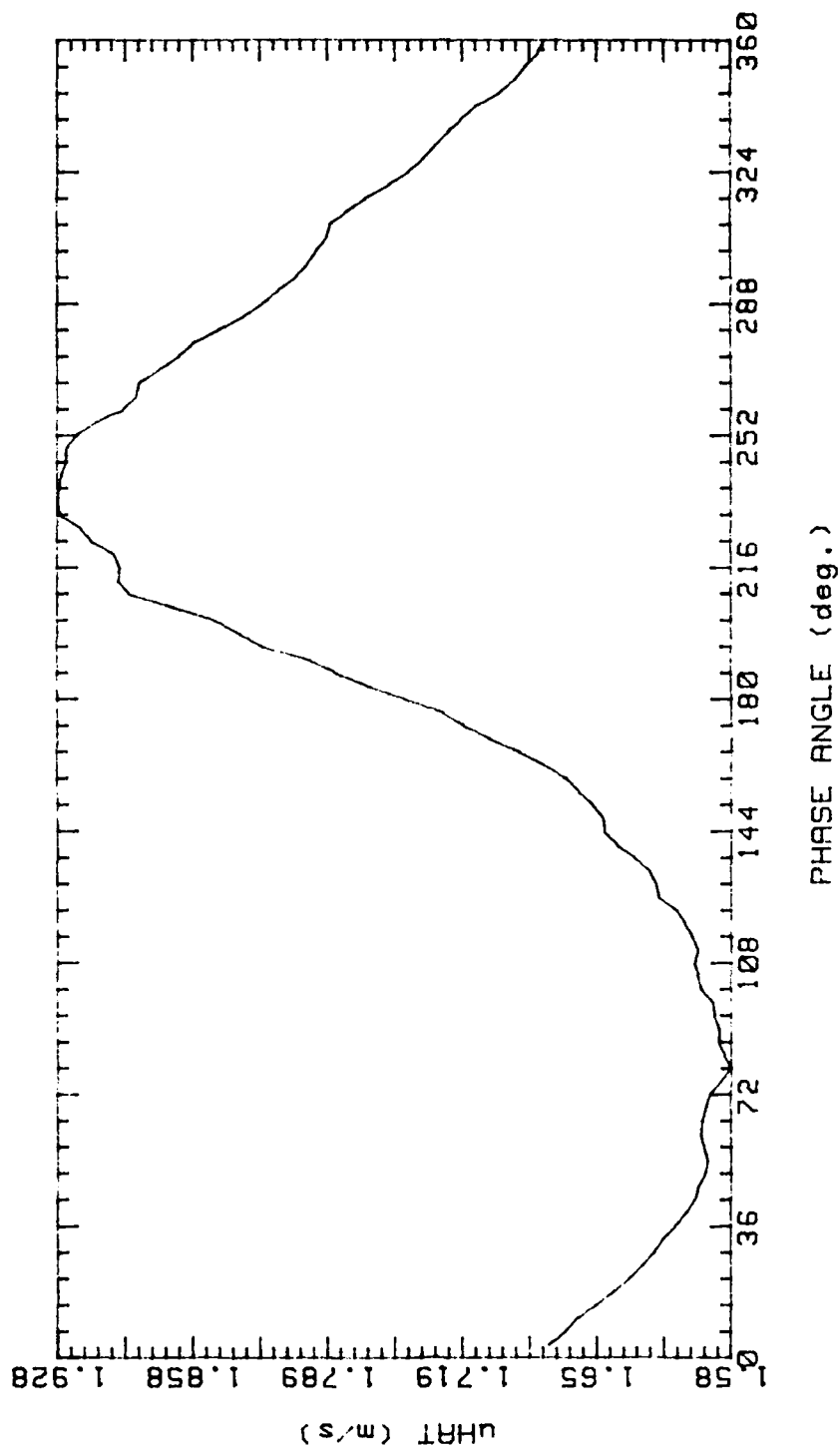


Figure 26.

MULTIRUN (AV3, 8 RUNS) PH. AVE., 161089  
 AVG. VEL 1.725m/s RMS VEL .337m/s  
 OSC. FREQ. 2Hz STR. # .0665  
 BULK VEL. 2.4m/s REY. # 2005

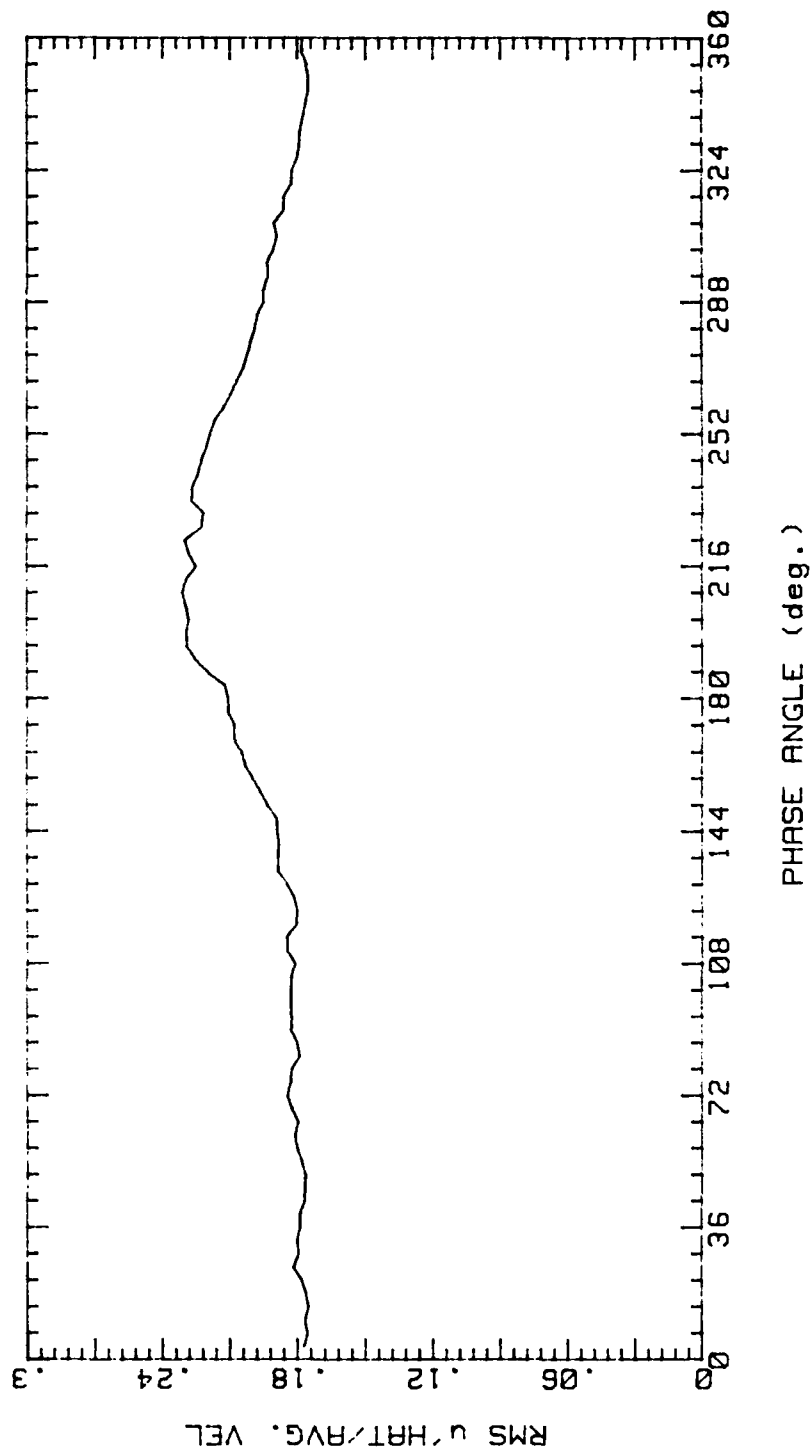


Figure 27.



MULTIRUN (AV4, 1 RUNS) PH. AVE., 161089  
 AVG. VEL 2.316m/s RMS VEL .438m/s  
 OSC. FREQ. 2Hz STR. # .05232  
 BULK VEL. 3.05m/s REY. # 2548

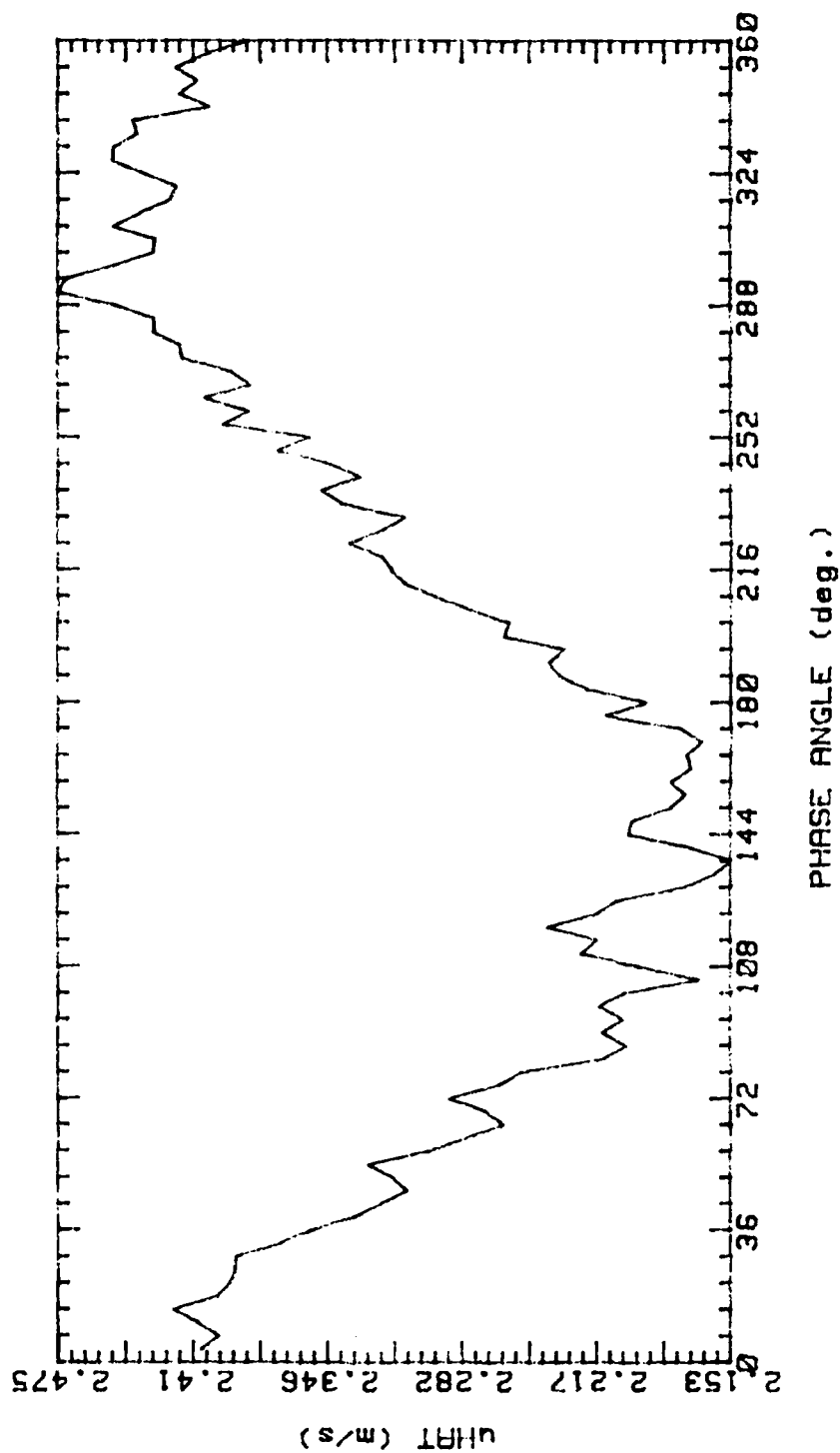


Figure 28.

MULTIRUN (AV4, 1 RUNS) PH. AVE., 161089  
 AVG. VEL 2.316m/s RMS VEL .438m/s  
 OSC. FREQ. 2Hz STR. # .05232  
 BULK VEL. 3.05m/s REY. # 2548

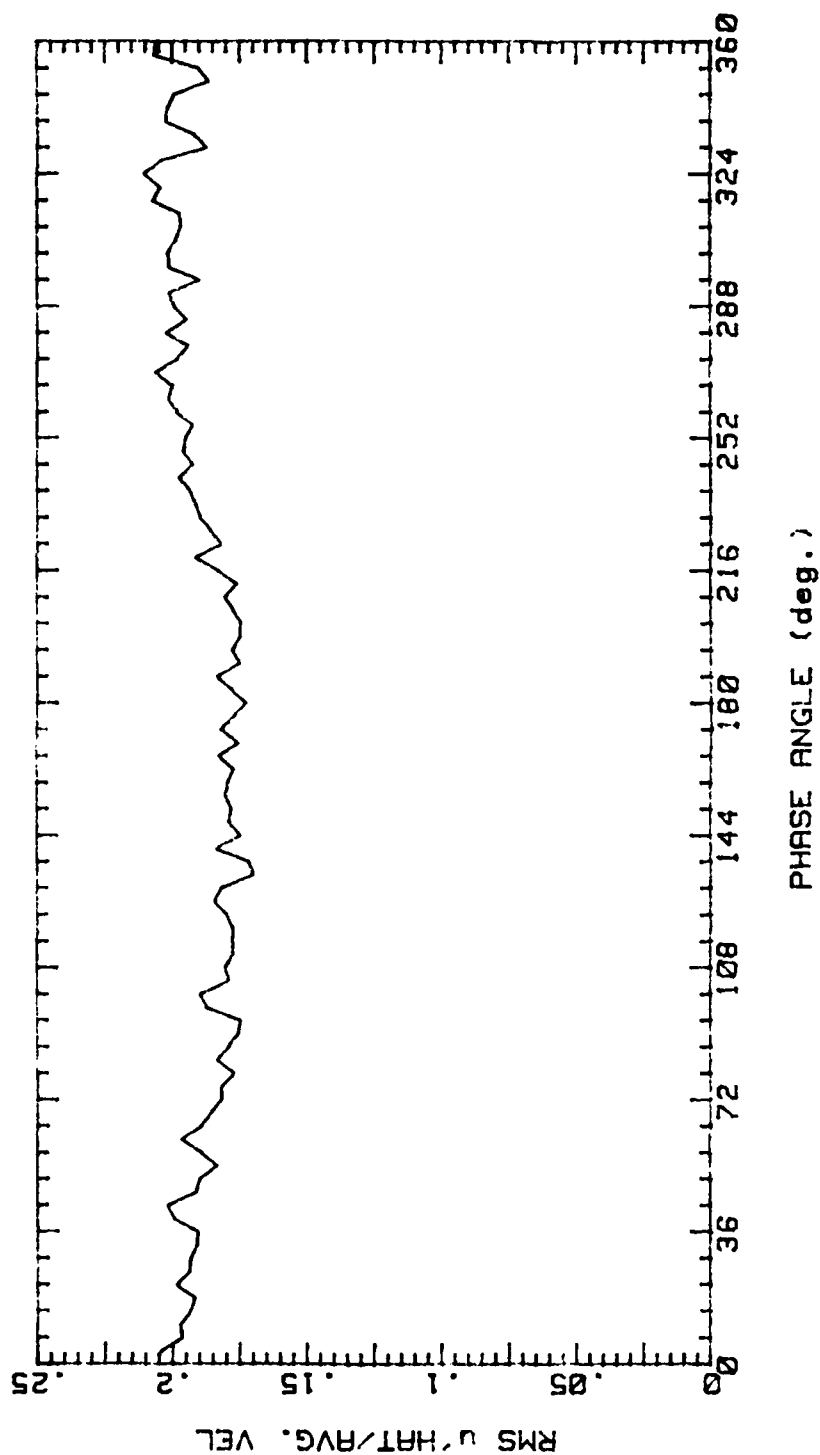


Figure 29.

MULTIRUN (AV4, 8 RUNS) PH. AVE., 161089

AVG. VEL 2.32m/s RMS VEL .4355m/s

OSC. FREQ. 2Hz STR. # .05232

BULK VEL. 3.05m/s REY. # 2548

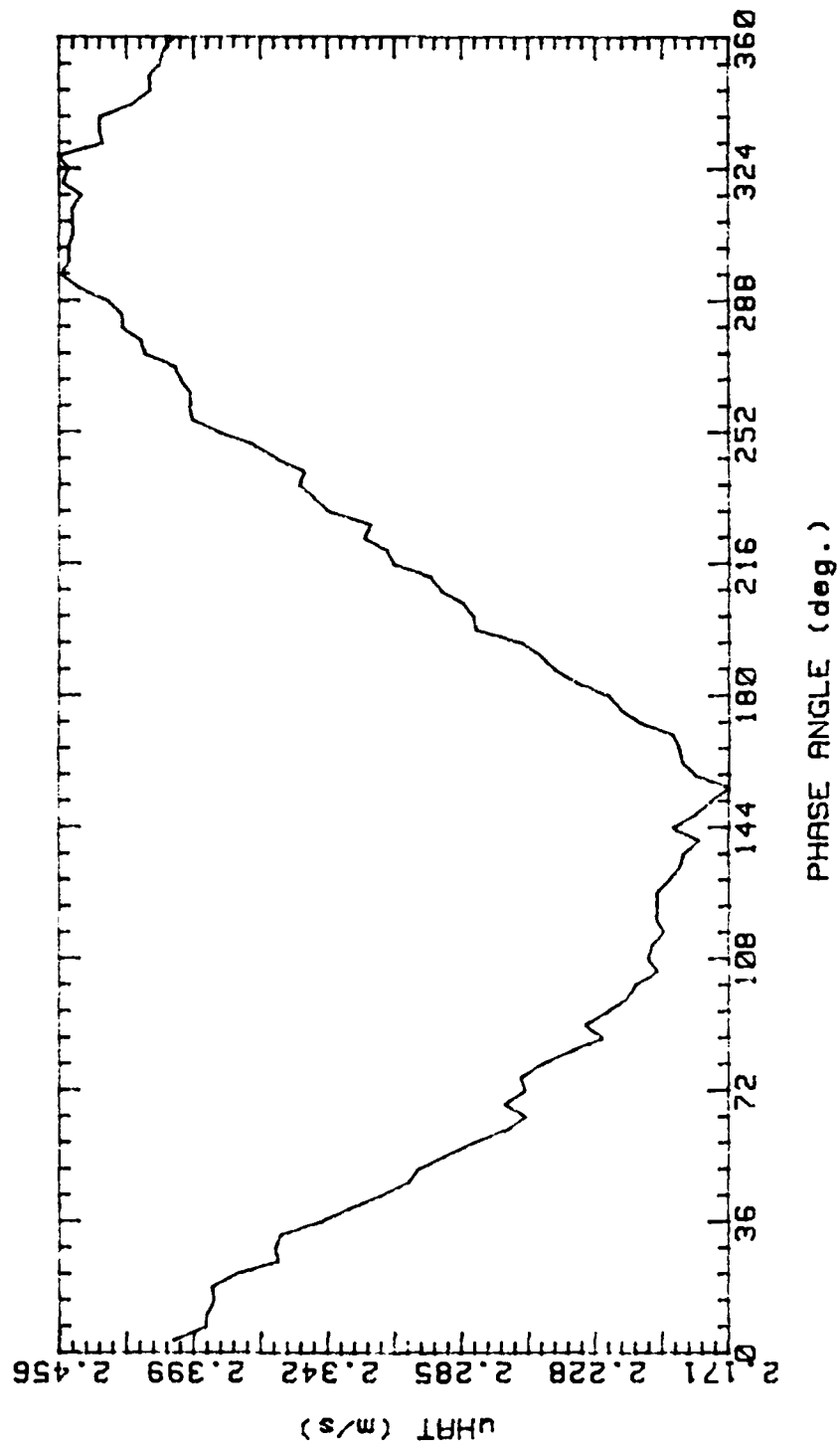


Figure 30.

MULTIRUN (AV4, 8 RUNS) PH. AVE., 161089

AVG. VEL 2.32m/s RMS VEL .4355m/s  
OSC. FREQ. 2Hz STR. # .05232  
BULK VEL. 3.05m/s REY. # 2548

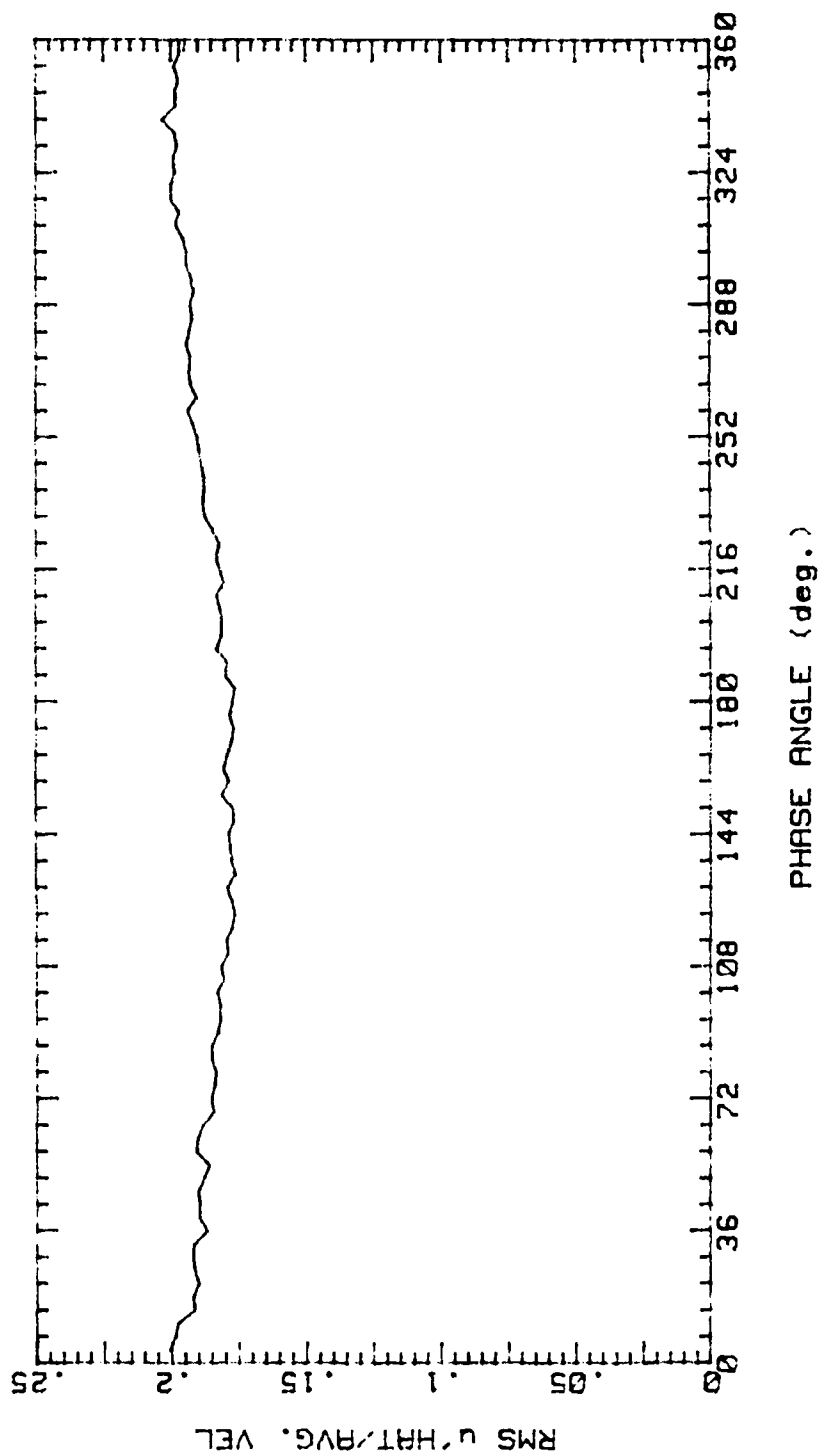


Figure 31.

MULTIRUN (AV5, 1 RUNS) PH. AVE., 181089  
 AVG. VEL 3.705m/s RMS VEL .5718m/s  
 OSC. FREQ. 2Hz STR. # .0399  
 BULK VEL. 4.38m/s REY. # 3660

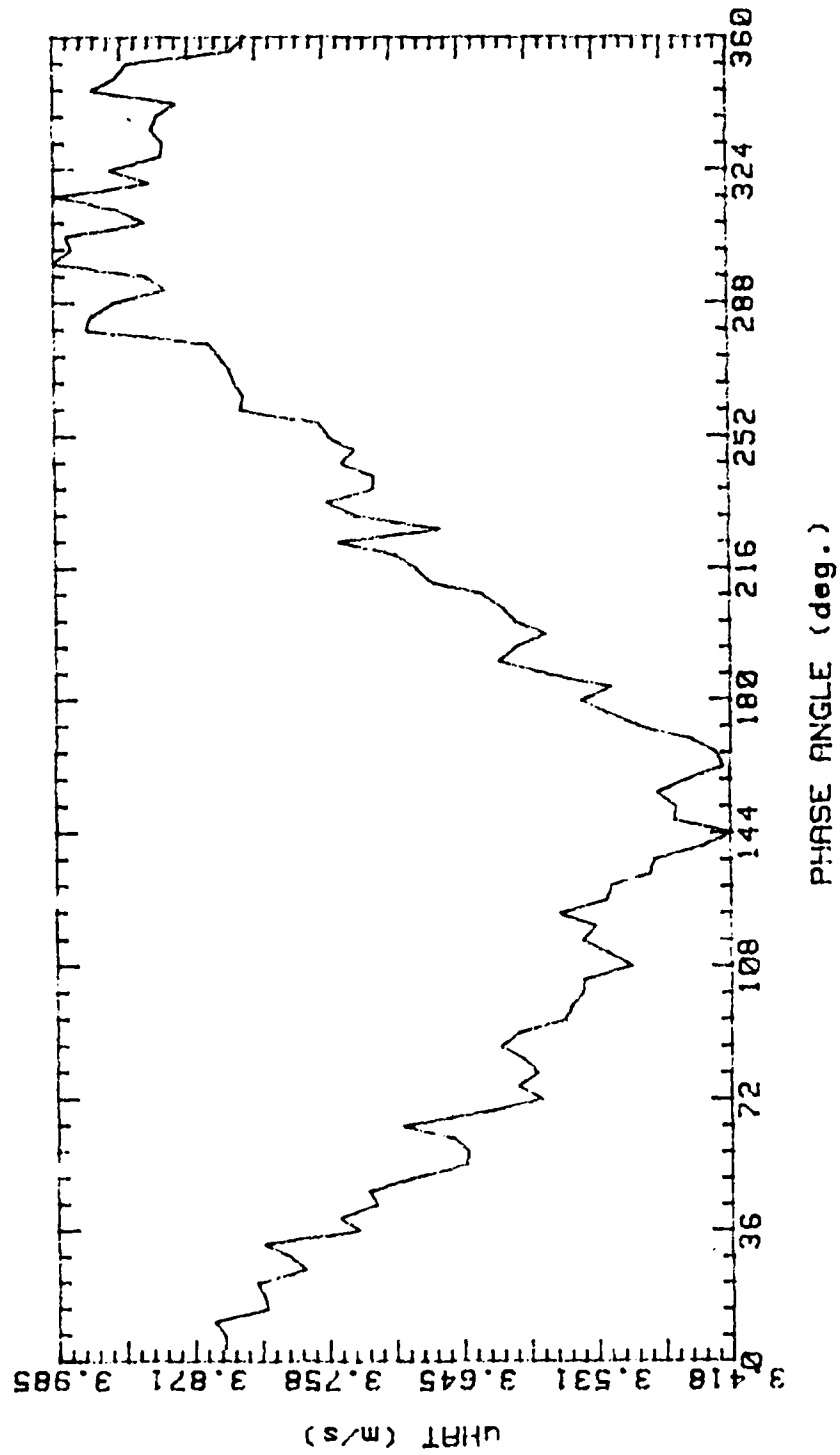


Figure 32.

MULTIRUN (AVS, 1 RUNS) PH. AVE., 181089  
 AVG. VEL 3.705m/s RMS VEL .5718m/s  
 OSC. FREQ. 2Hz STR. # .0399  
 BULK VEL. 4.38m/s REY. # 3660

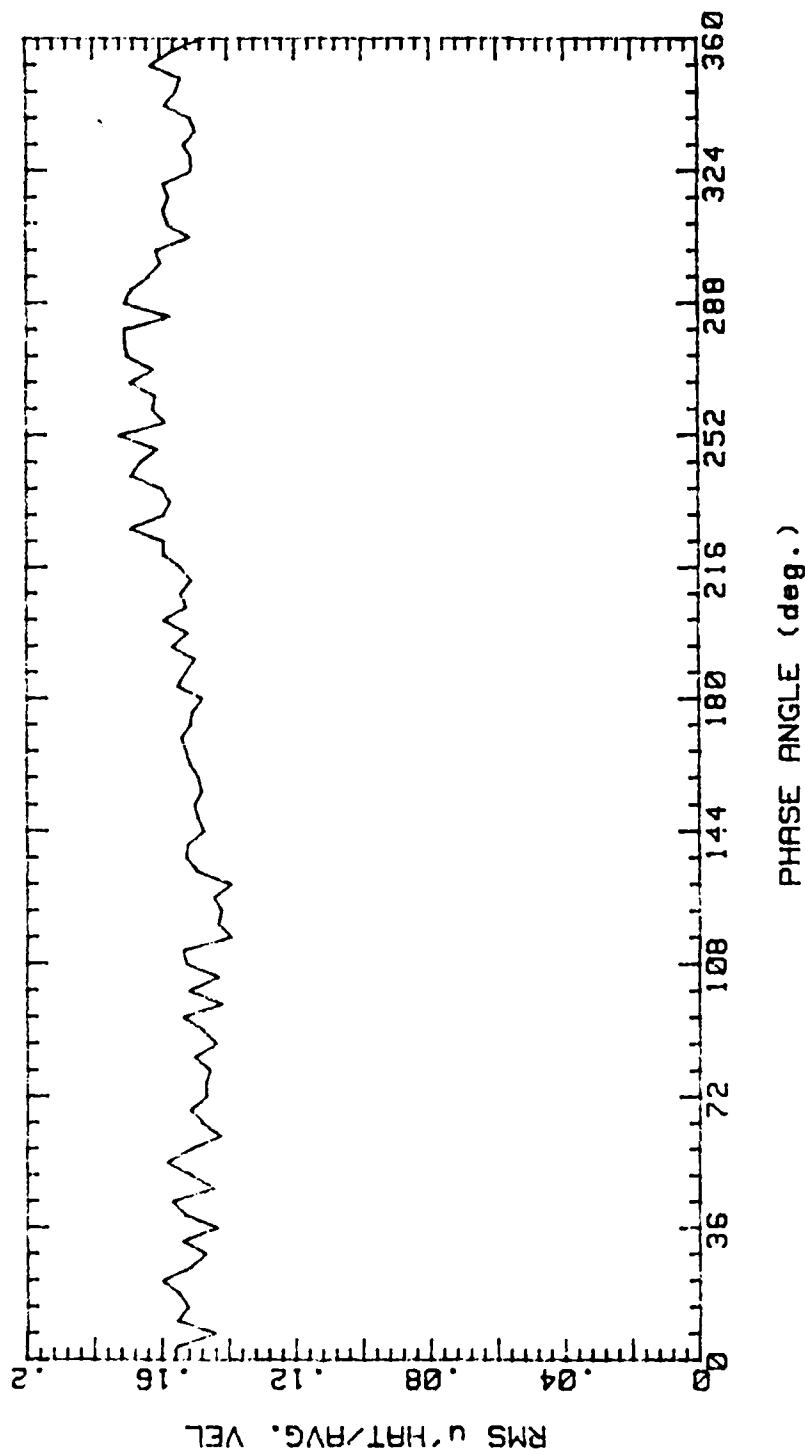


Figure 33.

MULTIRUN (AV5, 8 RUNS) PH. AVE., 181089  
 AVG. VEL 3.708m/s RMS VEL .5675m/s  
 OSC. FREQ. 2Hz STR. # .03644  
 BULK VEL. 4.38m/s REY. # 3660

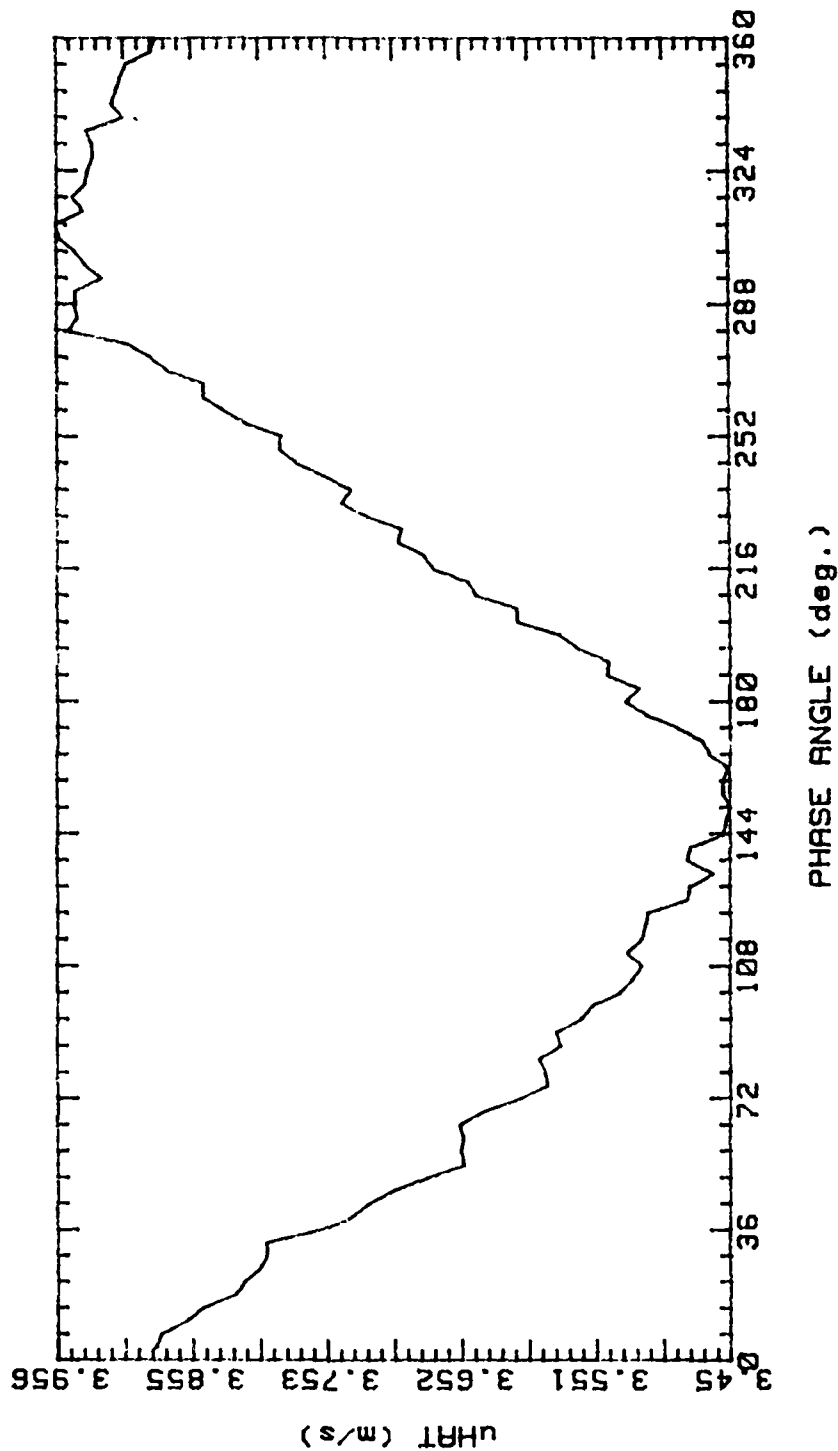


Figure 34.

MULTIRUN (AV5, 8 RUNS) PH. AVE., 181089  
 AVG. VEL 3.708m/s RMS VEL .5675m/s  
 OSC. FREQ. 2Hz STR. # .03644  
 BULK VEL. 4.38m/s REY. # 3660

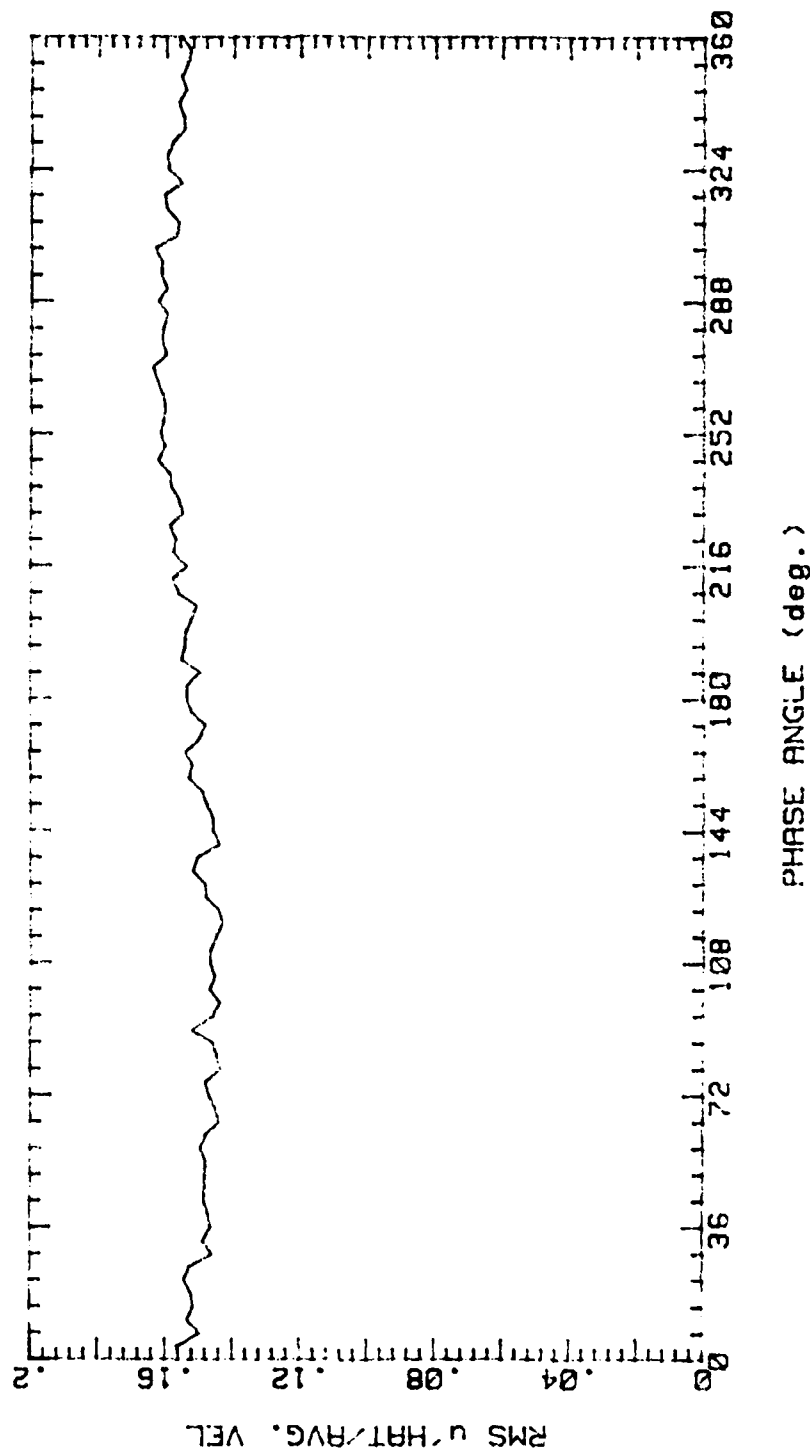


Figure 35.



Mean Velocity Profile Development

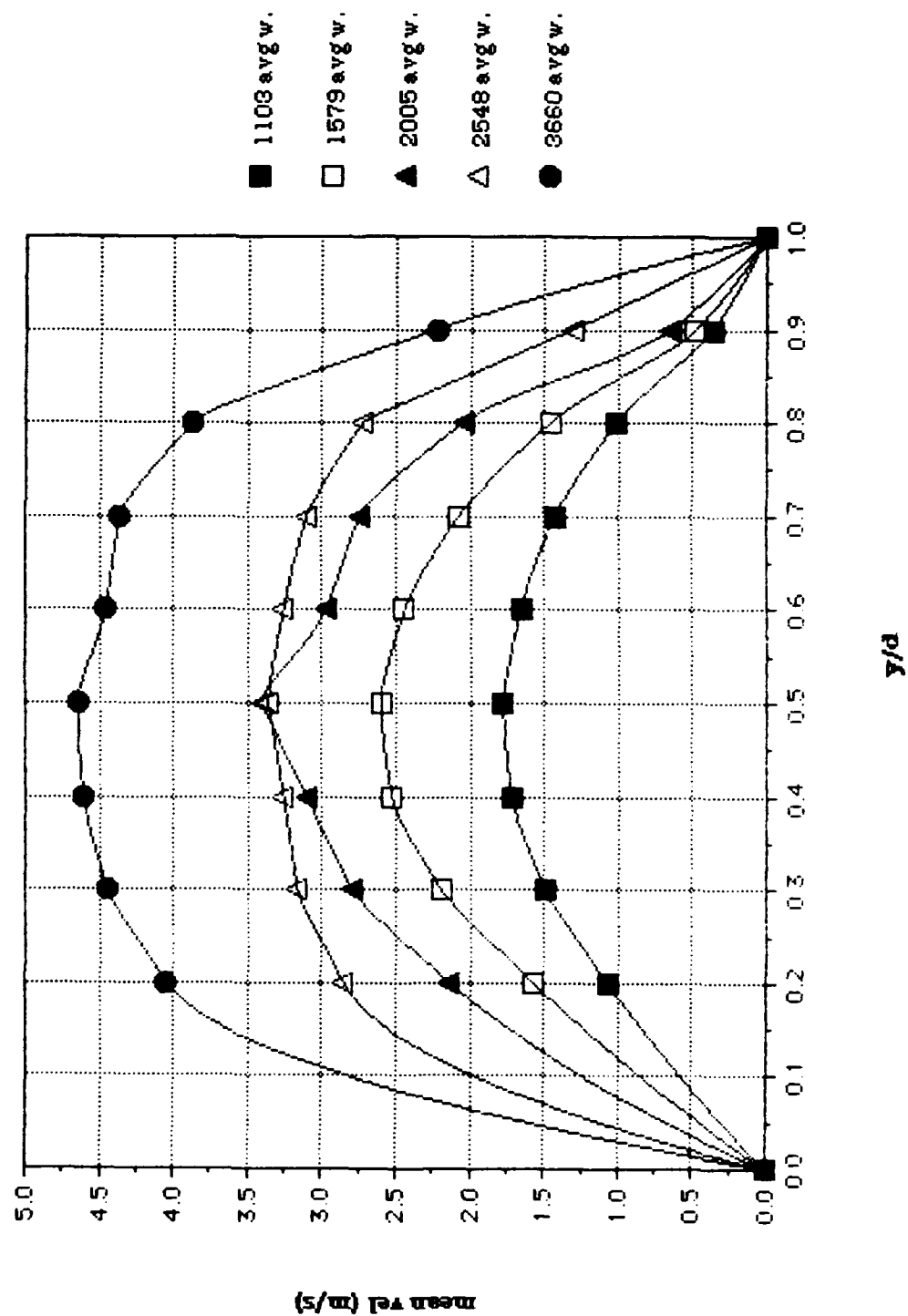


Figure 36.

Mean Velocity Profile Development  
with 2 Hz Imposed Unsteadiness

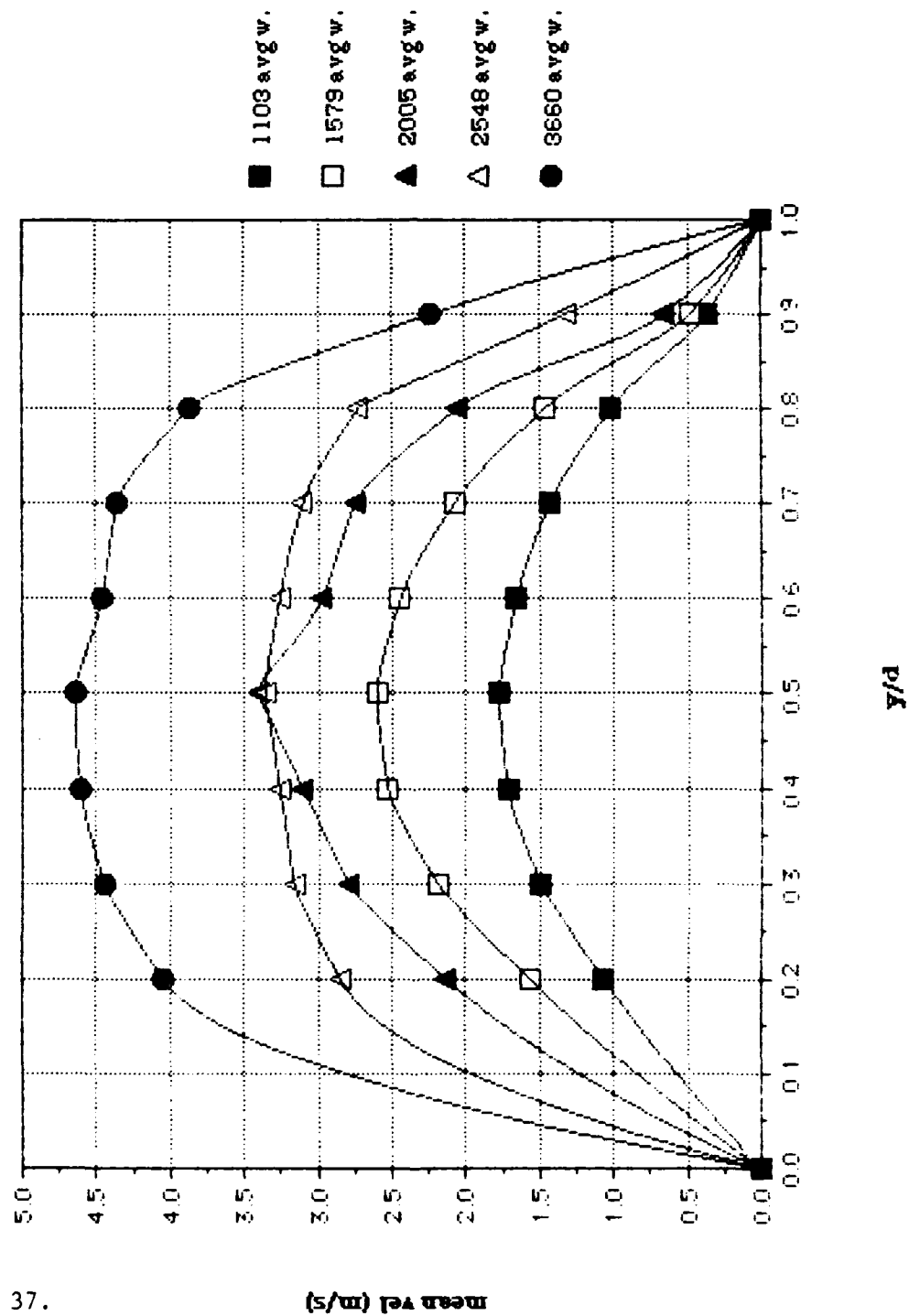


Figure 37.

mean vel (m/s)

Mean Velocity Profile at Re No. = 1103  
with 2 Hz Imposed Unsteadiness

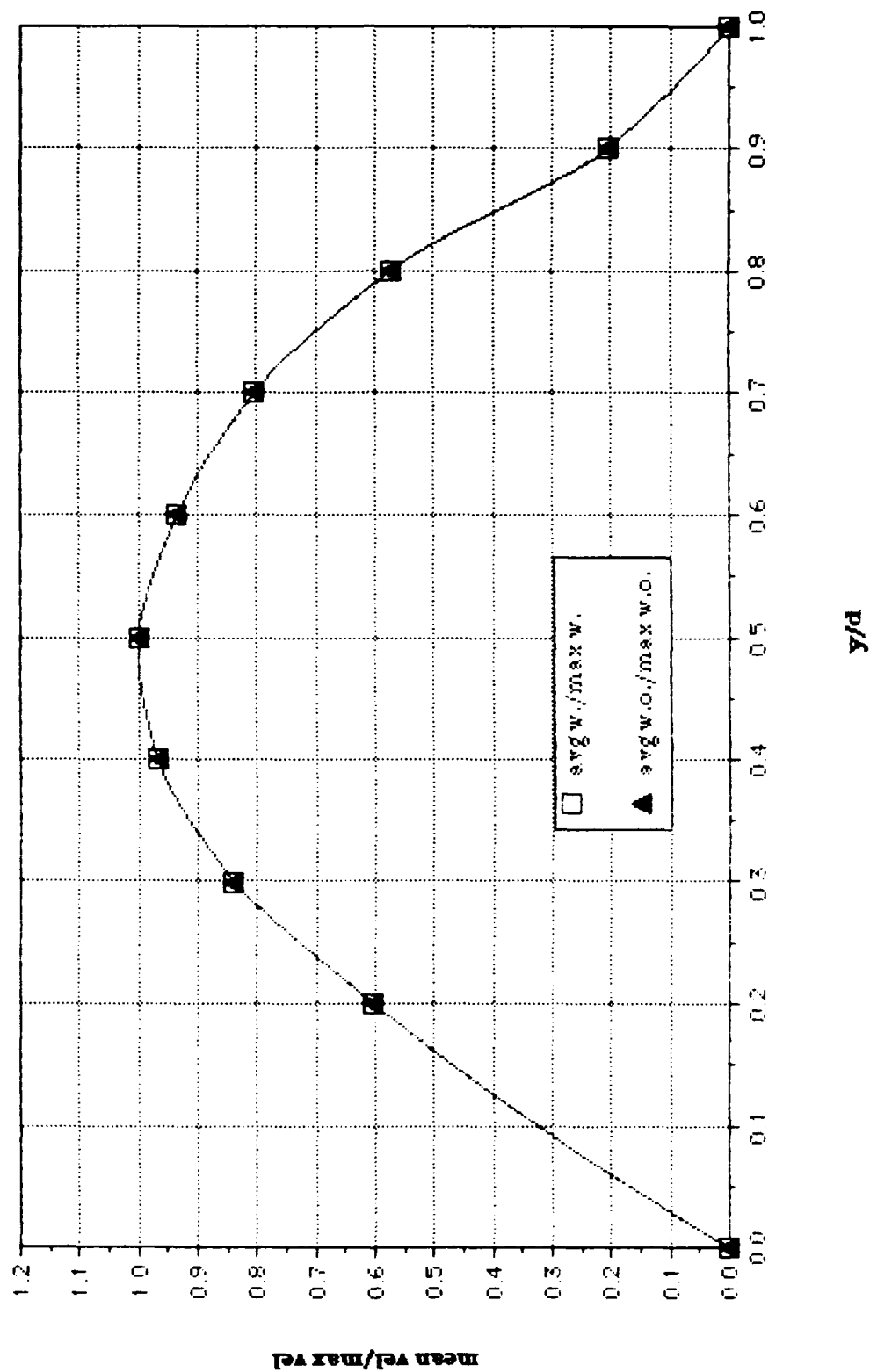


Figure 38.

Mean Velocity Profile at Re No. = 1579  
with 2 Hz Imposed Unsteadiness

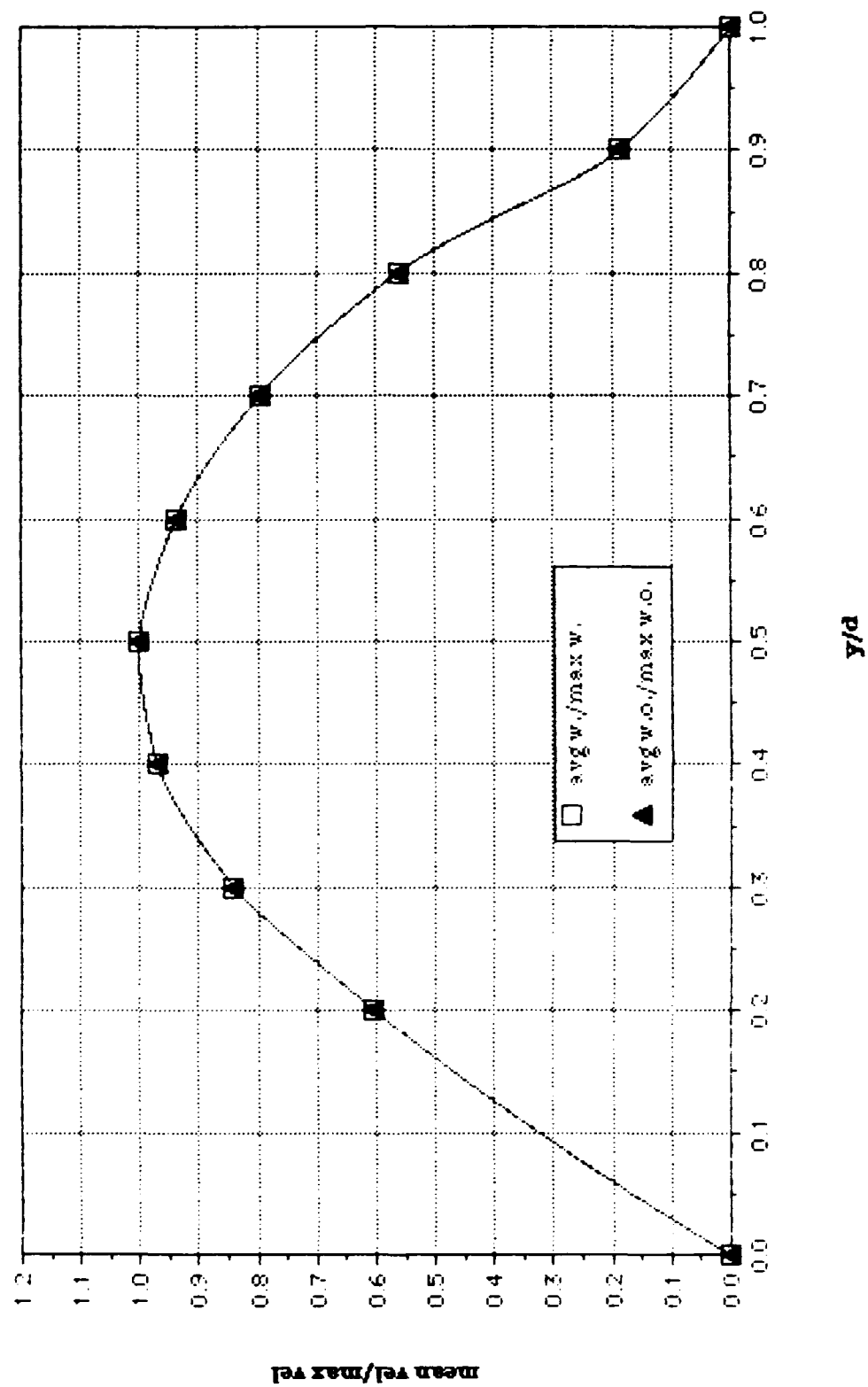


Figure 39.

Mean Velocity Profile at Re No. = 2005  
with 2 Hz Imposed Unsteadiness

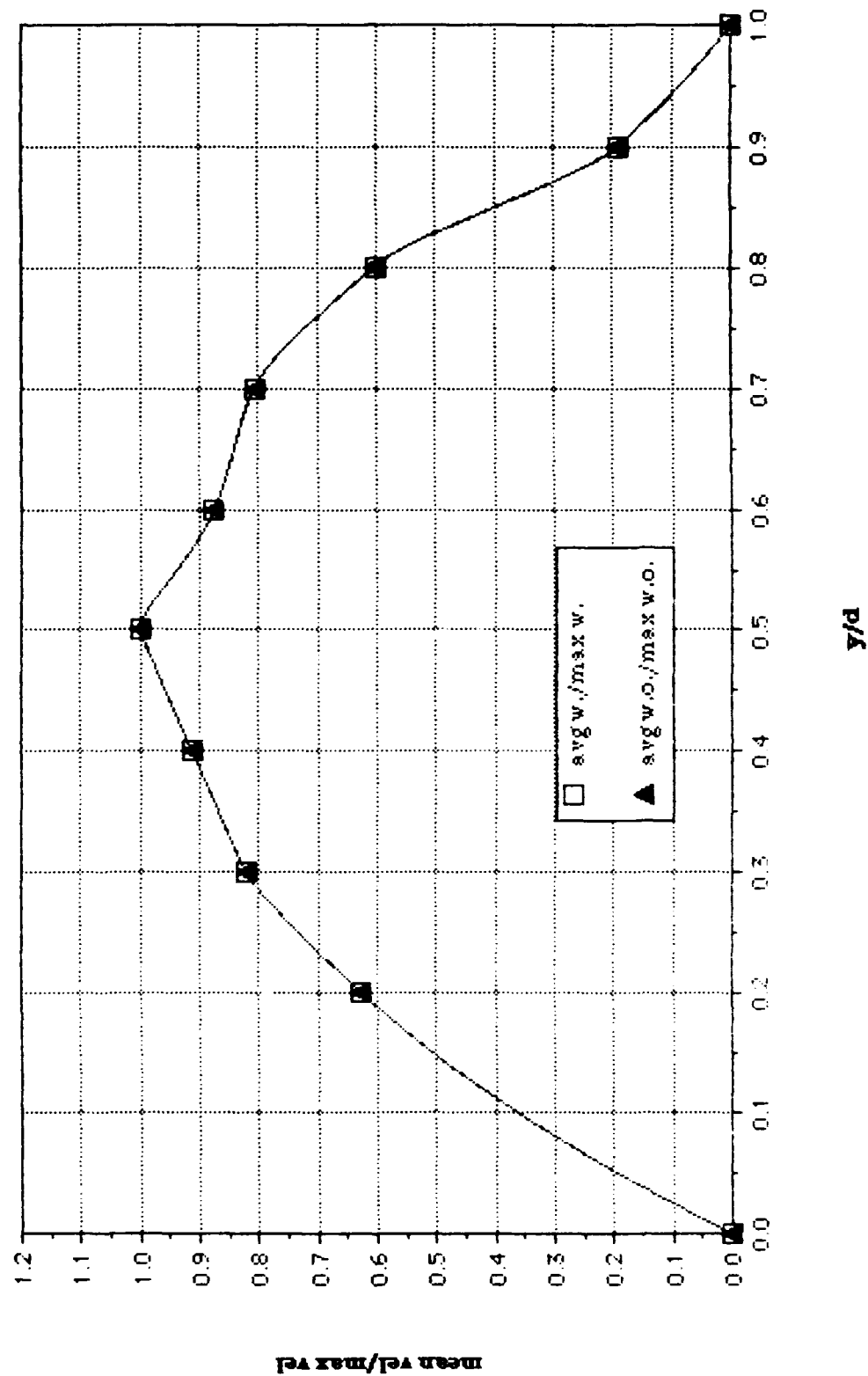


Figure 40.

Mean Velocity Profile at Re No. = 2548  
with 2 Hz Imposed Unsteadiness

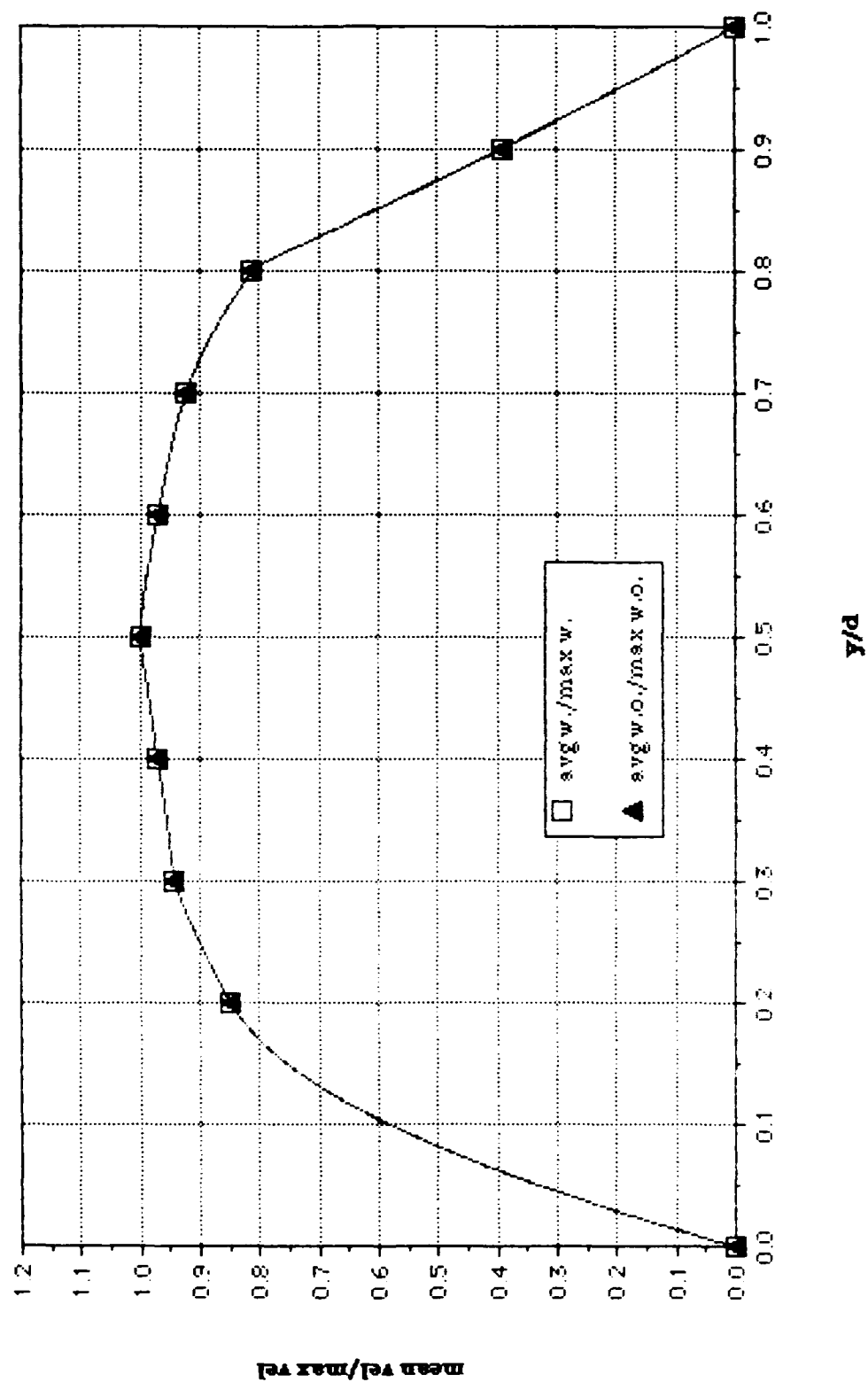


Figure 41.

Mean Velocity Profile at Re No. = 3660  
with 2 Hz Imposed Unsteadiness

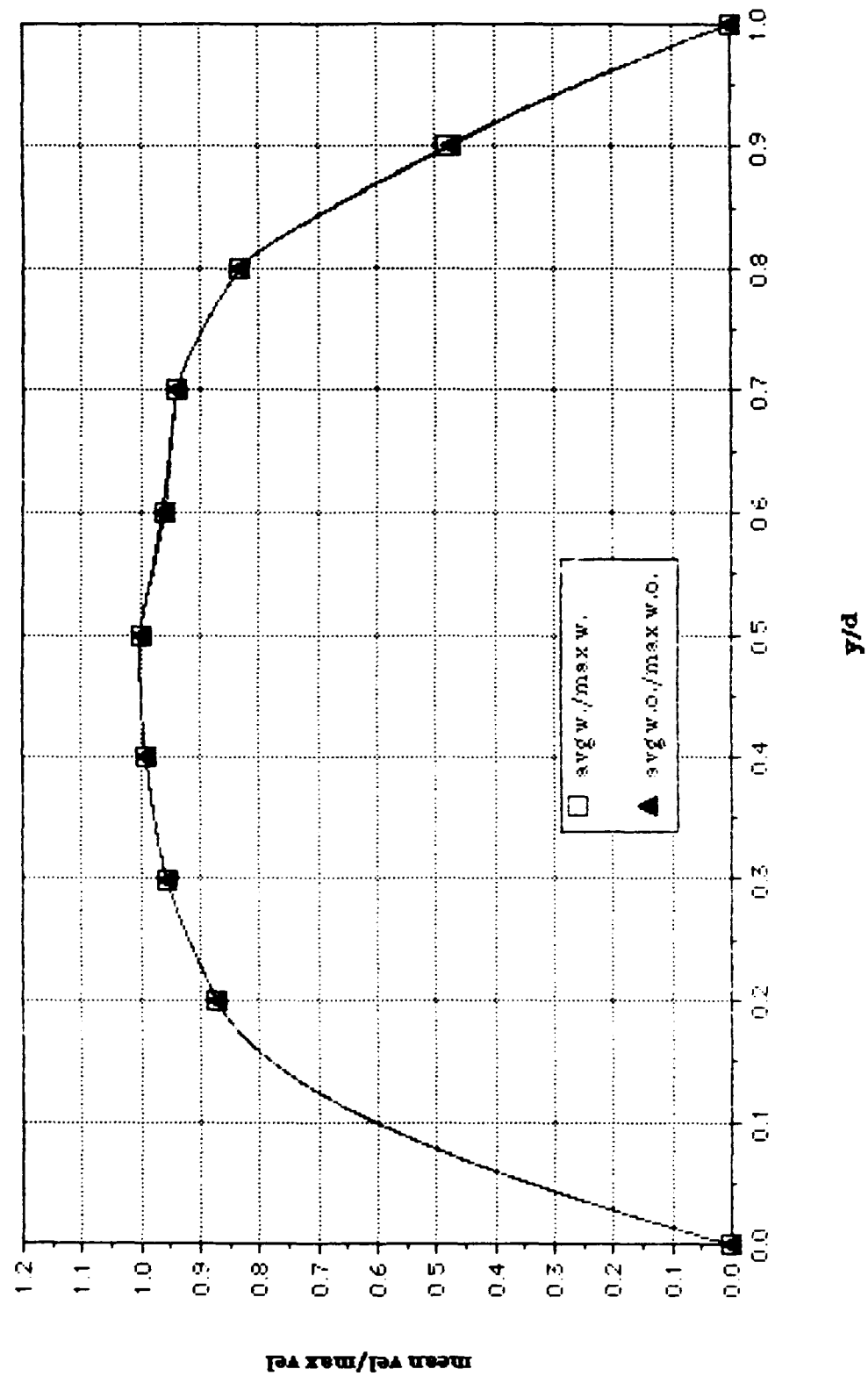


Figure 42.

RMS Velocity Profile Development

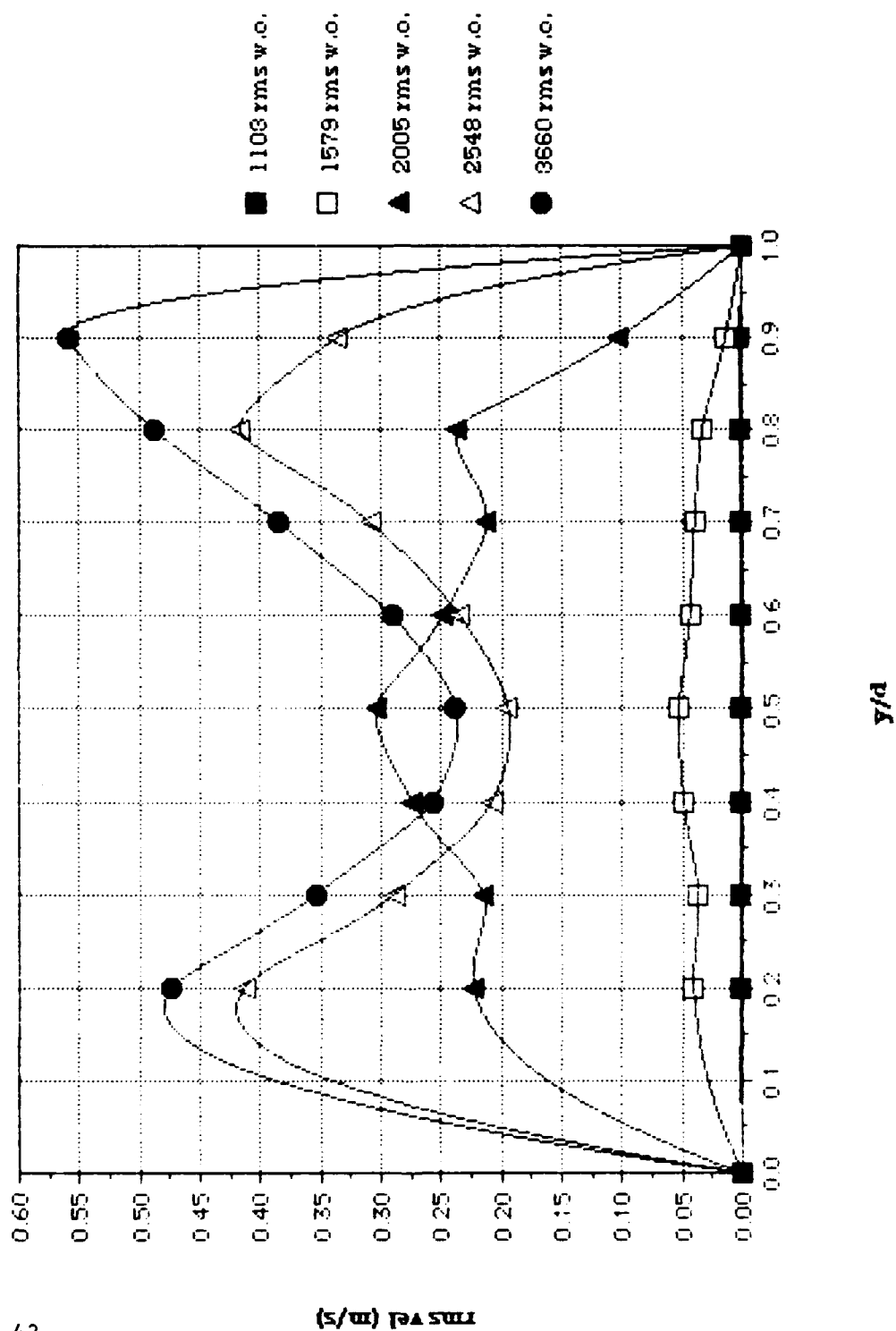


Figure 43.



RMS Velocity Profile Development  
with 2 Hz Imposed Unsteadiness

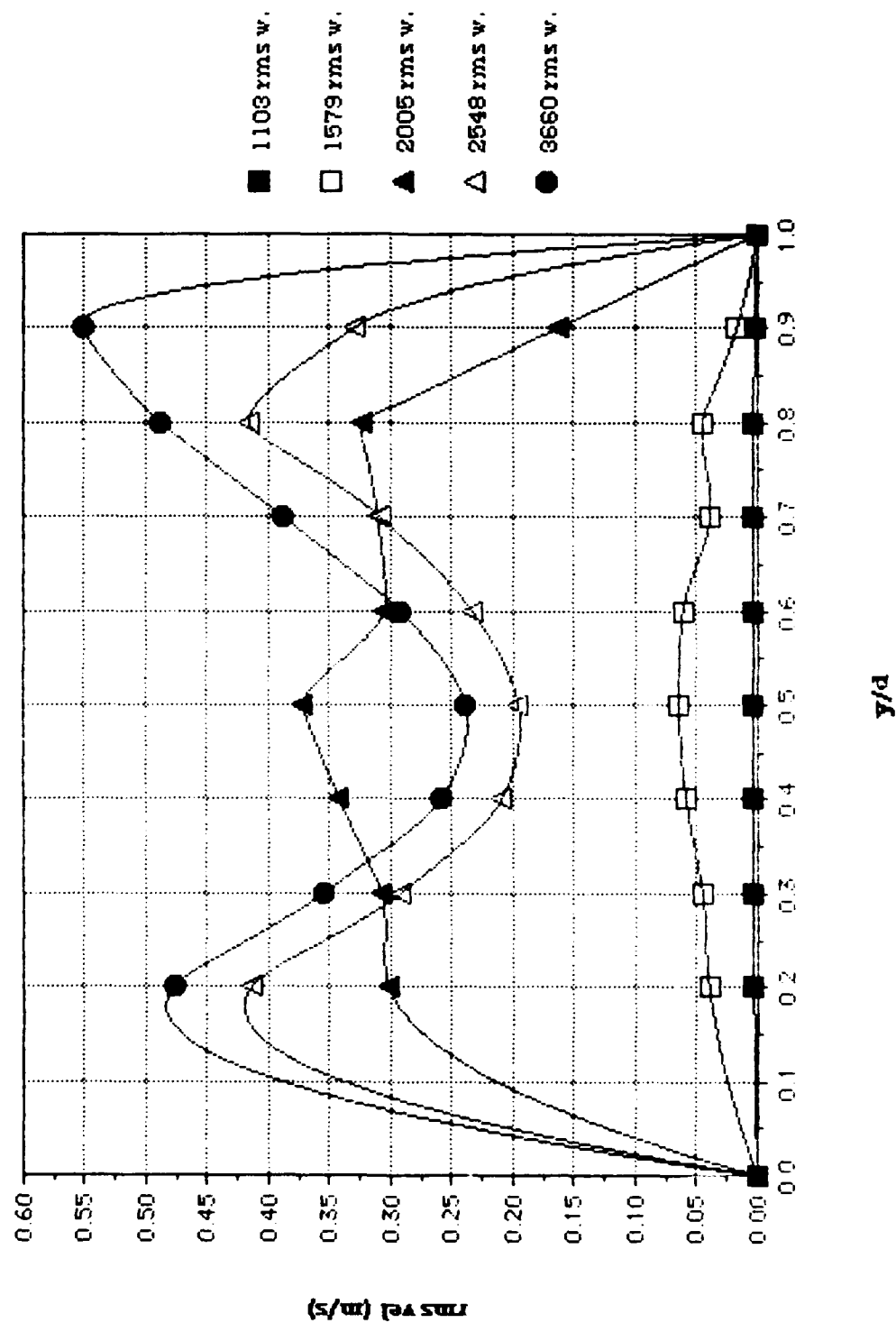


Figure 44.

RMS Velocity Profile at Re No. = 1103  
with 2 Hz Imposed Unsteadiness

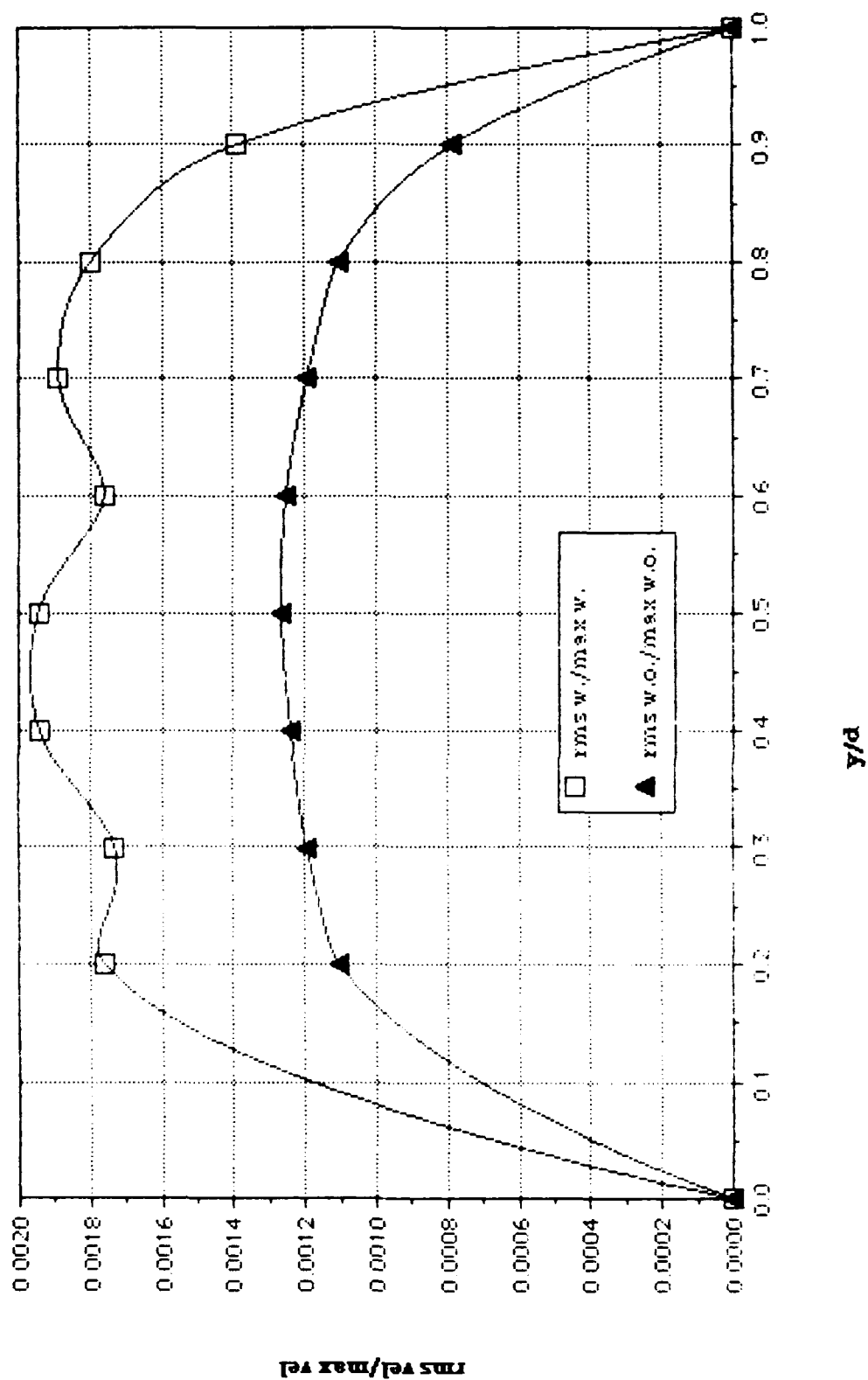


Figure 45.

RMS Velocity Profile at Re No. = 1579  
with 2 Hz Imposed Unsteadiness

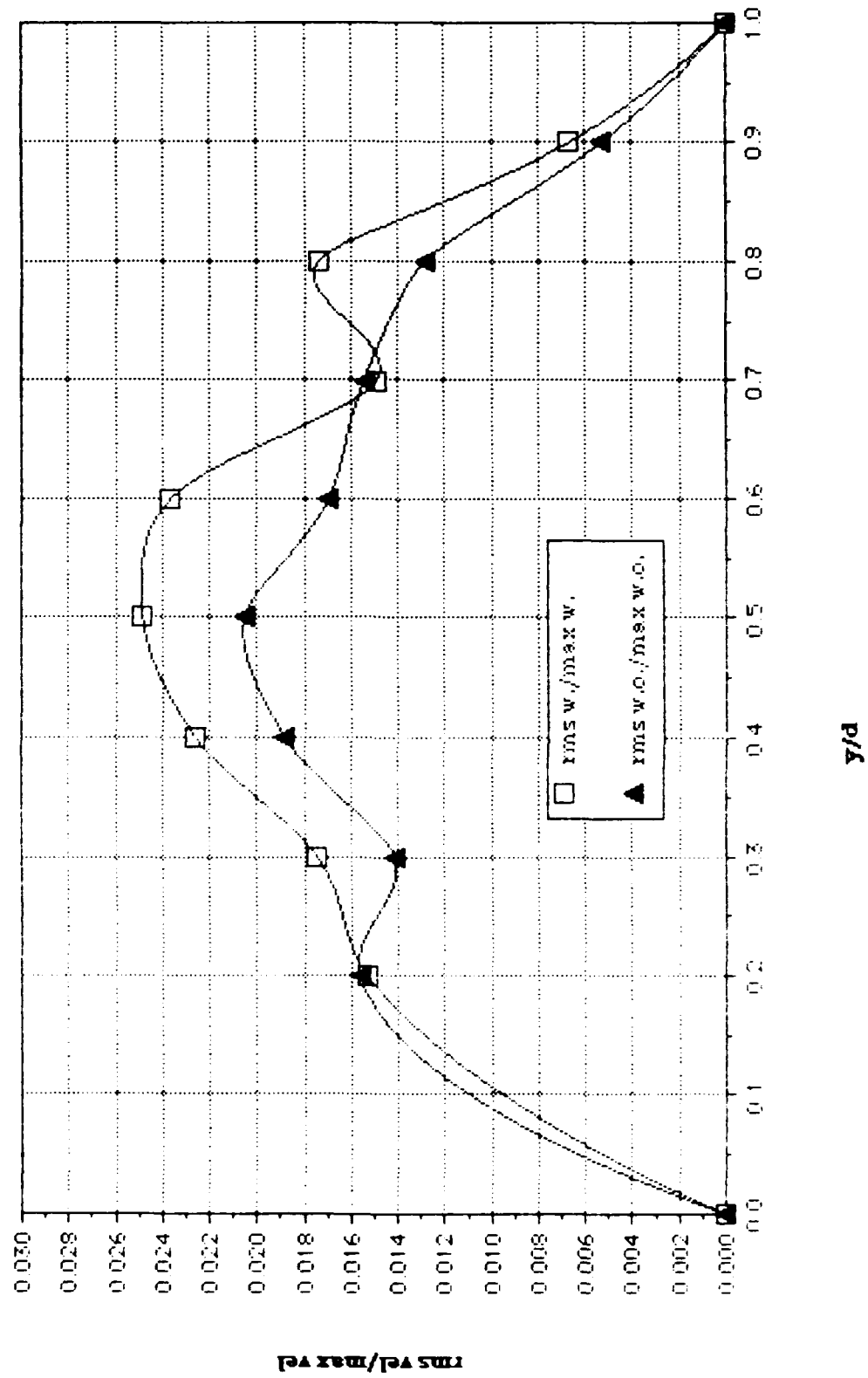


Figure 46.

RMS Velocity Profile at Re No. = 2005  
with 2 Hz Imposed Unsteadiness

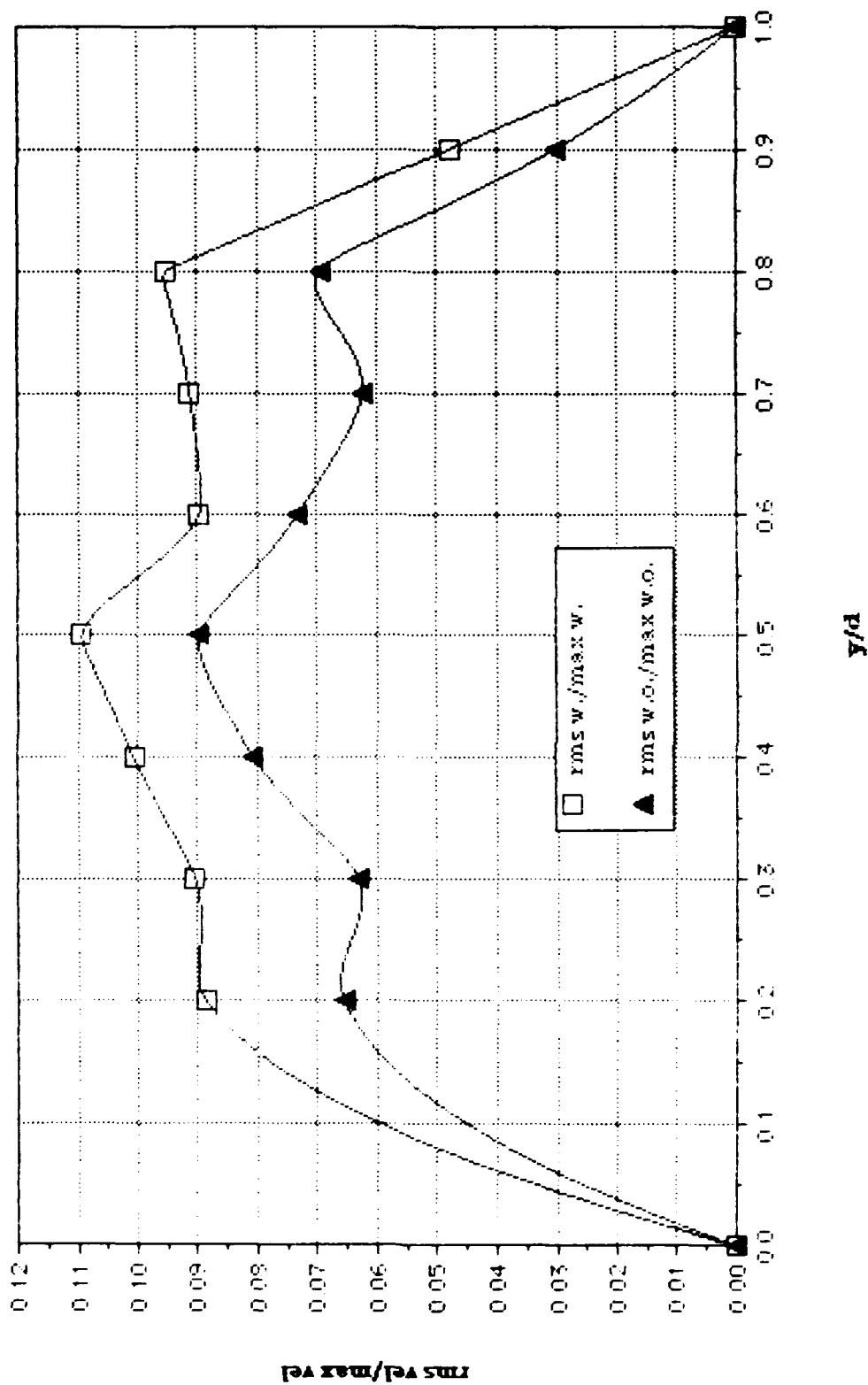


Figure 47.

RMS Velocity Profile at Re No. = 2548  
with 2 Hz Imposed Unsteadiness

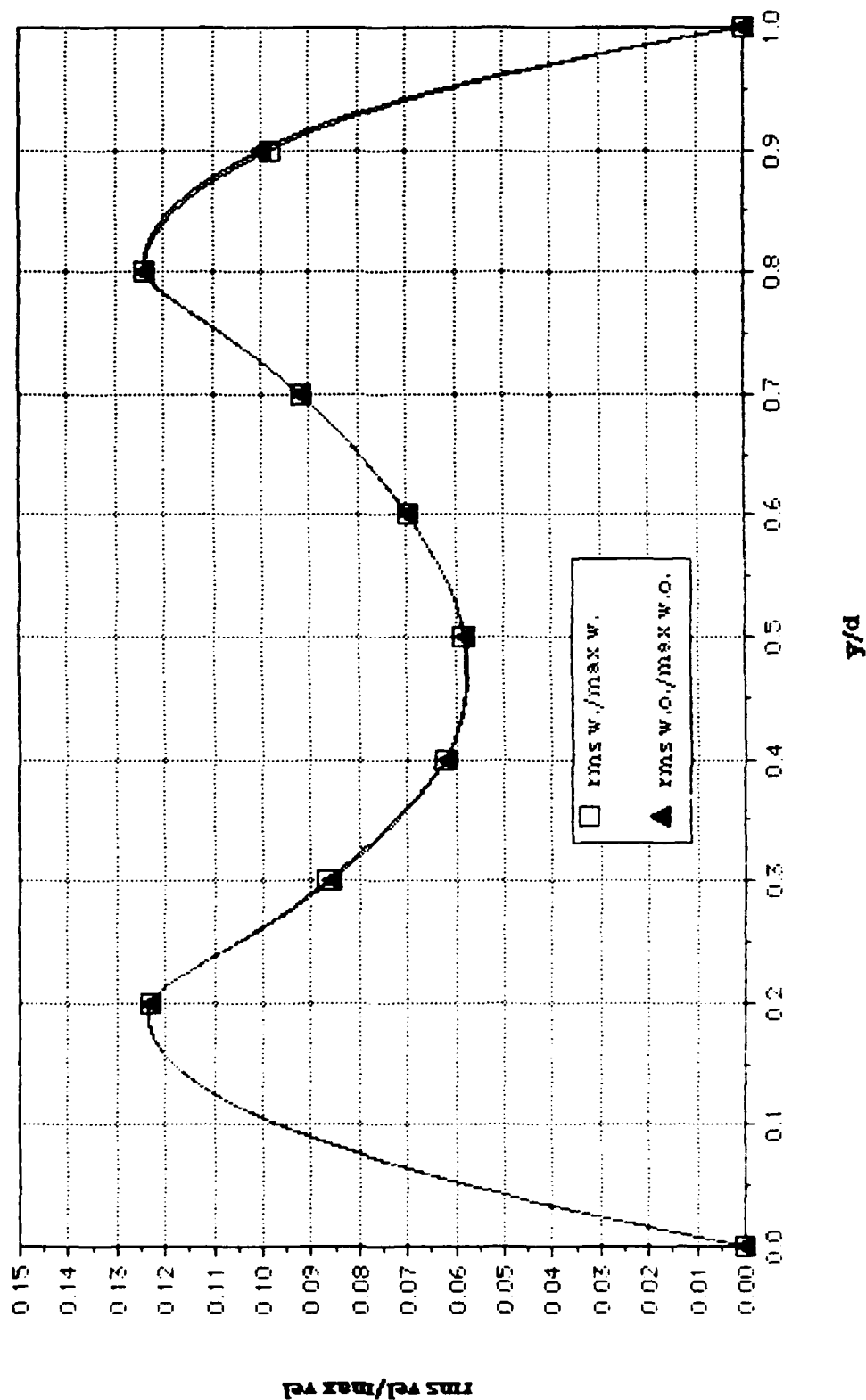


Figure 48.

RMS Velocity Profile at Re No. = 3660  
with 2 Hz Imposed Unsteadiness

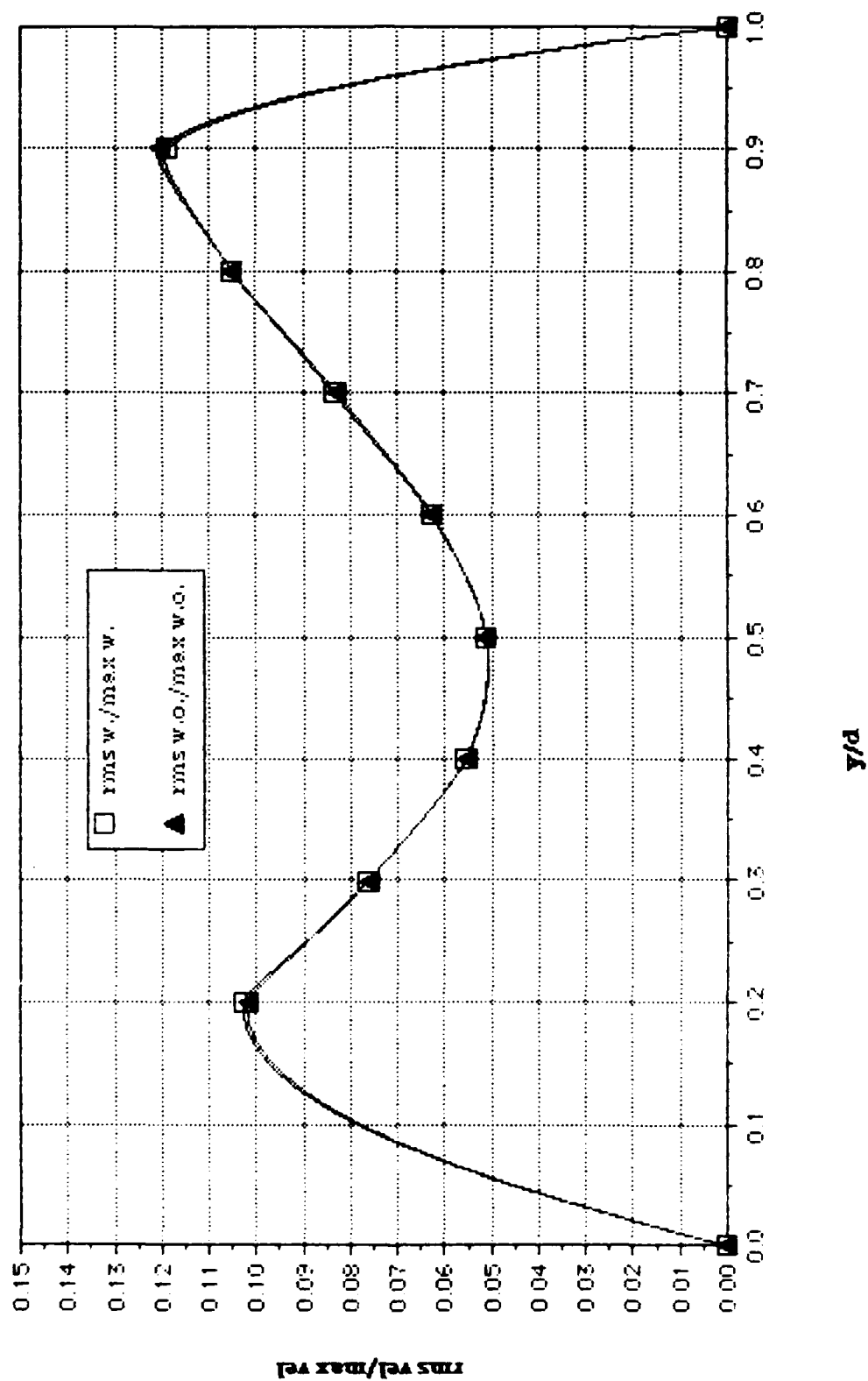


Figure 49.

2P3A1 201089.2235  
 AVG. VEL. .6568m/s RMS VEL .1026m/s  
 OSC. FREQ. 0Hz STR. # 0  
 BULK VEL. 2.4m/s REY. # 2005

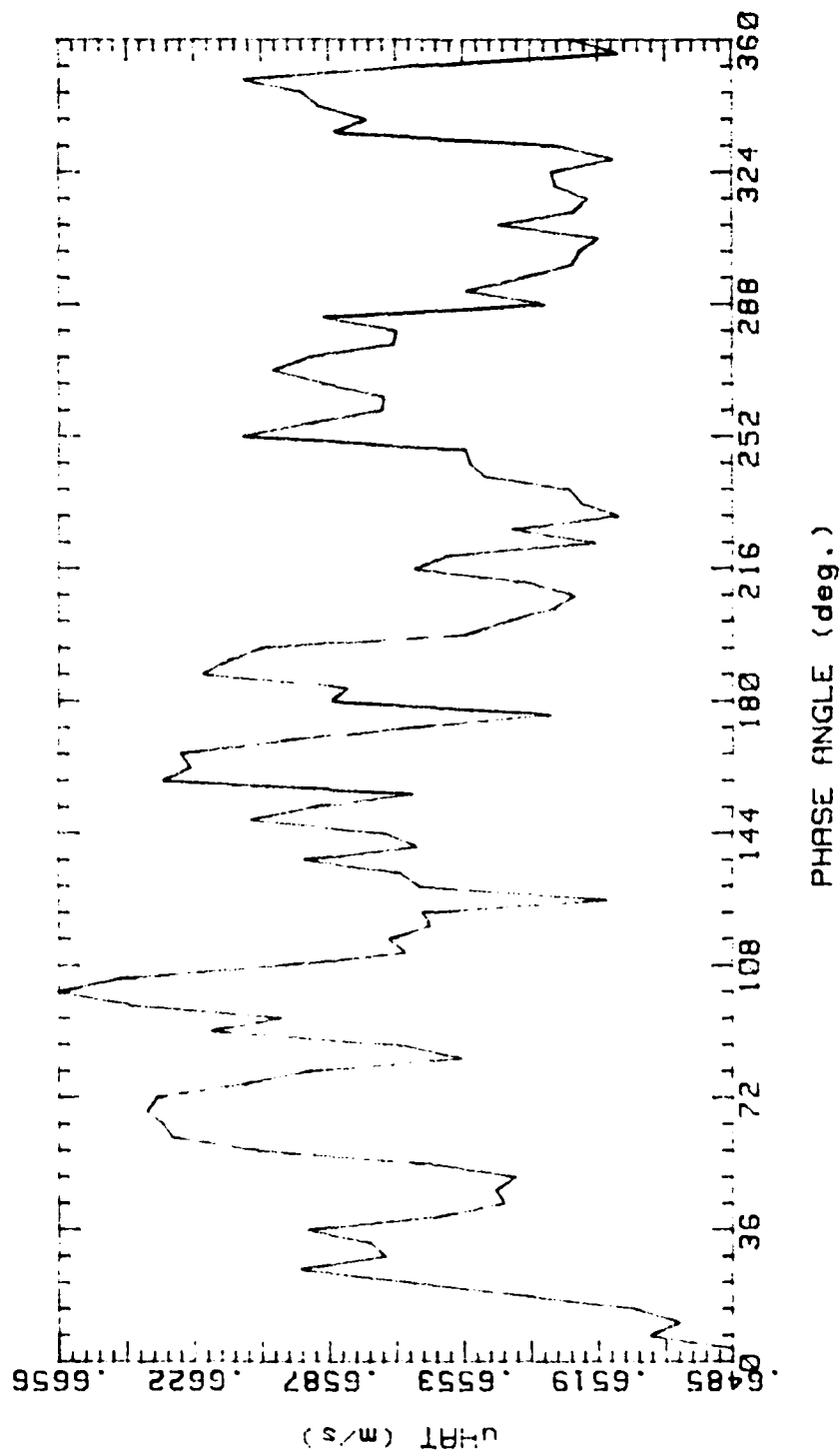


Figure 50.

2P3A2 201089.2251

AVG. VEL	2.051m/s	RMS VEL	.2364m/s
OSC. FREQ.	0Hz	STR.	# 0
BULK VEL.	2.4m/s	REY.	# 2005

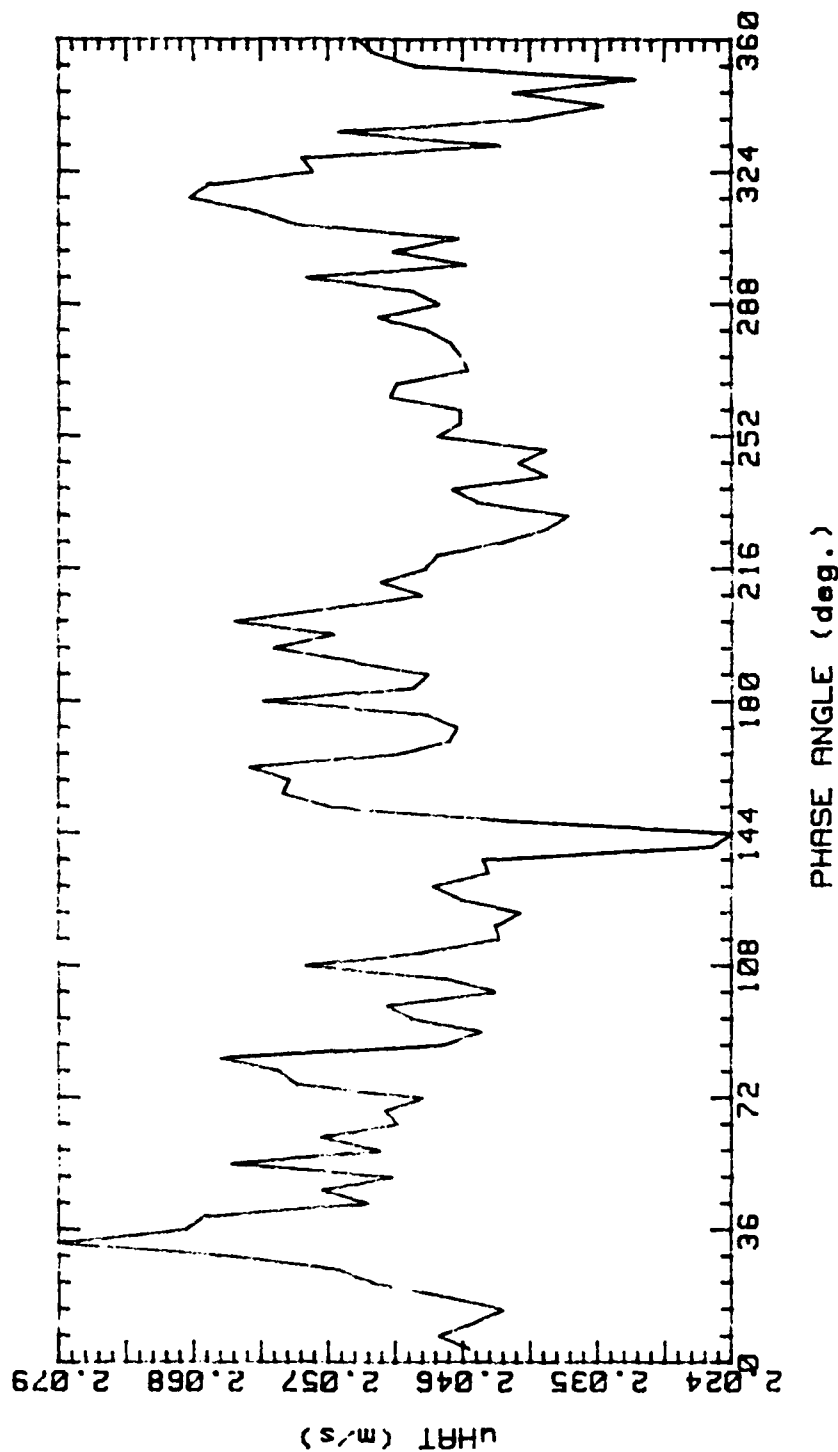


Figure 51.



2P3A3 201089.2304  
 AVG. VEL 2.744m/s RMS VEL .2122m/s  
 OSC. FREQ. 0Hz STR. # 0  
 BULK VEL. 2.4m/s REY. # 2005

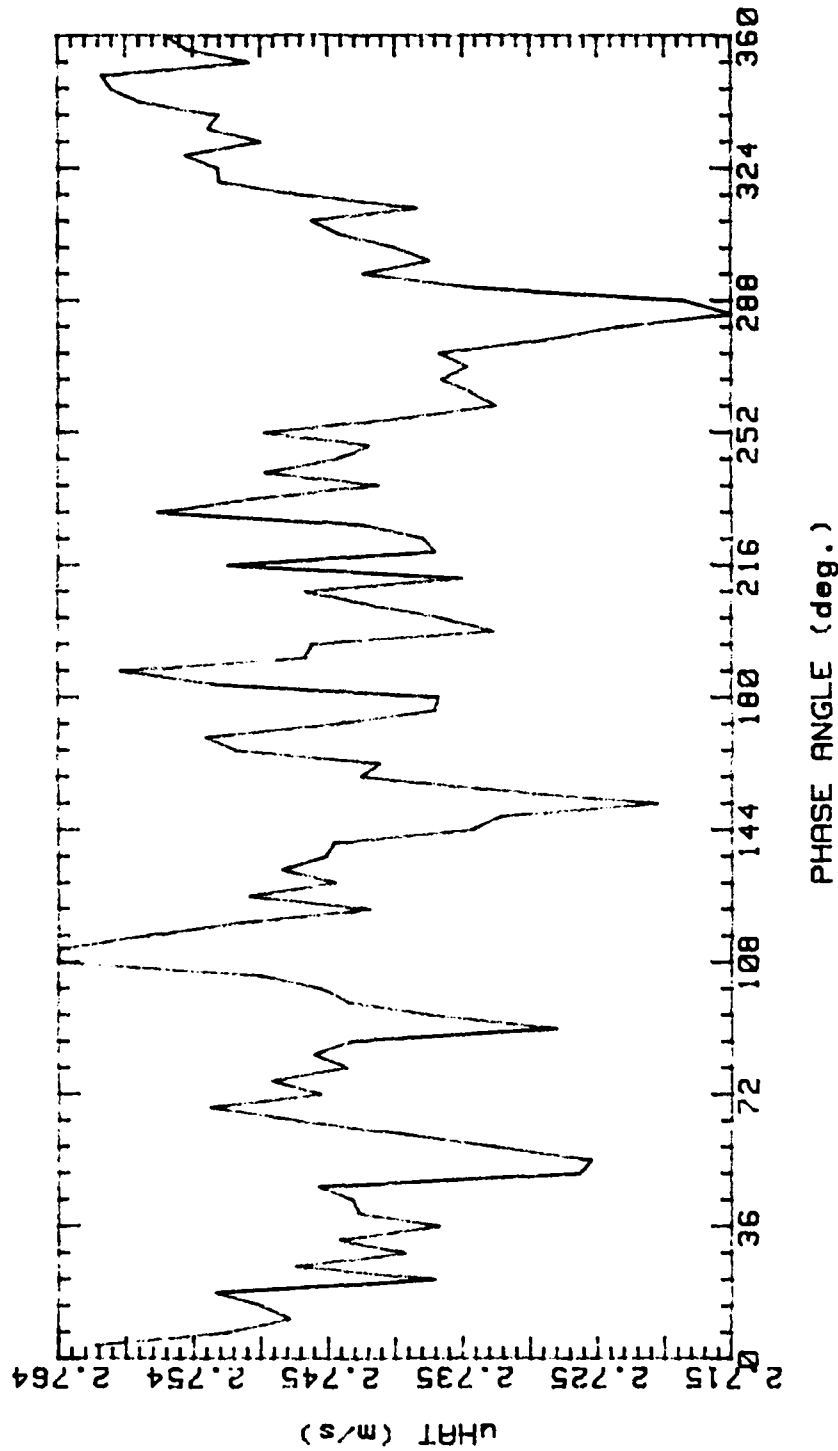


Figure 52.

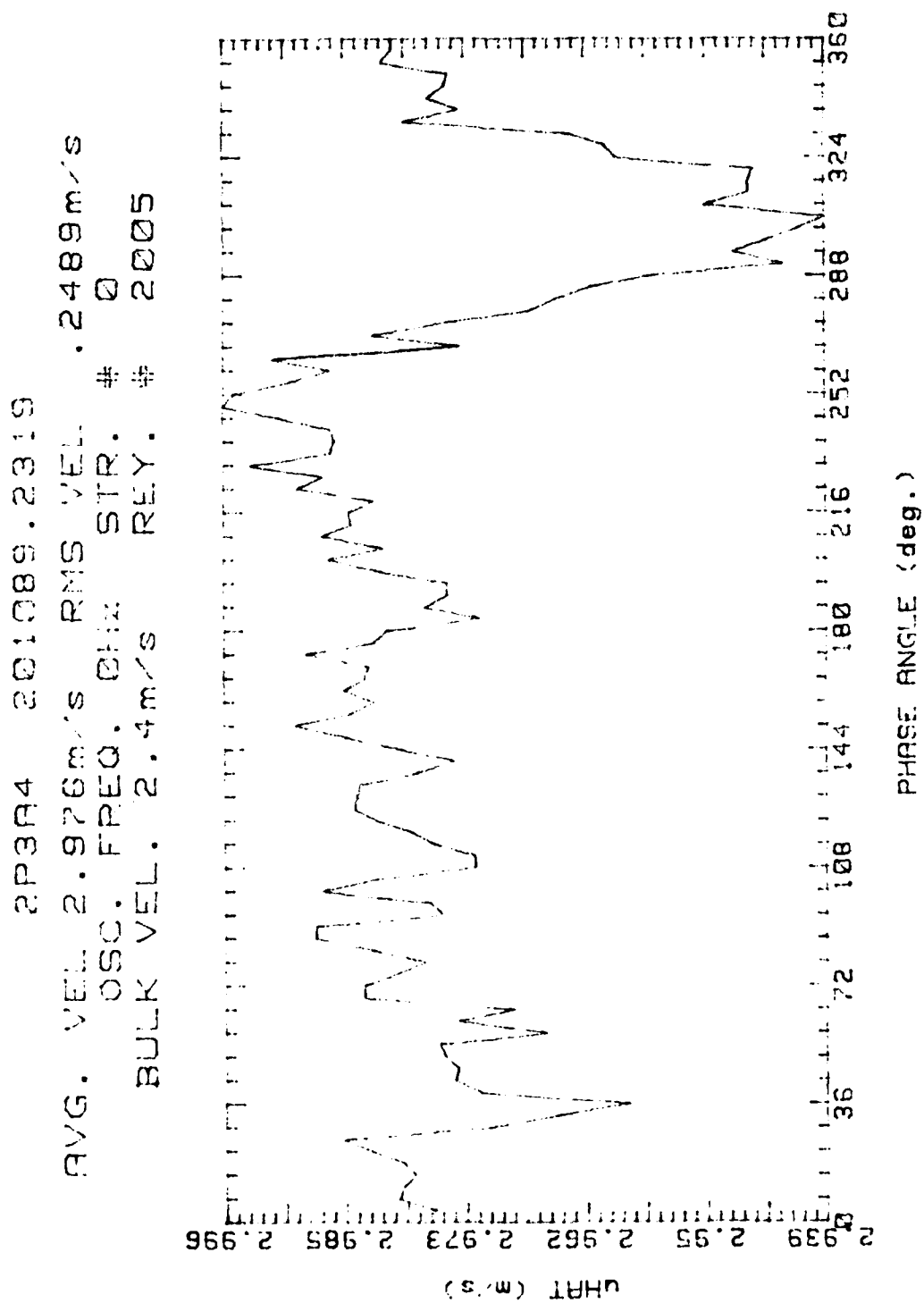


Figure 53.

2P3A5 201089.2334

AVG. VEL 3.4m/s RMS VEL .3048m/s  
OSC. FREQ. 0Hz STR. # 0  
BULK VEL. 2.4m/s REY. # 2005

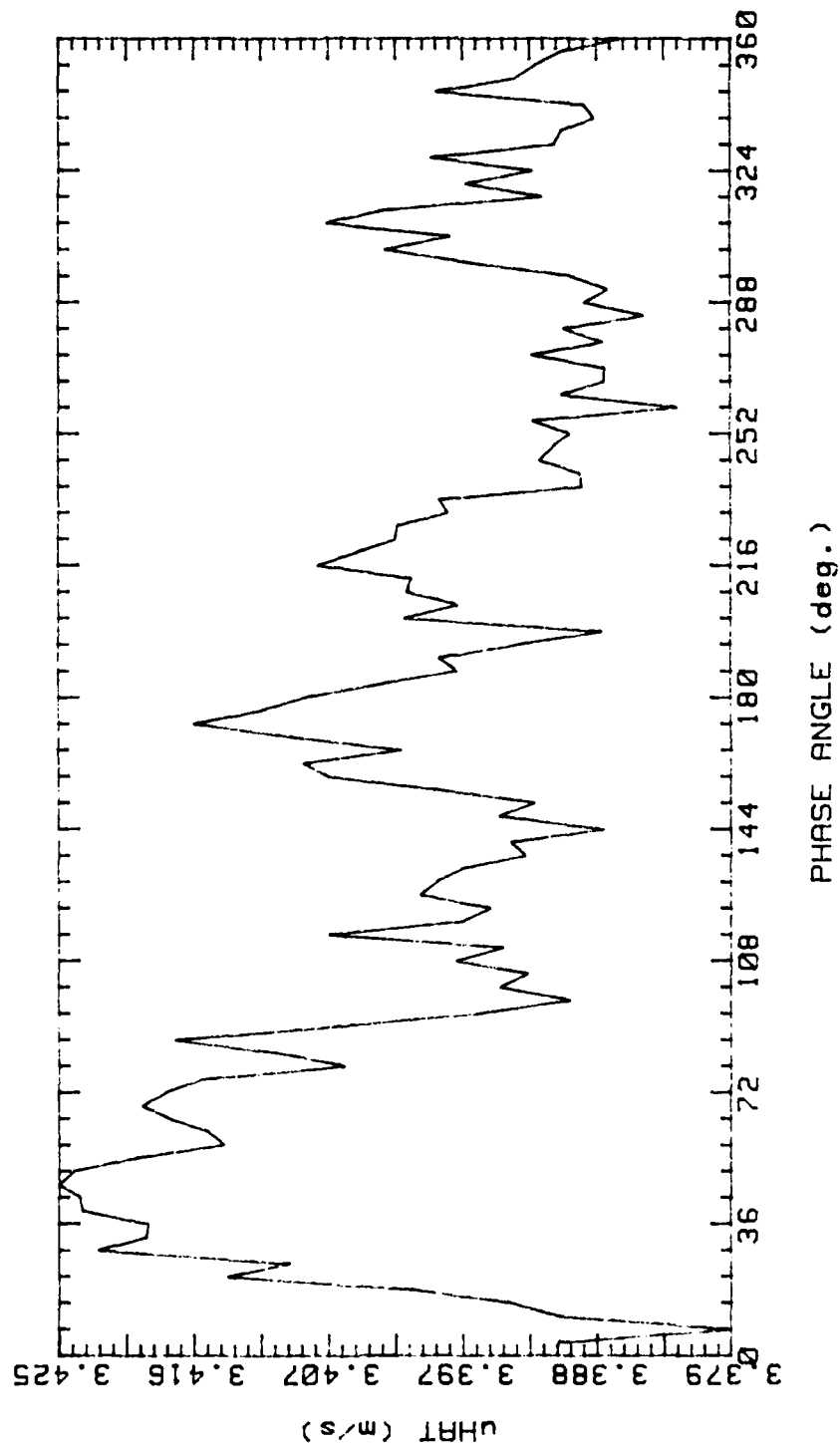


Figure 54.

2P3A6 201089.2349  
 AVG. VEL 3.103m/s RMS VEL .274m/s  
 OSC. FREQ. 0Hz STR. # 0  
 BULK VEL. 2.4m/s REY. # 2005

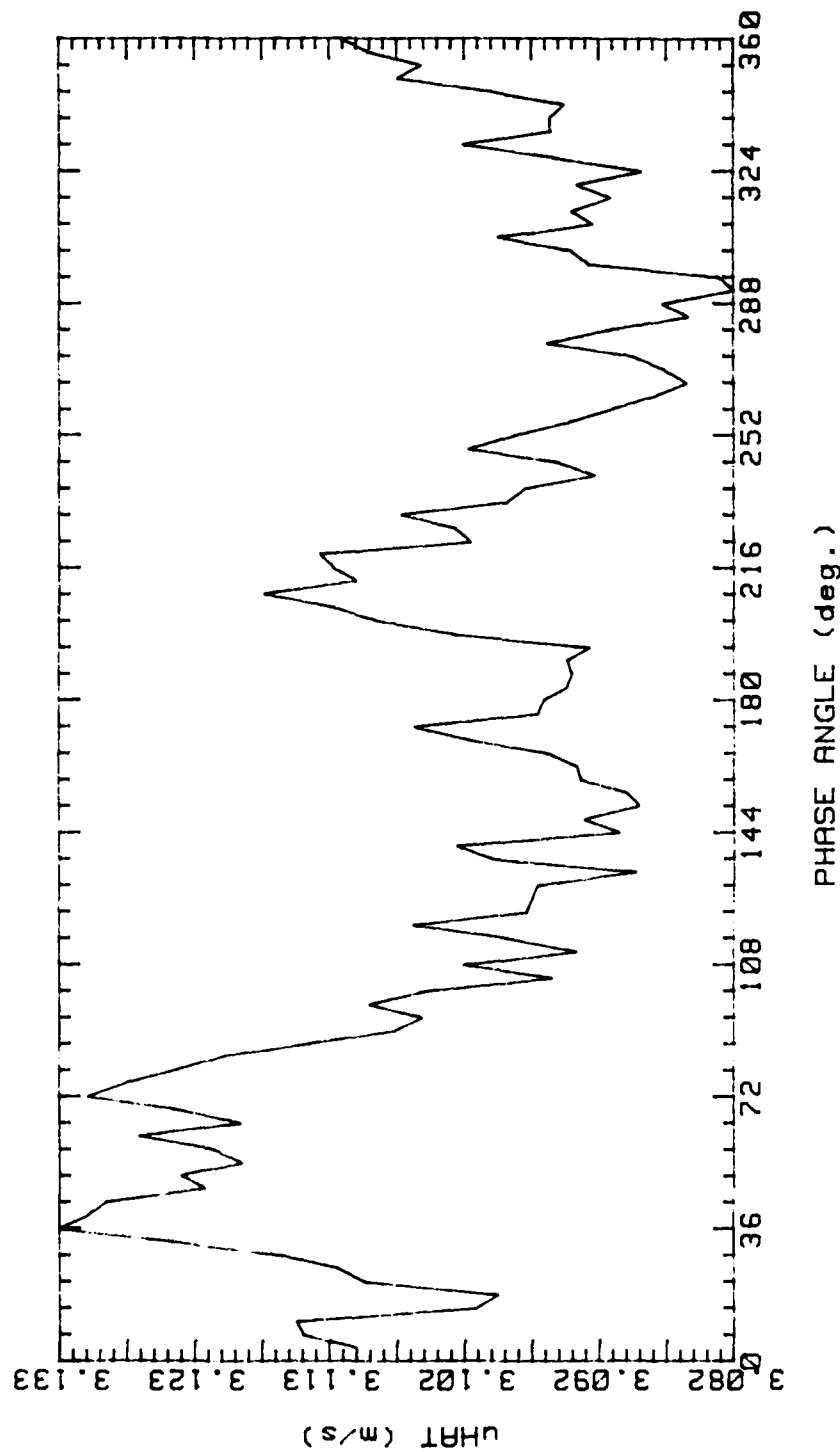


Figure 55.

2P3A7 211089.0004

AVG. VEL 2.792m/s RMS VEL .2149m/s

OSC. FREQ. 0Hz STR. # 0

BULK VEL. 2.4m/s REY. # 2005

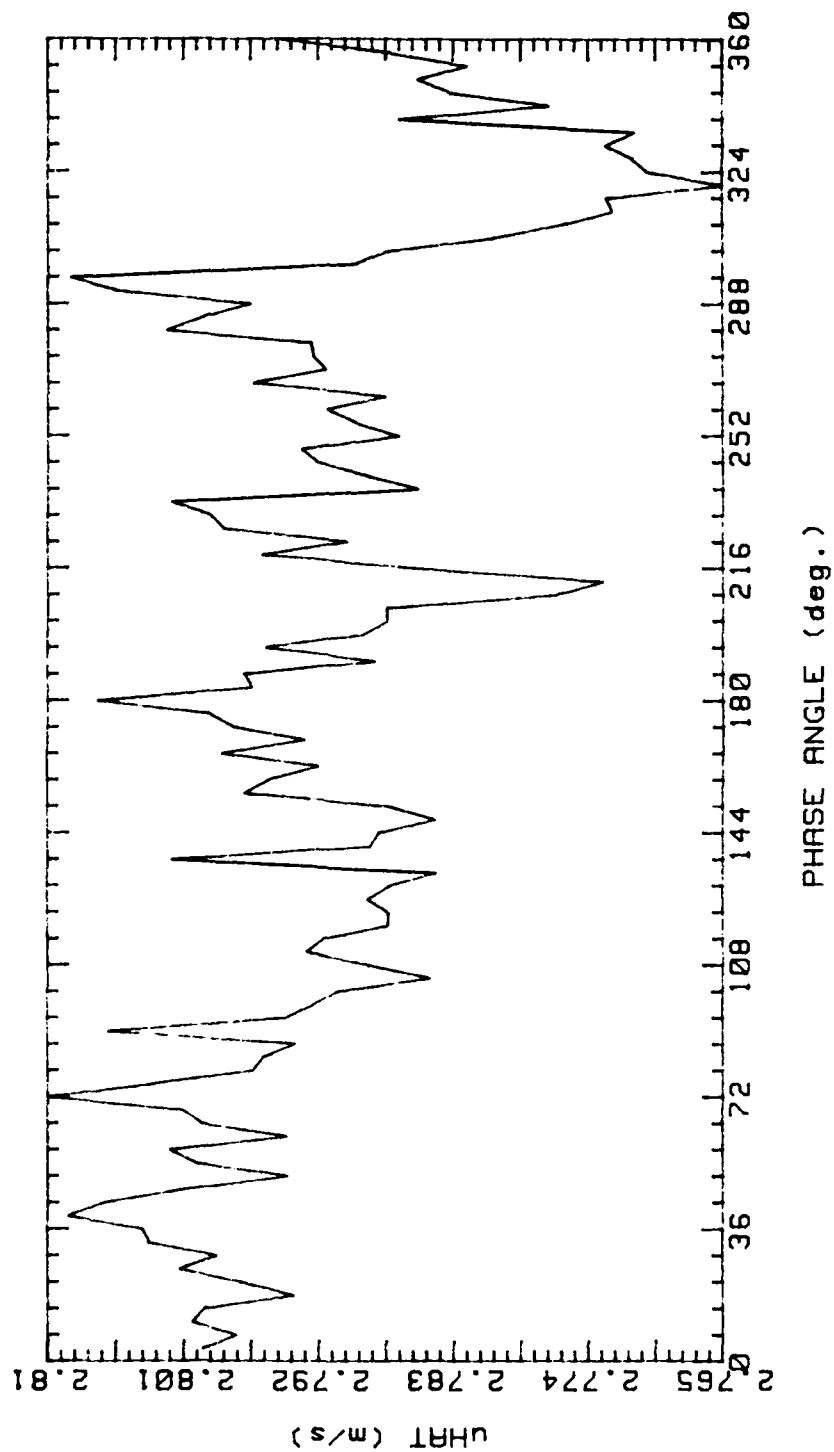


Figure 56.

2P3A8 211089.0018  
 AVG. VEL 2.129m/s RMS VEL .2231m/s  
 OSC. FREQ. 0Hz STR. # 0  
 BULK VEL. 2.4m/s REY. # 2005

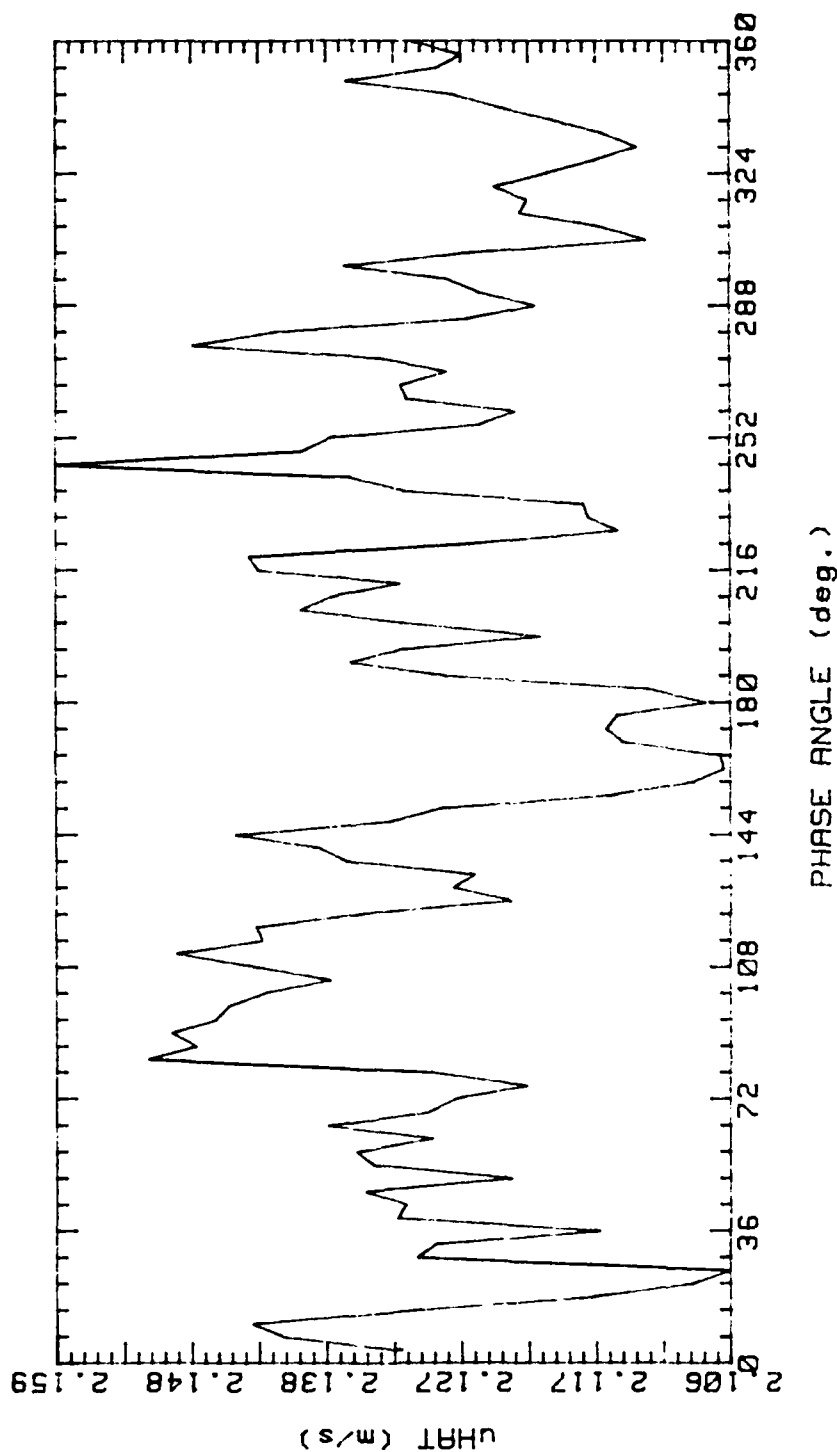


Figure 57.

2P391 201089.2235

AVG. VEL. .6568m/s RMS VEL. .1026m/s

OSC. FREQ. 0Hz STR. # 0

BULK VEL. 2.4m/s REY. # 2005

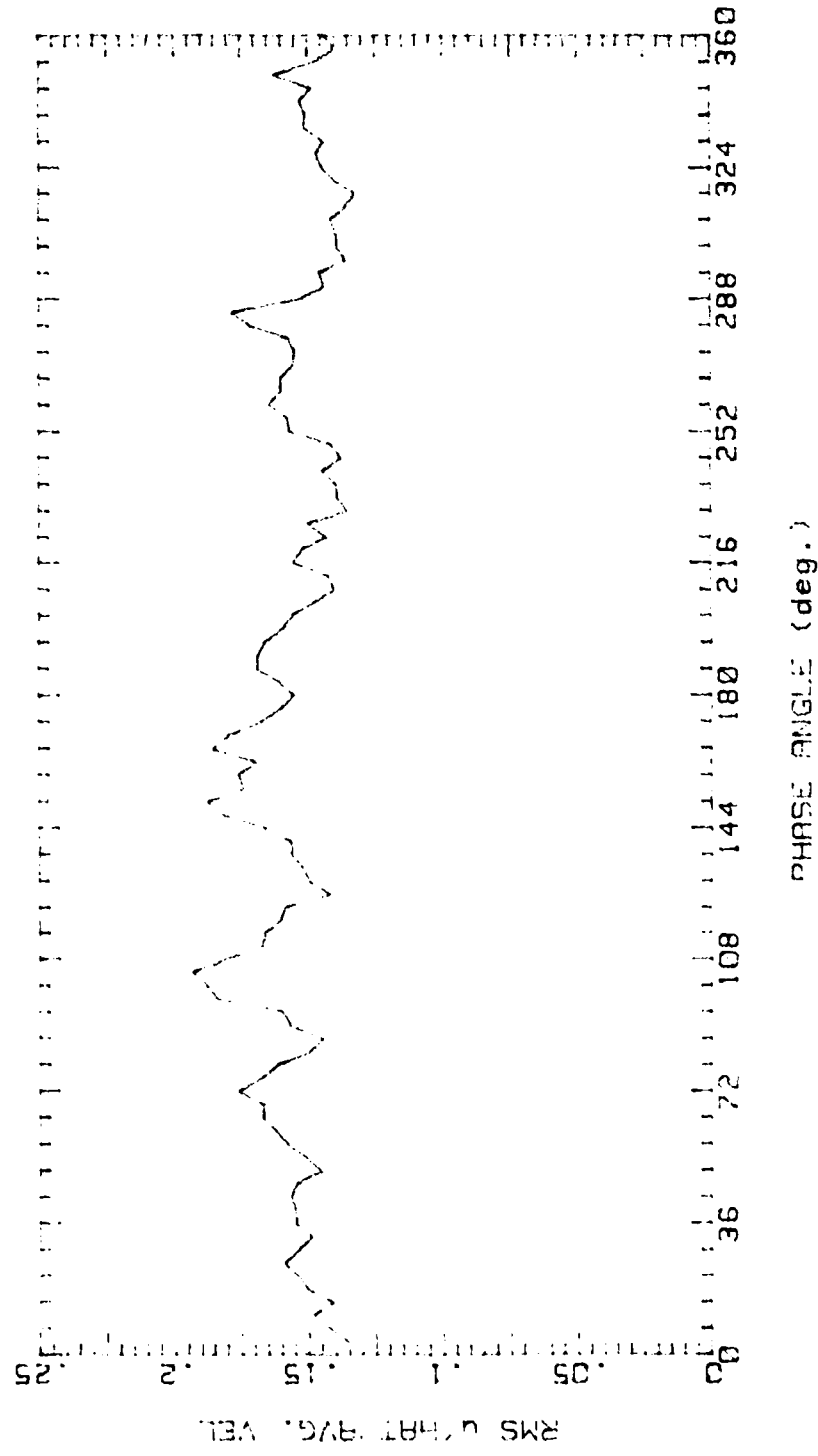


Figure 58.

2P3A2 201089.2251  
 AVG. VEL. 2.051m/s RMS VEL. .2364m/s  
 OSC. FREQ. 0Hz STR. # 0  
 BULK VEL. 2.4m/s REY. # 2005

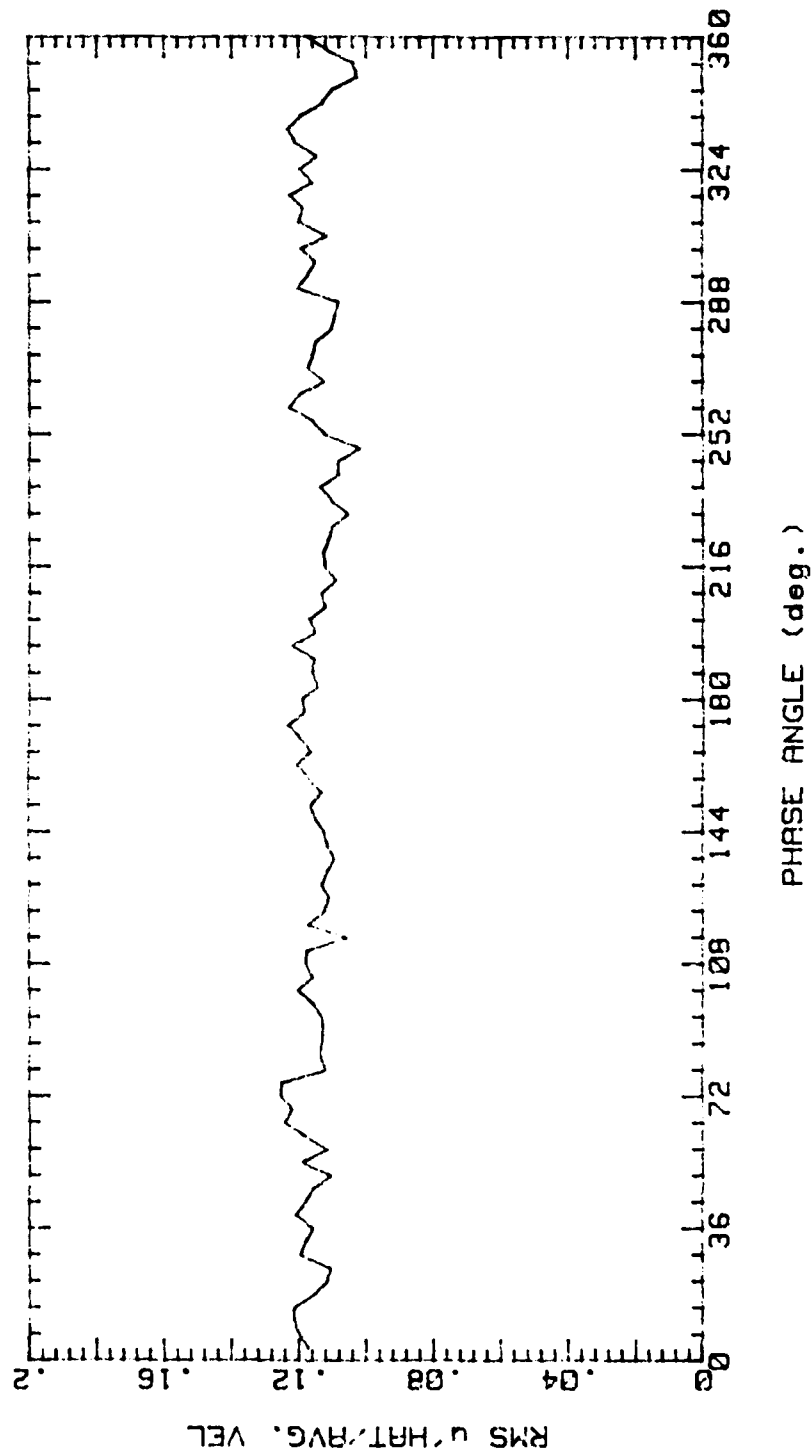


Figure 59.



2P3A3 201089.2304  
 AVG. VEL 2.744m/s RMS VEL .2122m/s  
 OSC. FREQ. 0Hz STR. # 0  
 BULK VEL. 2.4m/s REY. # 2005

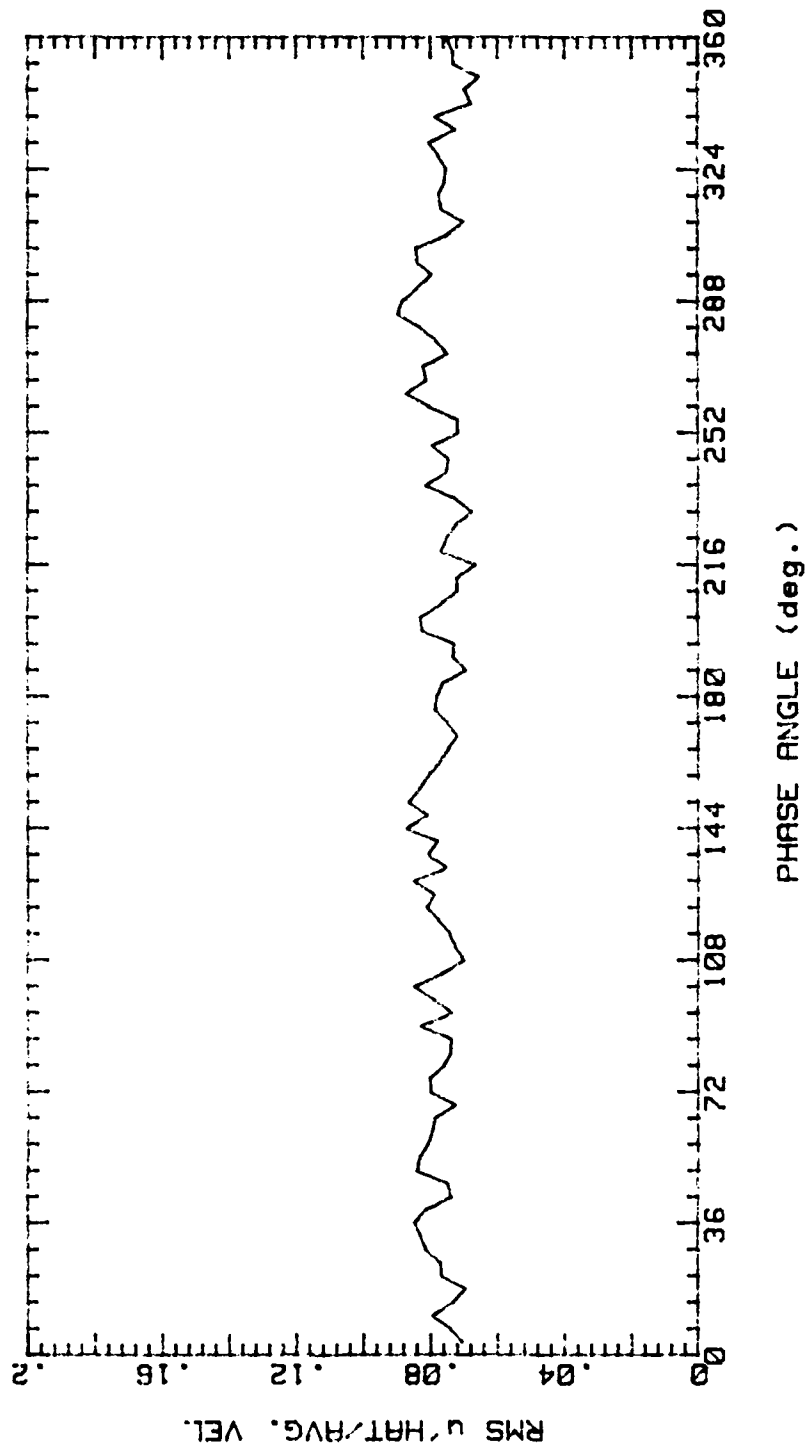


Figure 60.

2P3A4 201089.2319  
 AVG. VEL 2.976m/s RMS VEL .2489m/s  
 OSC. FREQ. 0Hz STR. # 0  
 BULK VEL. 2.4m/s REY. # 2005

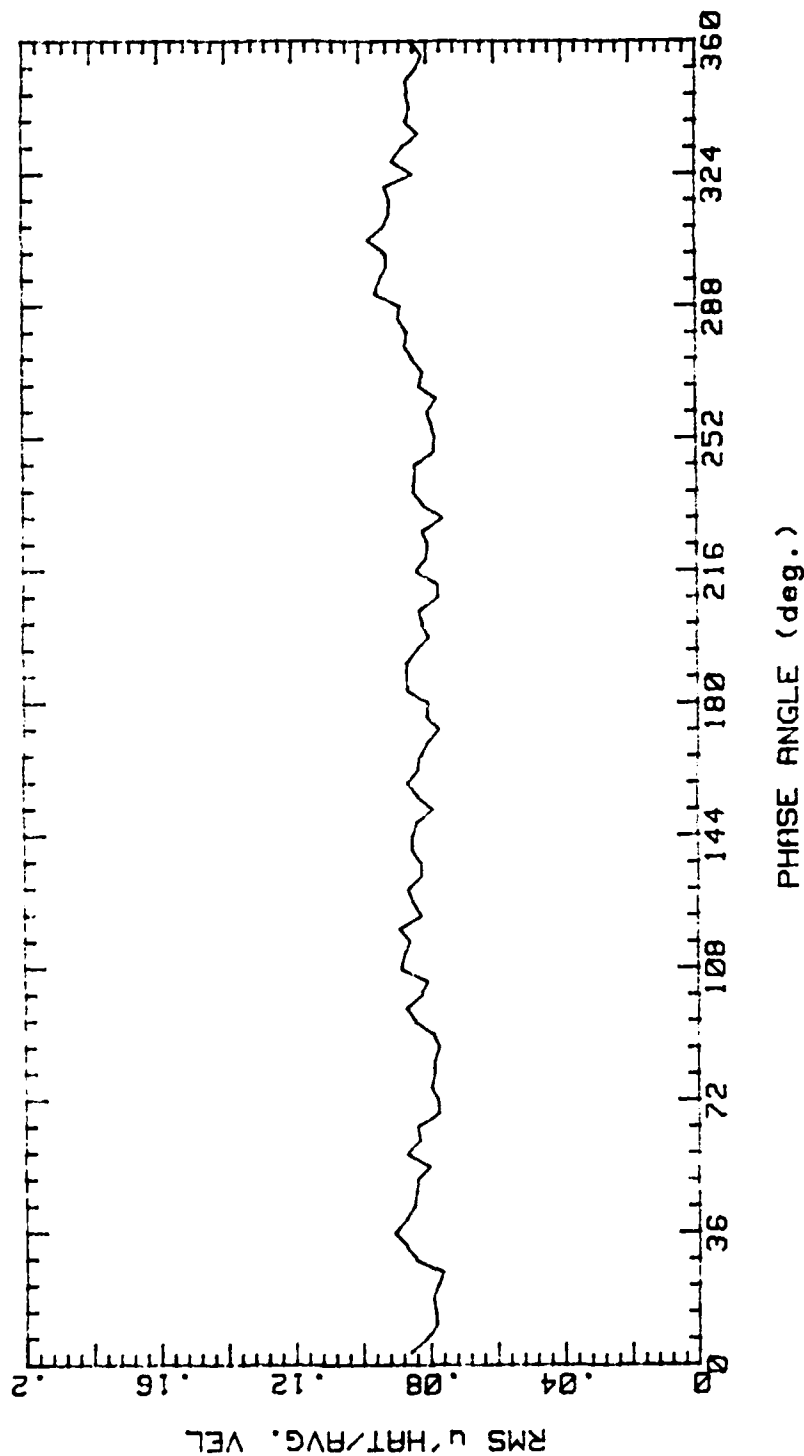


Figure 61.

2P3A5 201089.2334  
 AVG. VEL 3.4m/s RMS VEL .3048m/s  
 OSC. FREQ. 0Hz STR. # 0  
 BULK VEL. 2.4m/s REY. # 2005

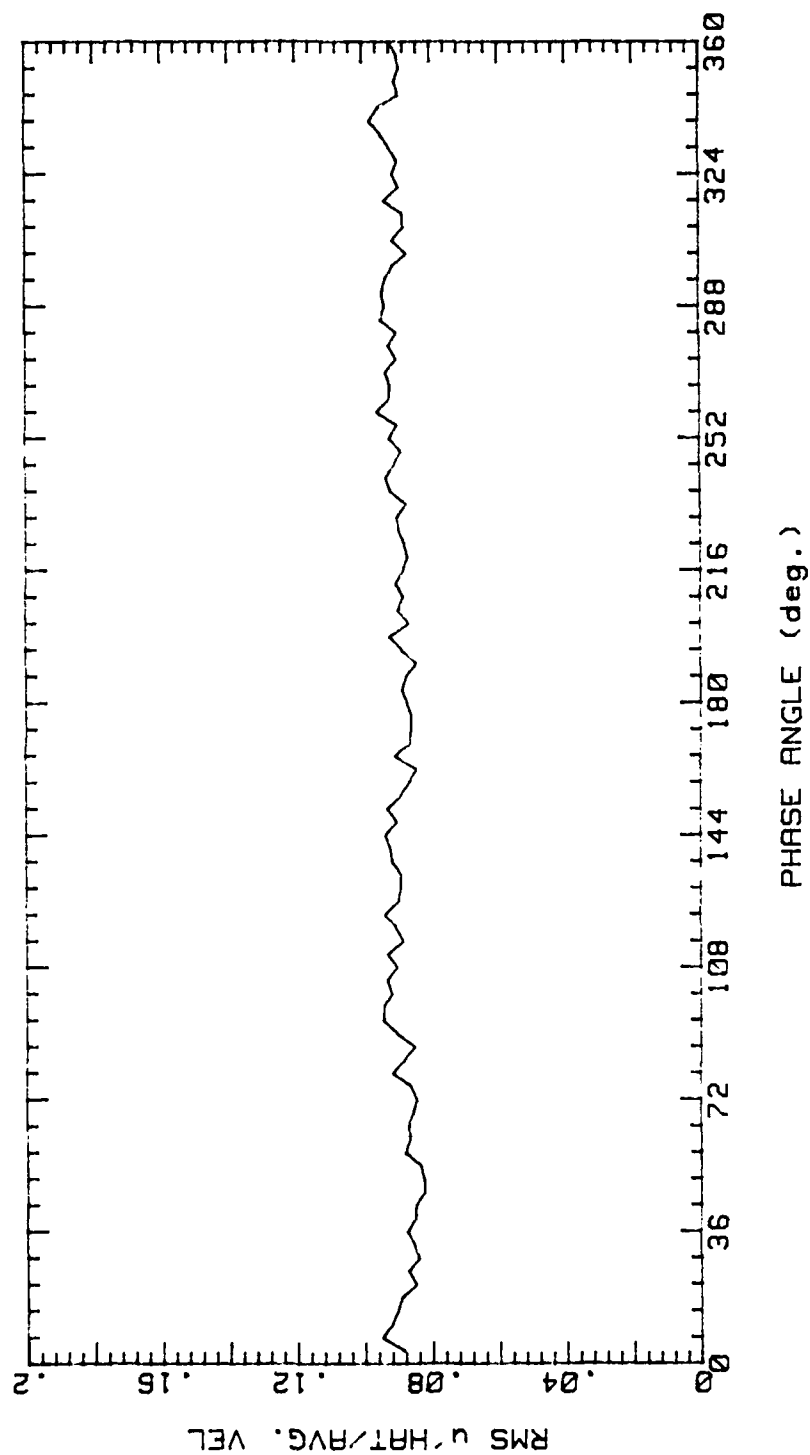


Figure 62.

2P3A6 201089.2349  
 AVG. VEL 3.103m/s RMS VEL .274m/s  
 OSC. FREQ. 0Hz STR. # 0  
 BULK VEL. 2.4m/s REY. # 2005

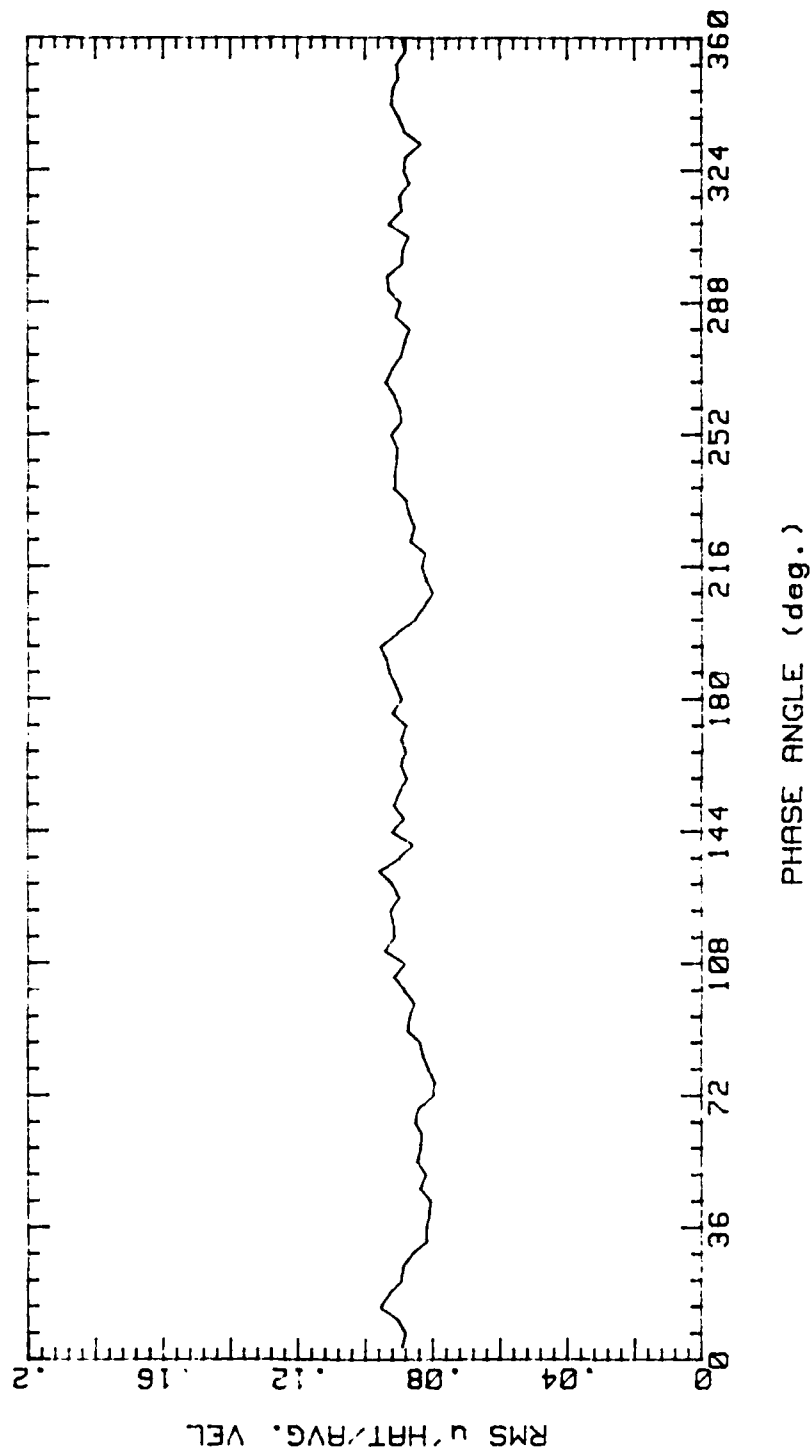


Figure 63.

2P3A7 211089.0004  
 AVG. VEL 2.792m/s RMS VEL .2149m/s  
 OSC. FREQ. 0Hz STR. # 0  
 BULK VEL. 2.4m/s REY. # 2005

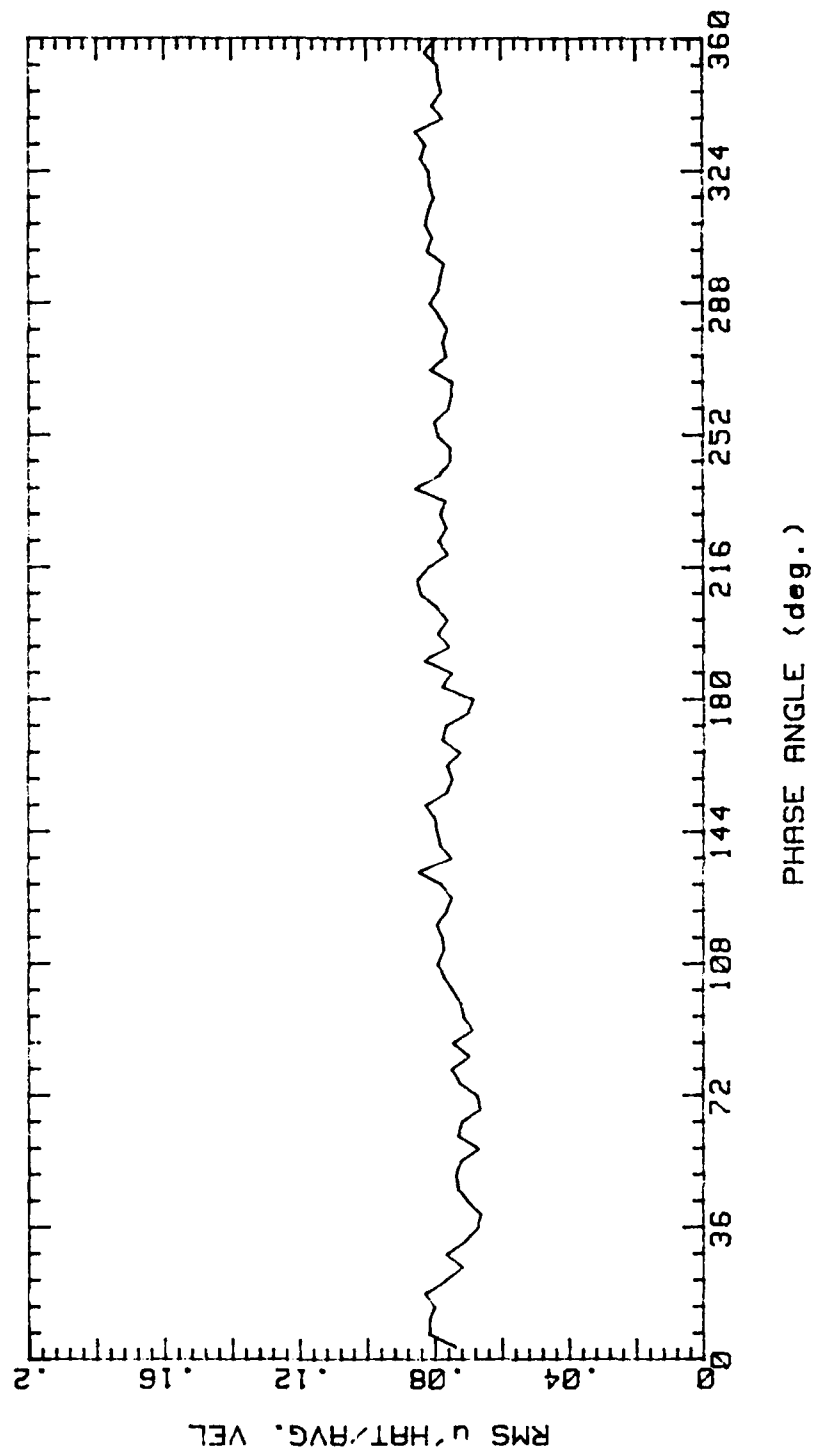


Figure 64.

2P3A8 211089.0018  
 AVG. VEL 2.129m/s RMS VEL .2231m/s  
 OSC. FREQ. 0Hz STR. # 0  
 BULK VEL. 2.4m/s REY: # 2005

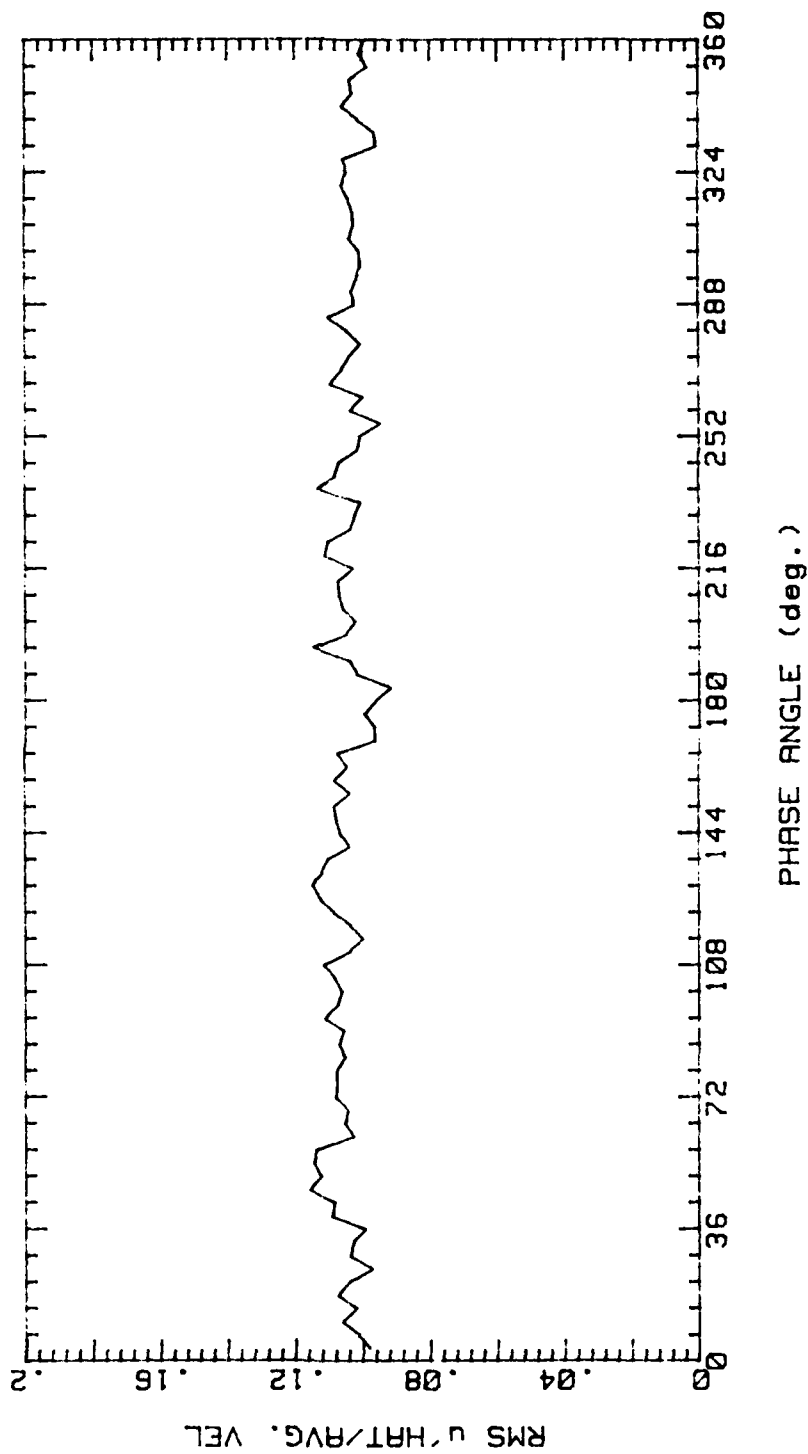


Figure 65.

2P3B1 201089.2242

AVG. VEL .651m/s RMS VEL .1629m/s  
OSC. FREQ. 2Hz STR. # .0665  
BULK VEL. 2.4m/s REY. # 2005

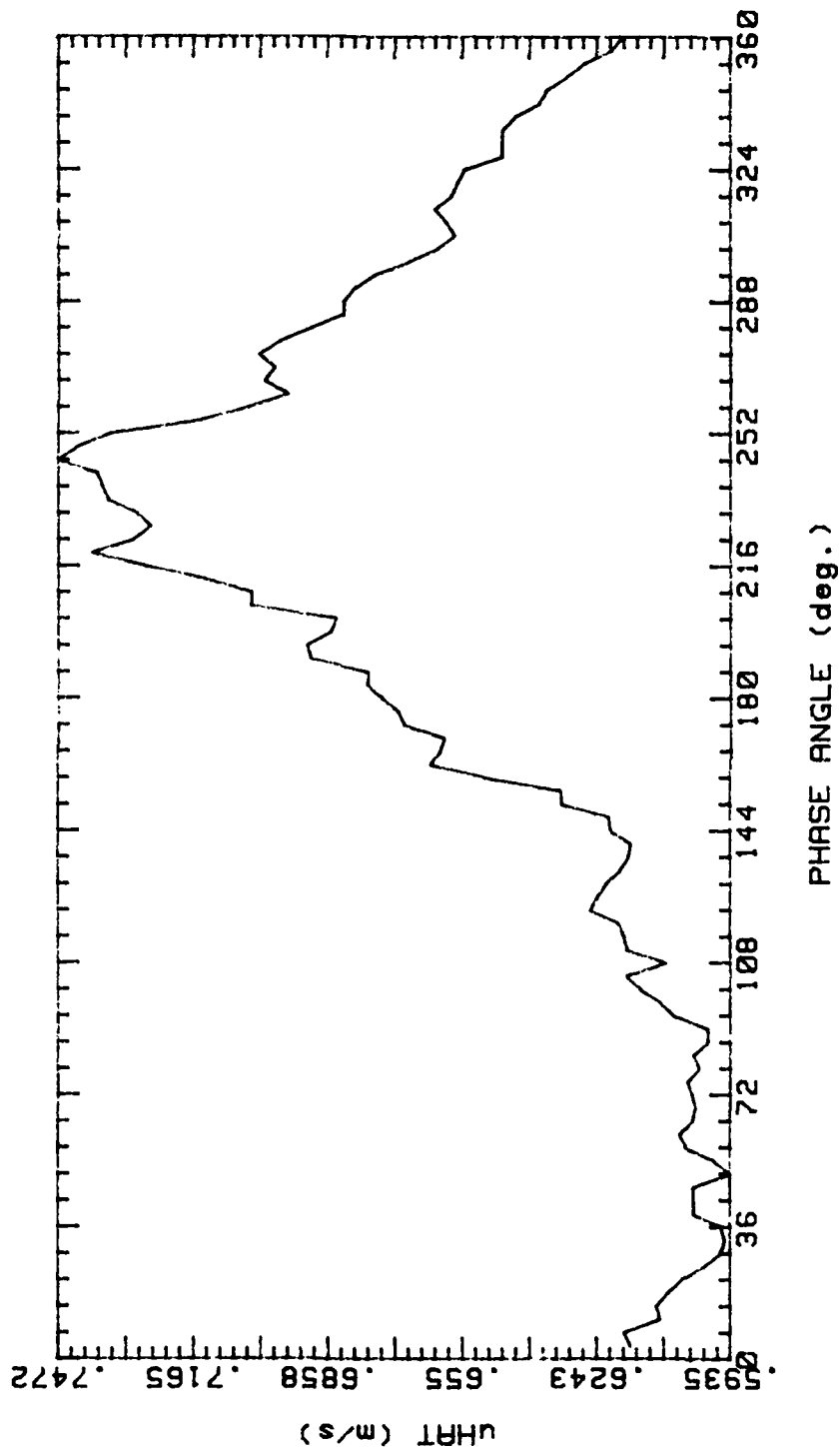


Figure 66.

2P3B2 201089.225S  
 AVG. VEL 2.049m/s RMS VEL .3241m/s  
 OSC. FREQ. 2Hz STR. # .0665  
 BULK VEL. 2.4m/s REY. # 2005

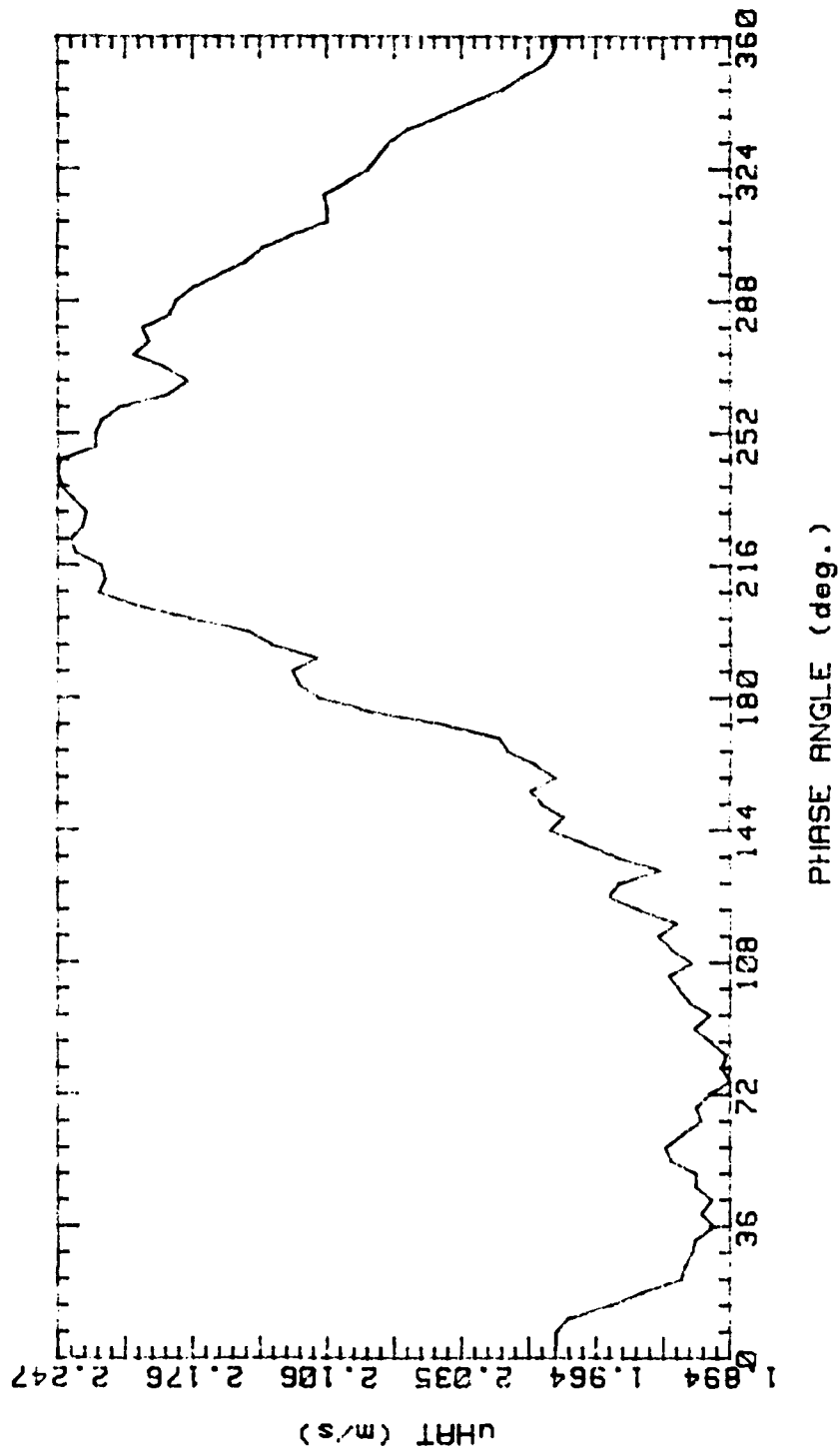


Figure 67.



2P3B3 201089.2311

AVG. VEL 2.746m/s RMS VEL .3107m/s  
OSC. FREQ. 2Hz STR. # .0665  
BULK VEL. 2.4m/s REY. # 2005

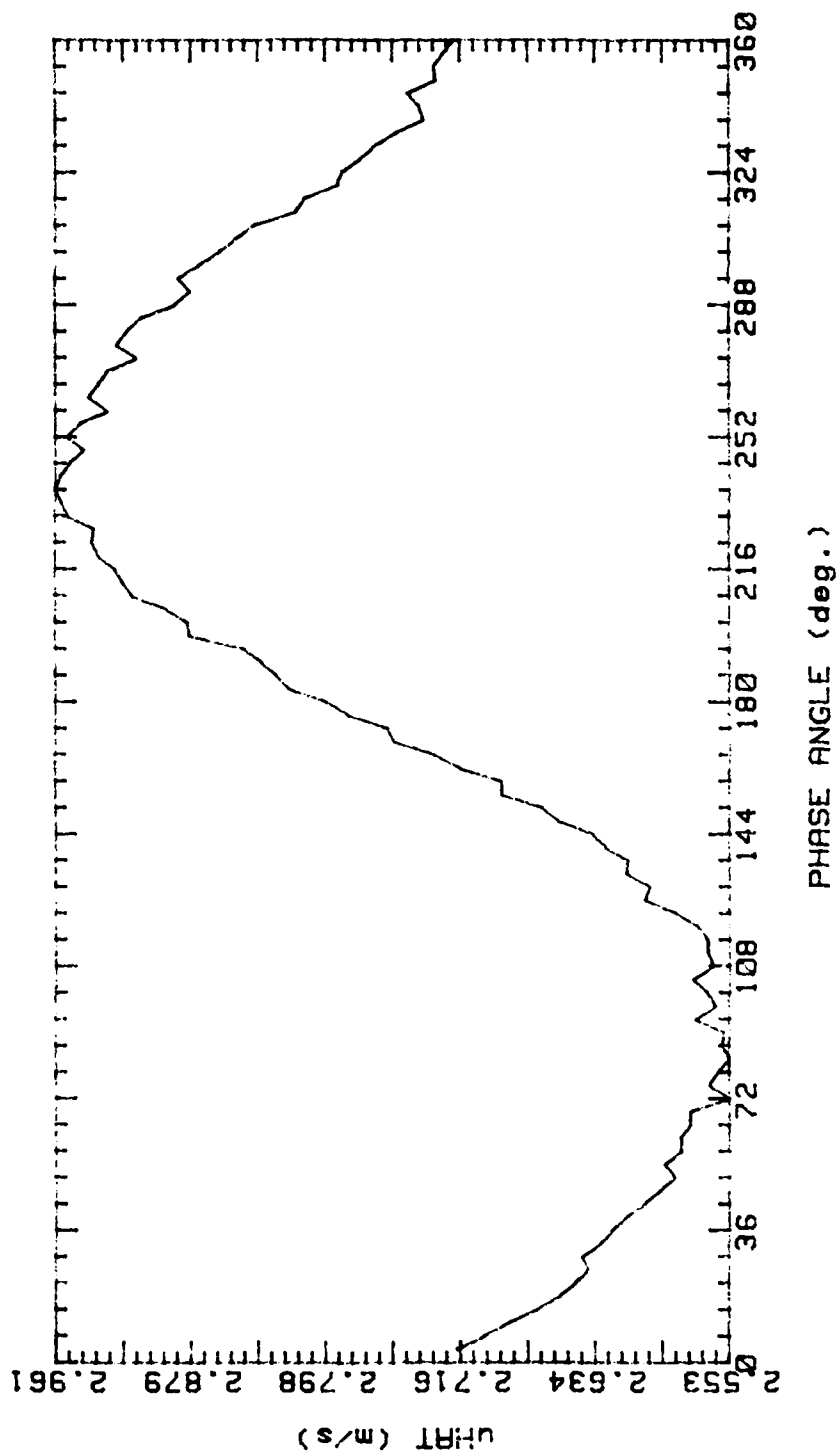


Figure 68.

2P3B4 201089.2326  
 AVG. VEL 2.978m/s RMS VEL .3052m/s  
 OSC. FREQ. 2Hz STR. # .0665  
 BULK VEL. 2.4m/s REY. # 2005

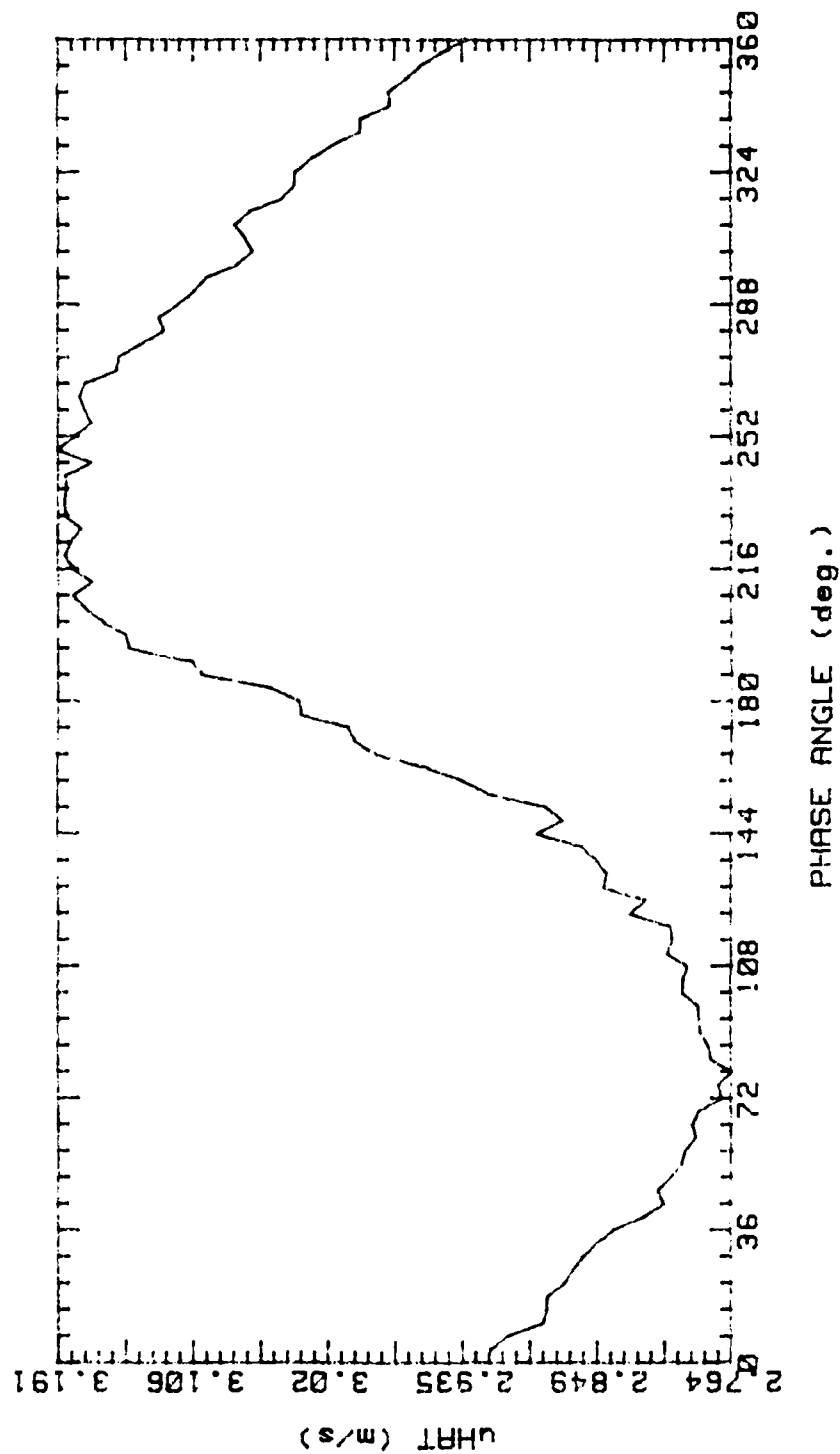


Figure 69.

2P3B5 201089.234

AVG. VEL 3.404m/s RMS VEL .3718m/s  
OSC. FREQ. 2Hz STR. # .0665  
BULK VEL. 2.4m/s REY. # 2005

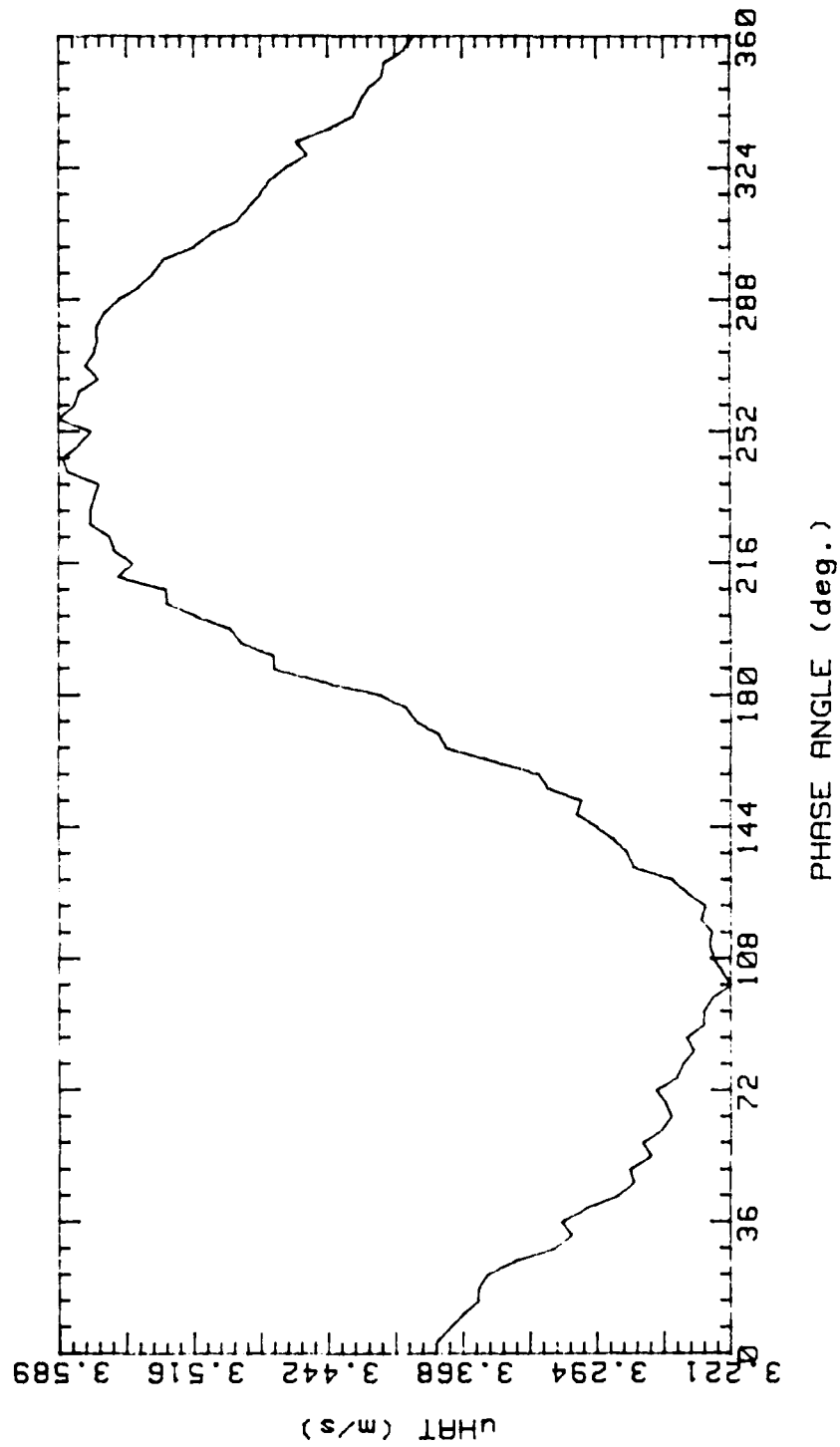


Figure 70.

2P3B6 201089.2356

AVG. VEL 3.106m/s RMS VEL .3423m/s  
OSC. FREQ. 2Hz STR. # .0665  
BULK VEL. 2.4m/s REY. # 2005

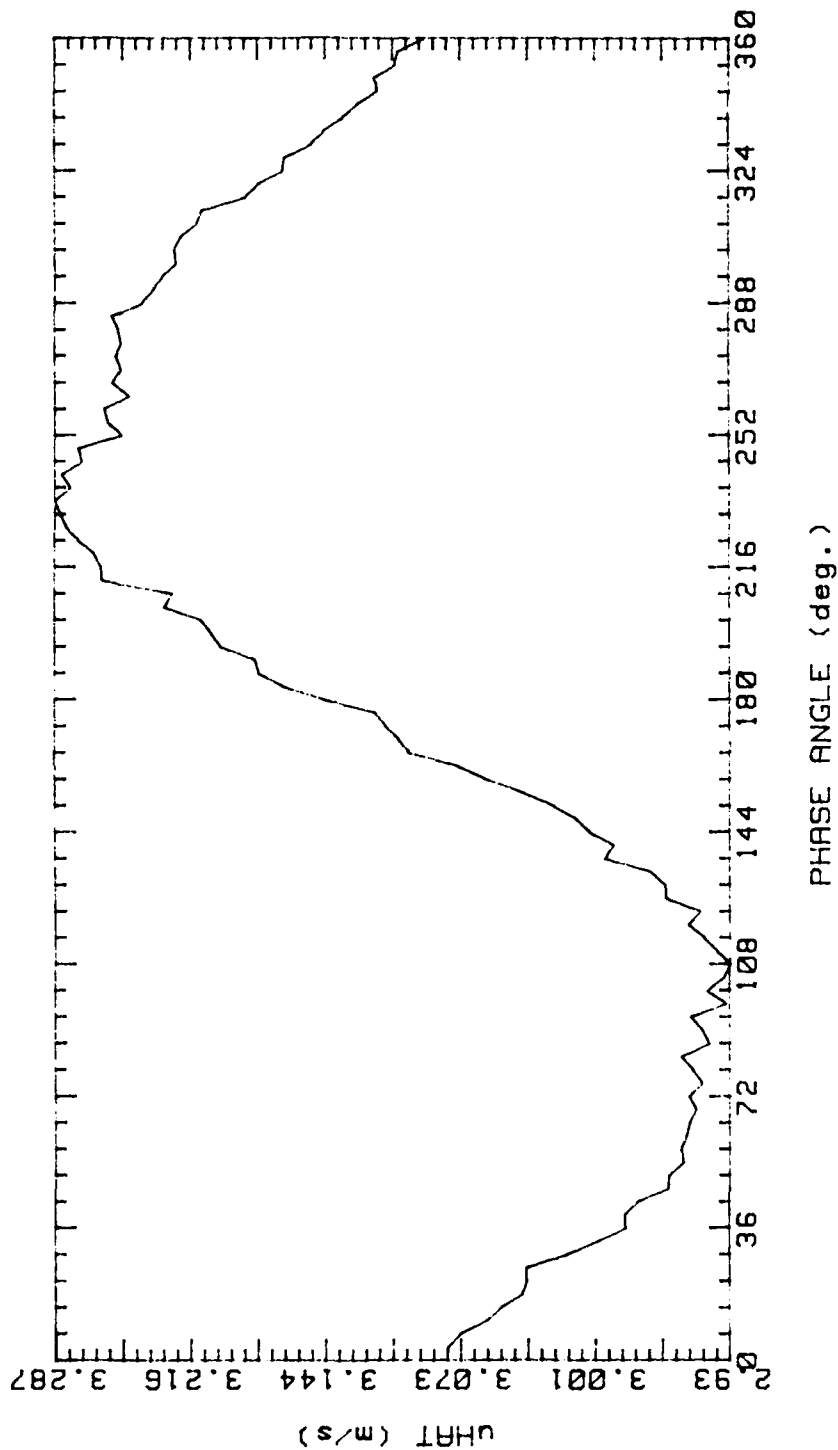


Figure 71.

2P3B7 211089.0011

AVG. VEL 2.795m/s RMS VEL .3078m/s

OSC. FREQ. 2Hz STR. # .0665

BULK VEL. 2.4m/s REY. # 2005

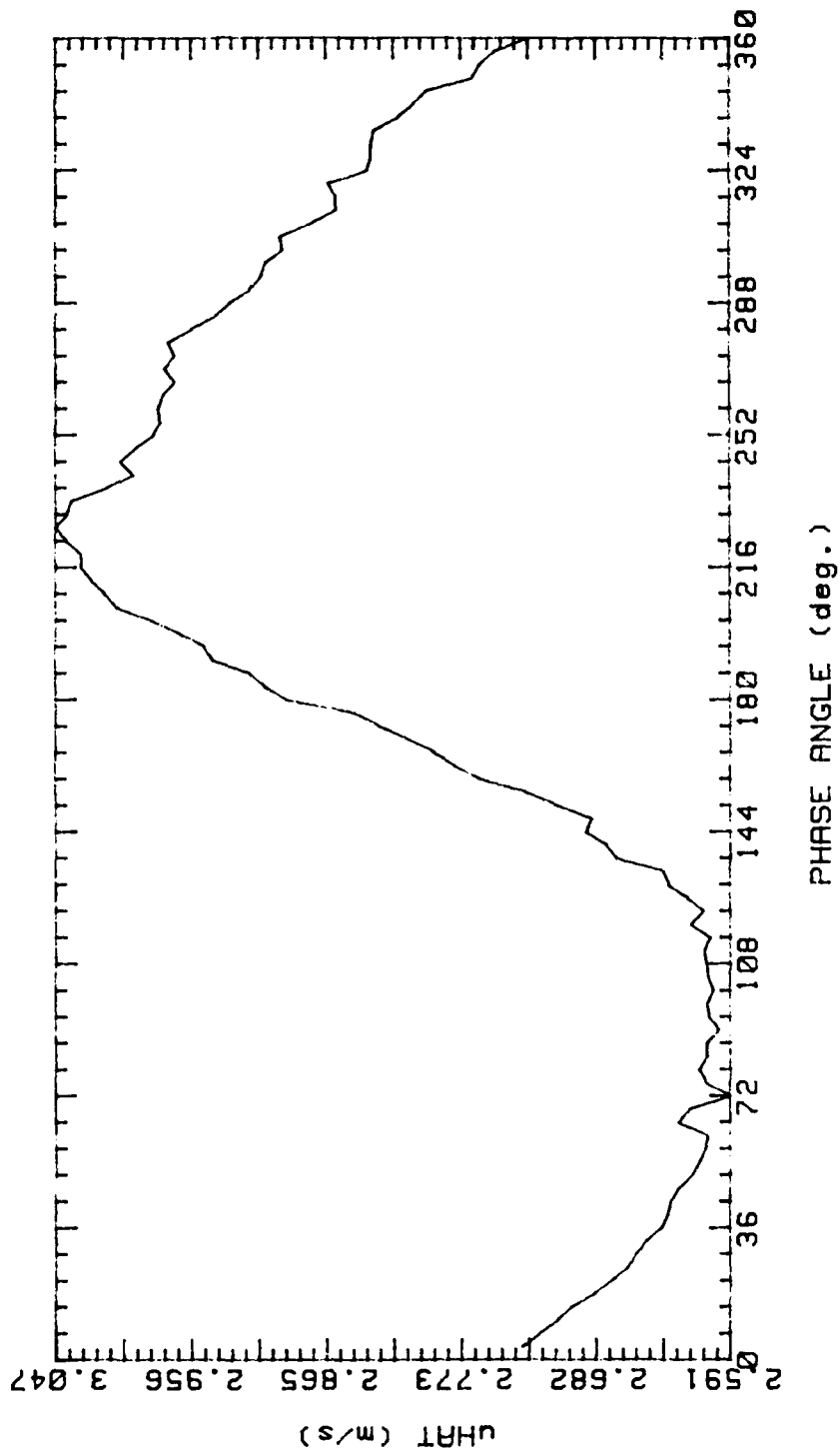


Figure 72.

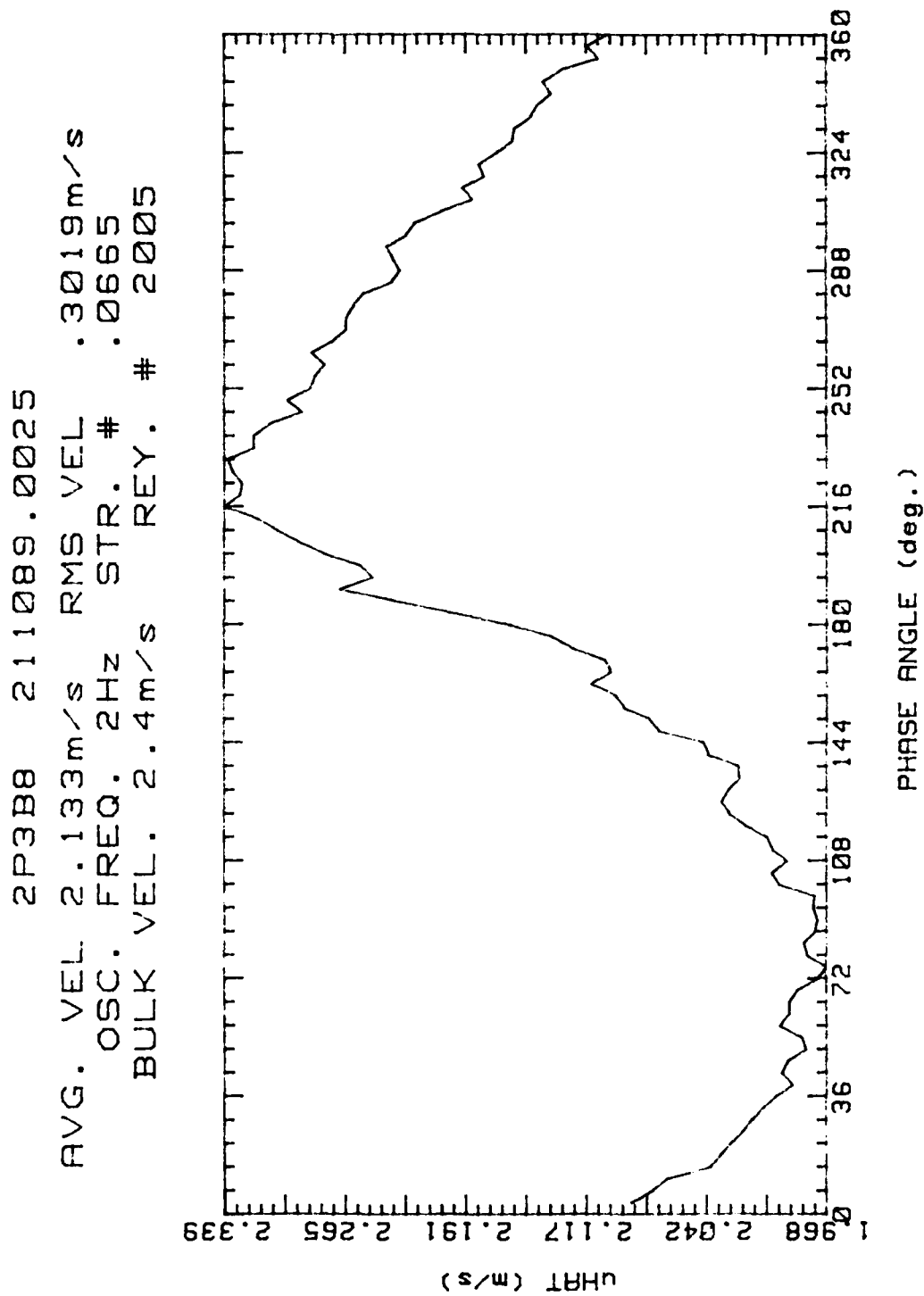


Figure 73.

2P3B1 201089.2242  
 AVG. VEL .651m/s RMS VEL .1629m/s  
 OSC. FREQ. 2Hz STR. # .0665  
 BULK VEL. 2.4m/s REY. # 2005

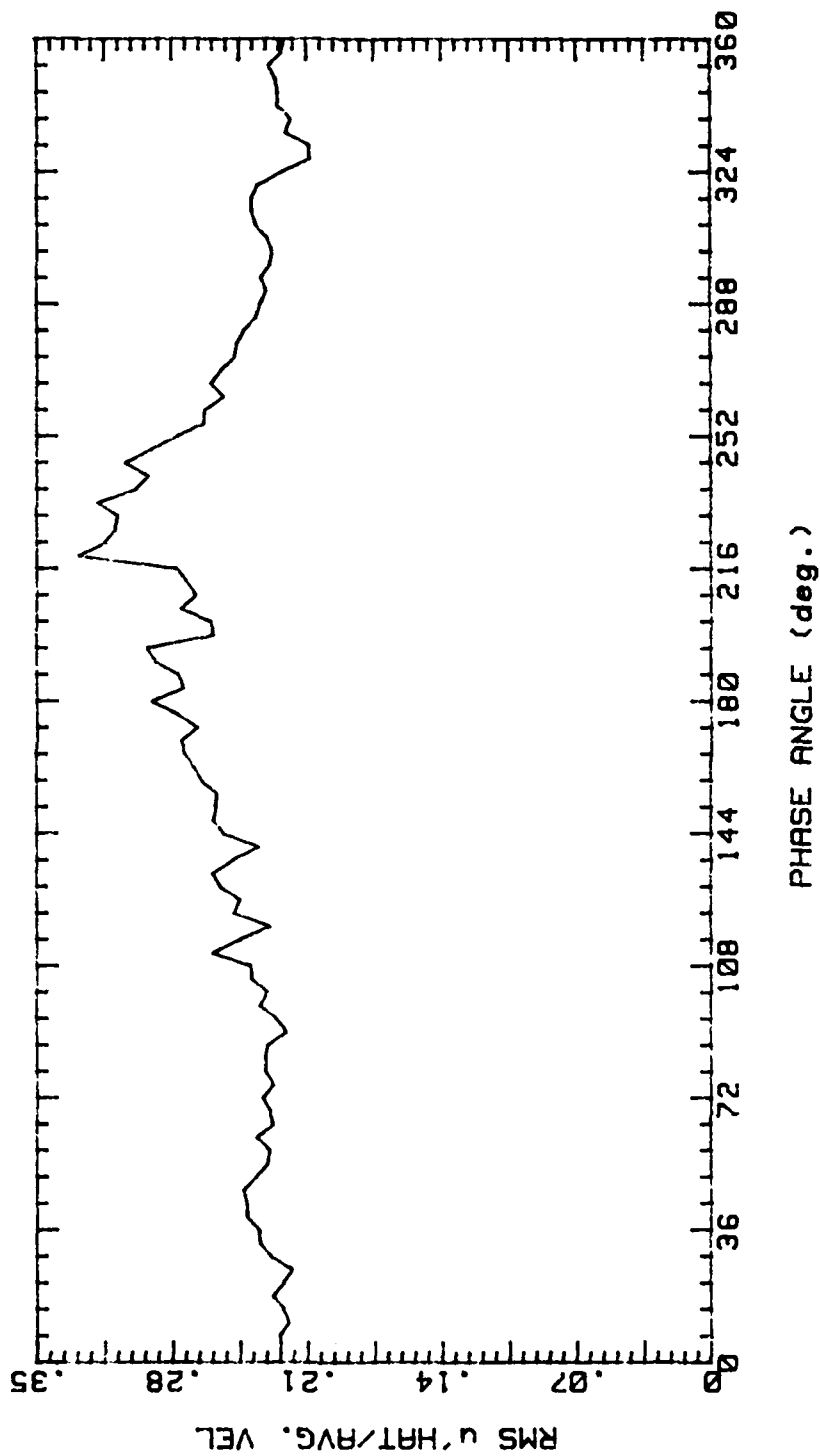


Figure 74.

2P3B2 201089.2256  
 AVG. VEL 2.049m/s RMS VEL .3241m/s  
 OSC. FREQ. 2Hz STR. # .0665  
 BULK VEL. 2.4m/s REY. # 2005

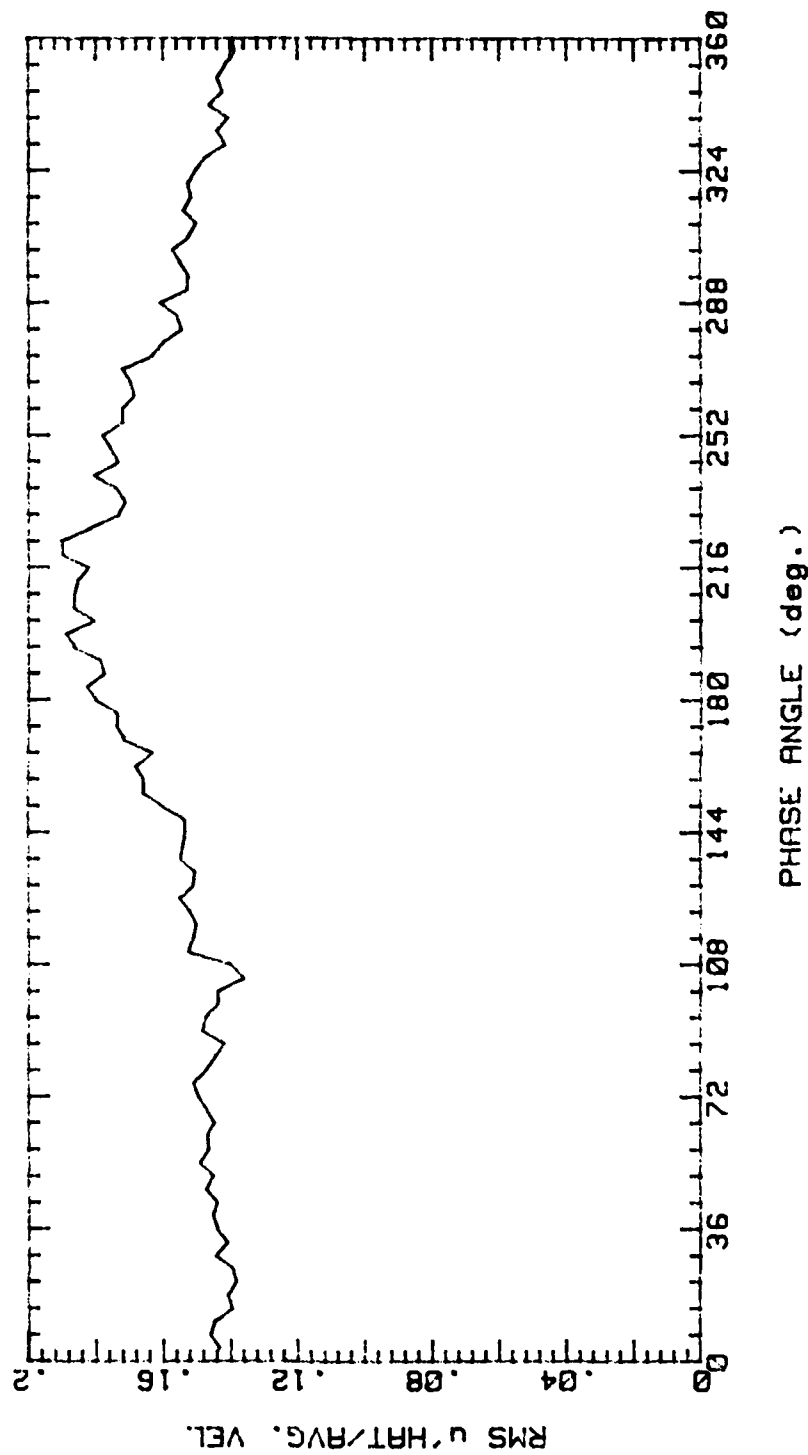


Figure 75.



2P3B3 201089.2311  
 AVG. VEL 2.746m/s RMS VEL .3107m/s  
 OSC. FREQ. 2Hz STR. # .0665  
 BULK VEL. 2.4m/s REY. # 2005

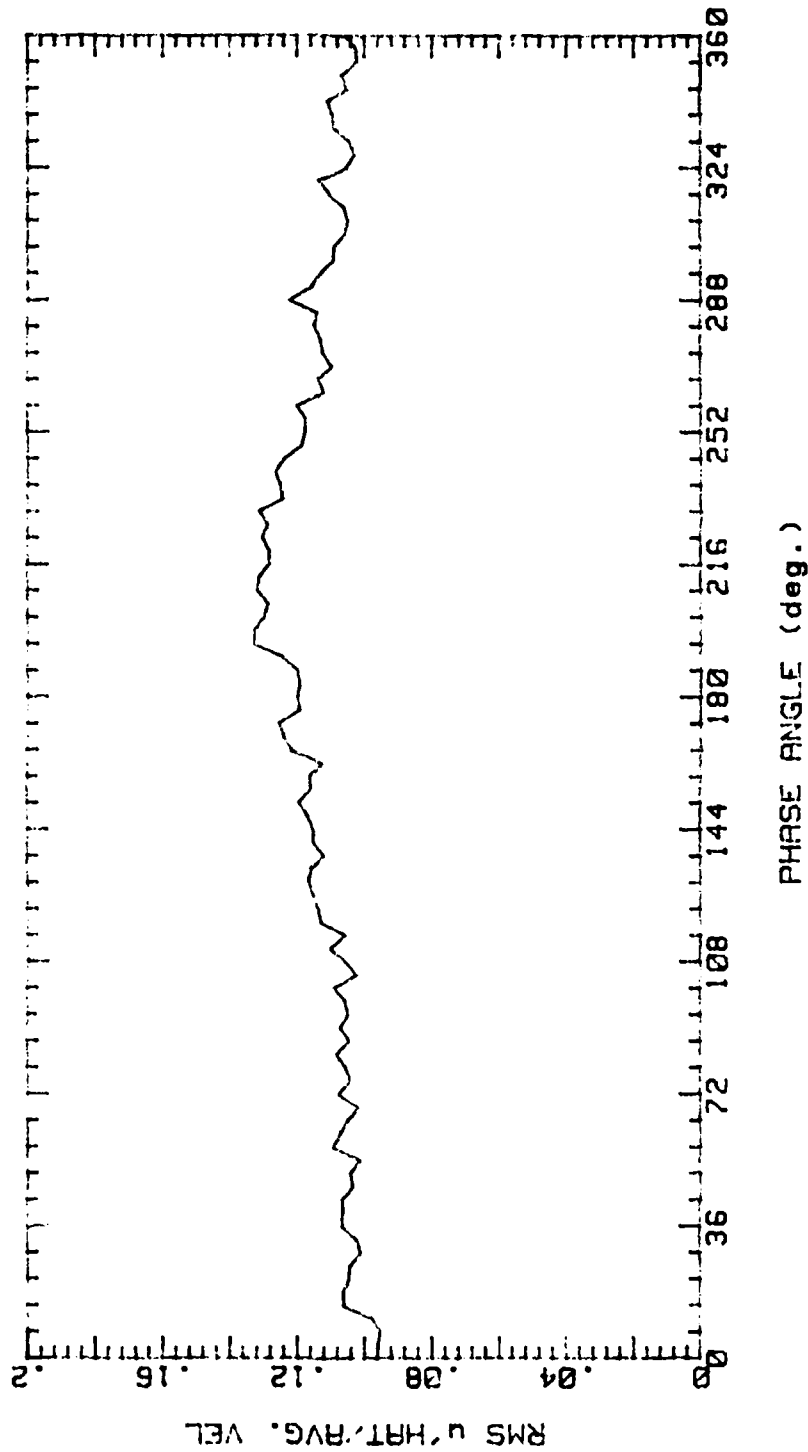


Figure 76.

2P3B4 201089.2326  
 AVG. VEL 2.978m/s RMS VEL .3052m/s  
 OSC. FREQ. 2Hz STR. # .0665  
 BULK VEL. 2.4m/s REY. # 2005

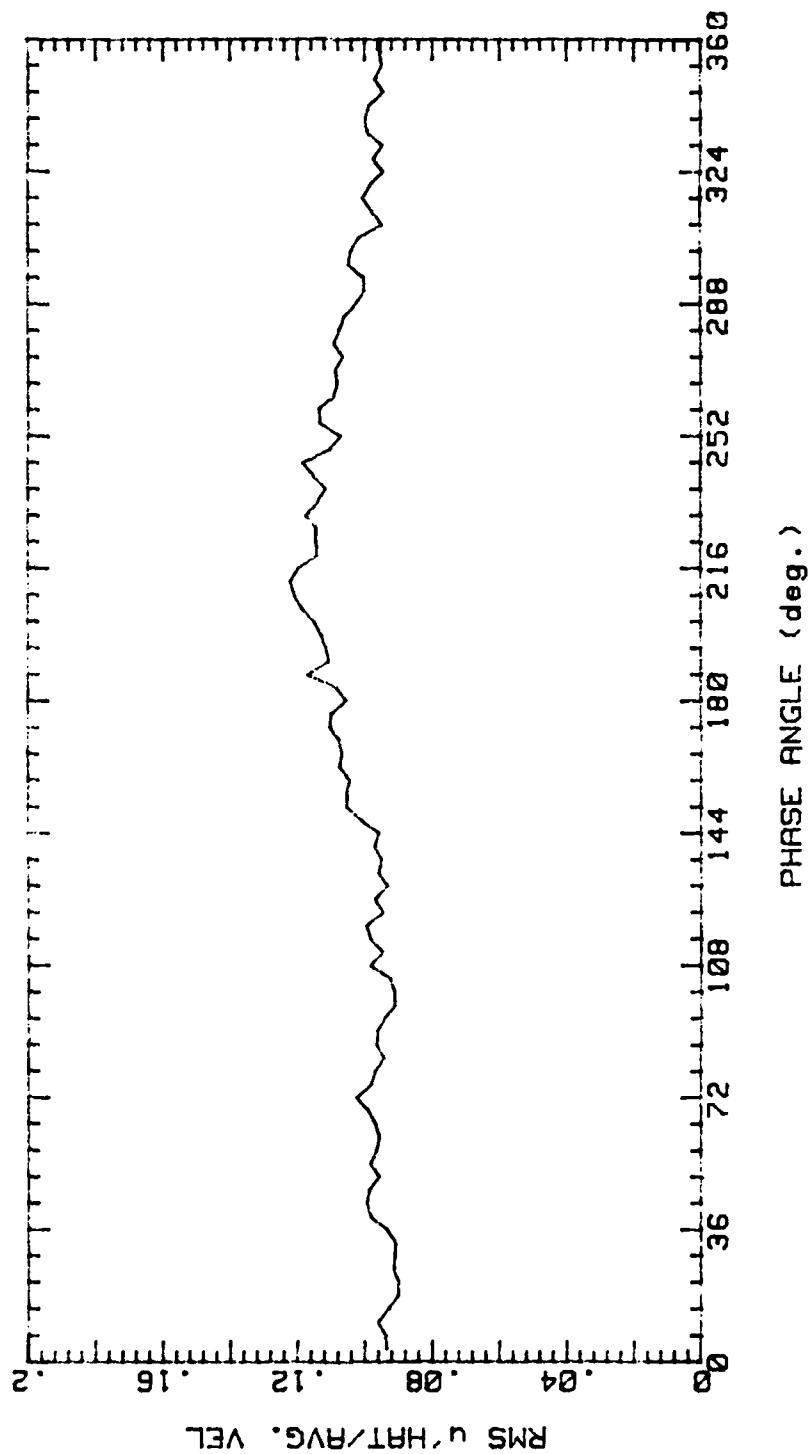


Figure 77.

2P3B5 201089.234  
 AVG. VEL 3.404m/s RMS VEL .3718m/s  
 OSC. FREQ. 2Hz STR. # .0665  
 BULK VEL. 2.4m/s REY. # 2005

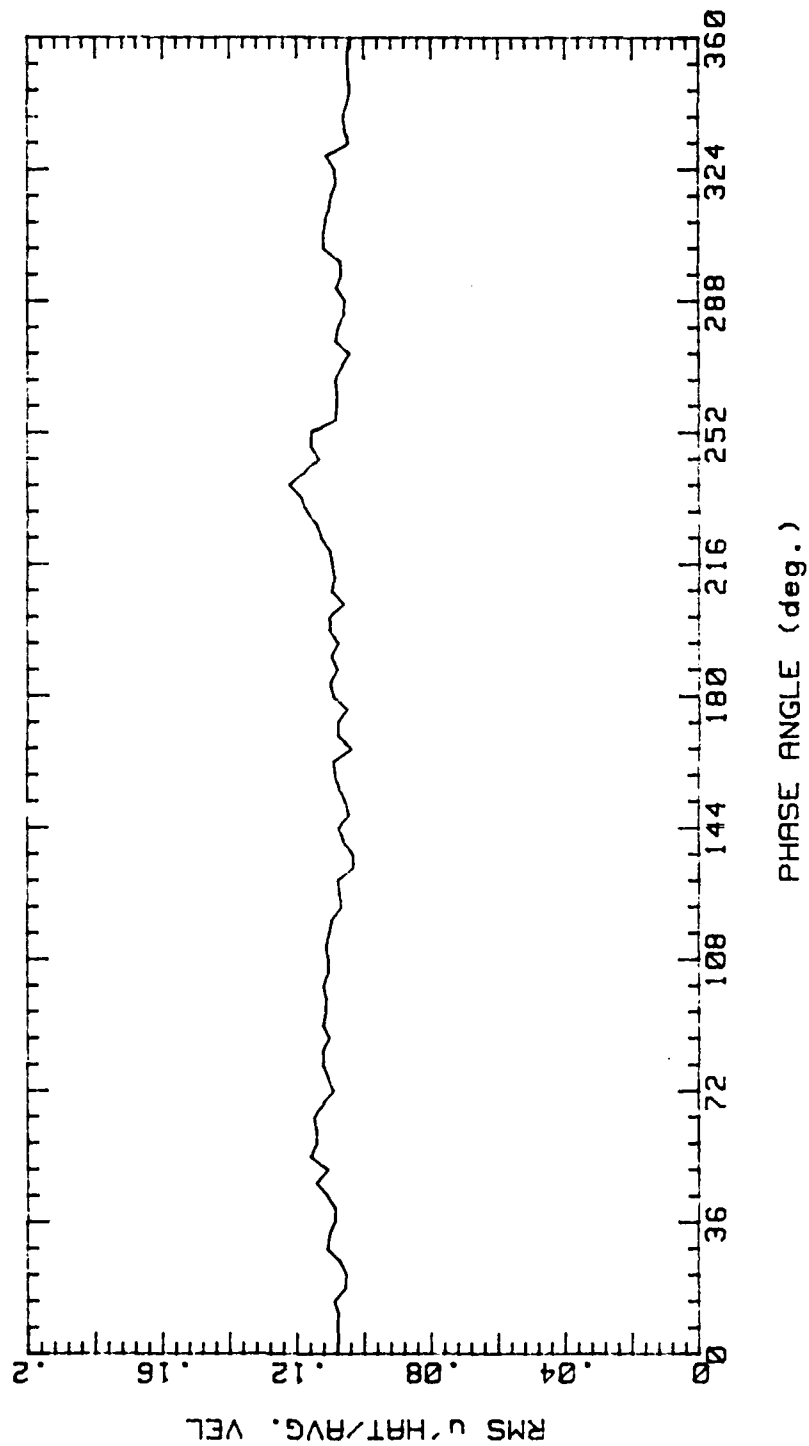


Figure 78.

2P3B6 201089.2356  
 AVG. VEL 3.106m/s RMS VEL .3423m/s  
 OSC. FREQ. 2Hz STR. # .0665  
 BULK VEL. 2.4m/s REY. # 2005

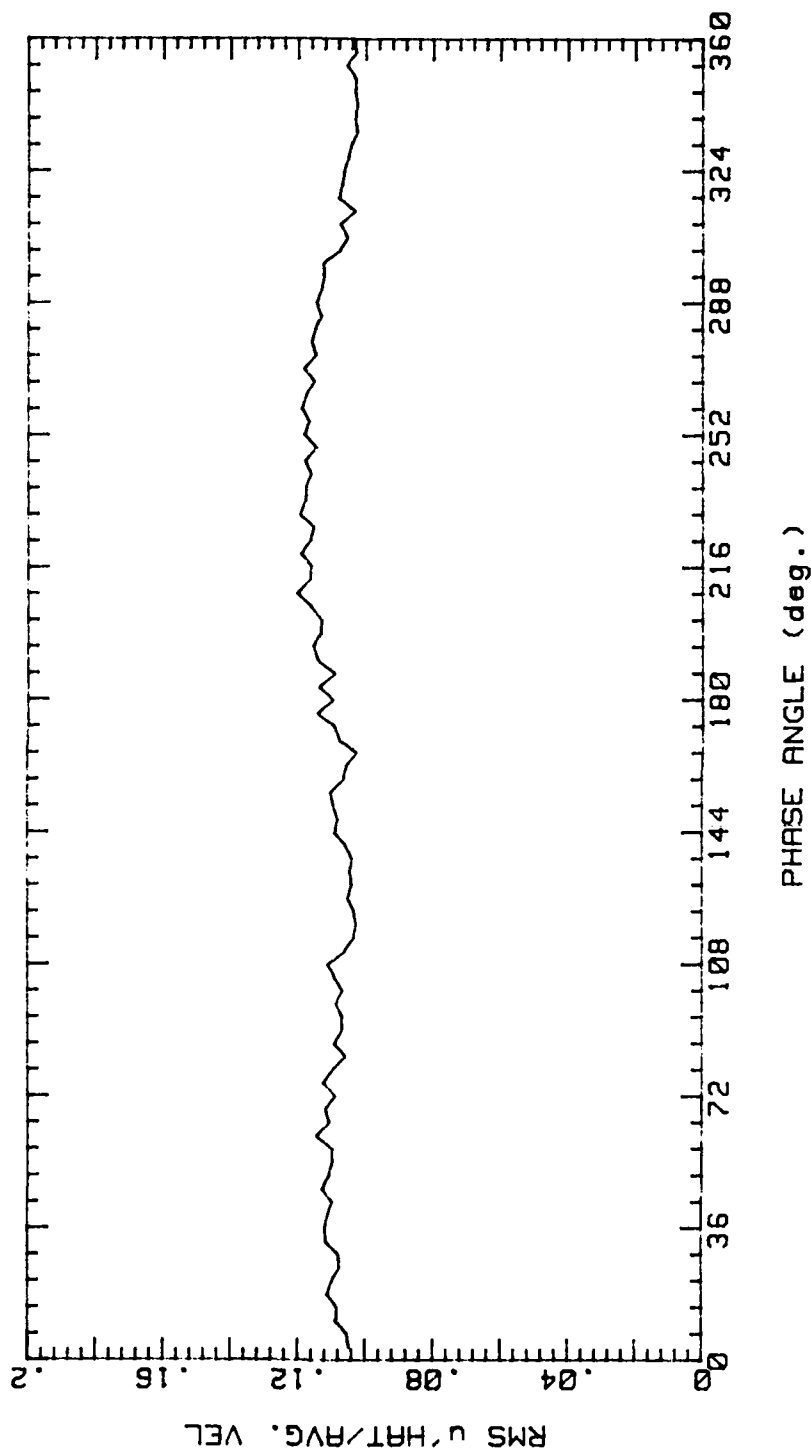


Figure 79.

2P3B7 211089.0011  
 AVG. VEL 2.795m/s RMS VEL .3078m/s  
 OSC. FREQ. 2Hz STR. # .0665  
 BULK VEL. 2.4m/s REY. # 2005

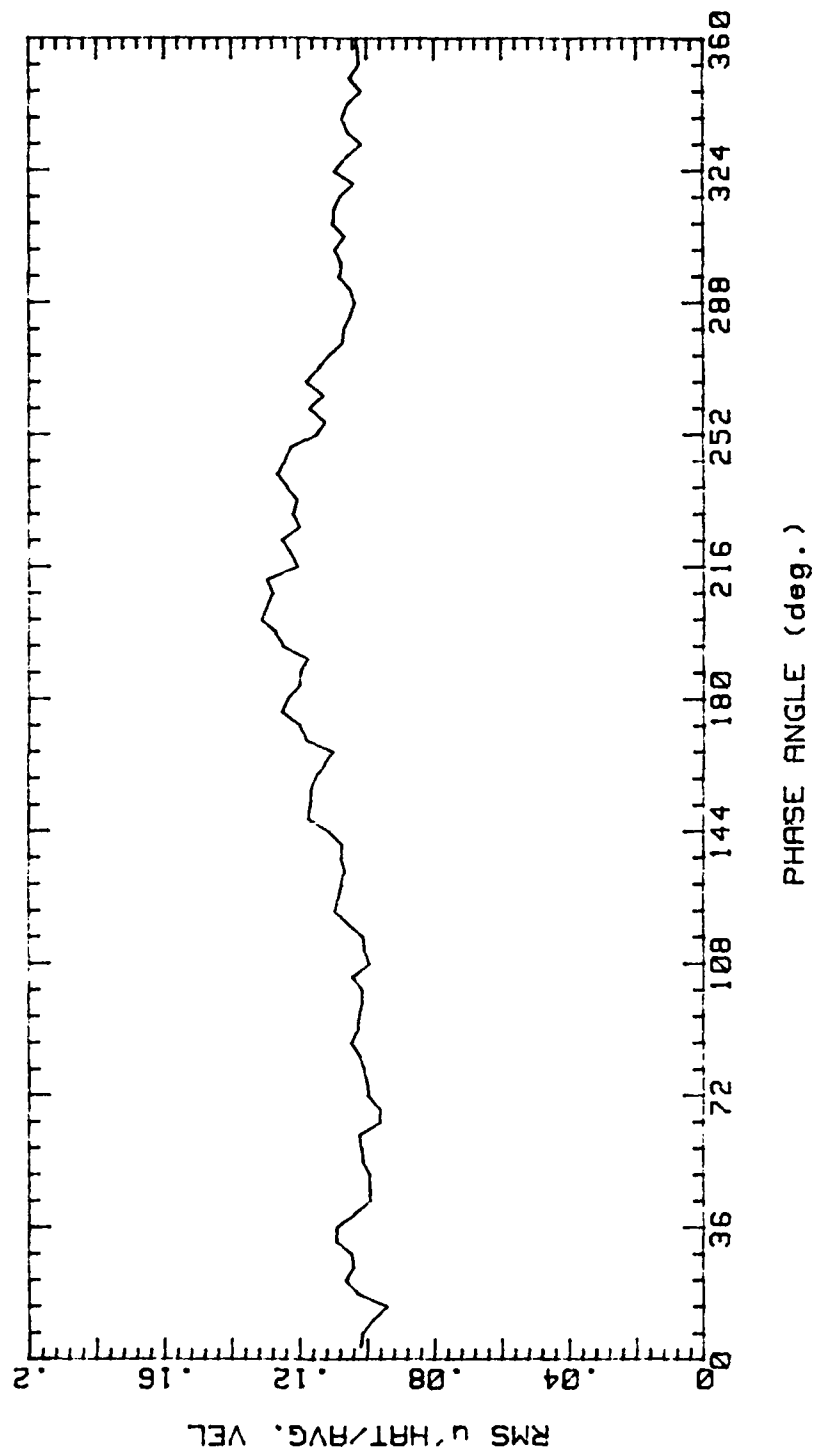


Figure 80.

2P3B8 211089.0025  
 AVG. VEL 2.133m/s RMS VEL .3019m/s  
 OSC. FREQ. 2Hz STR. # .0665  
 BULK VEL. 2.4m/s REY. # 2005

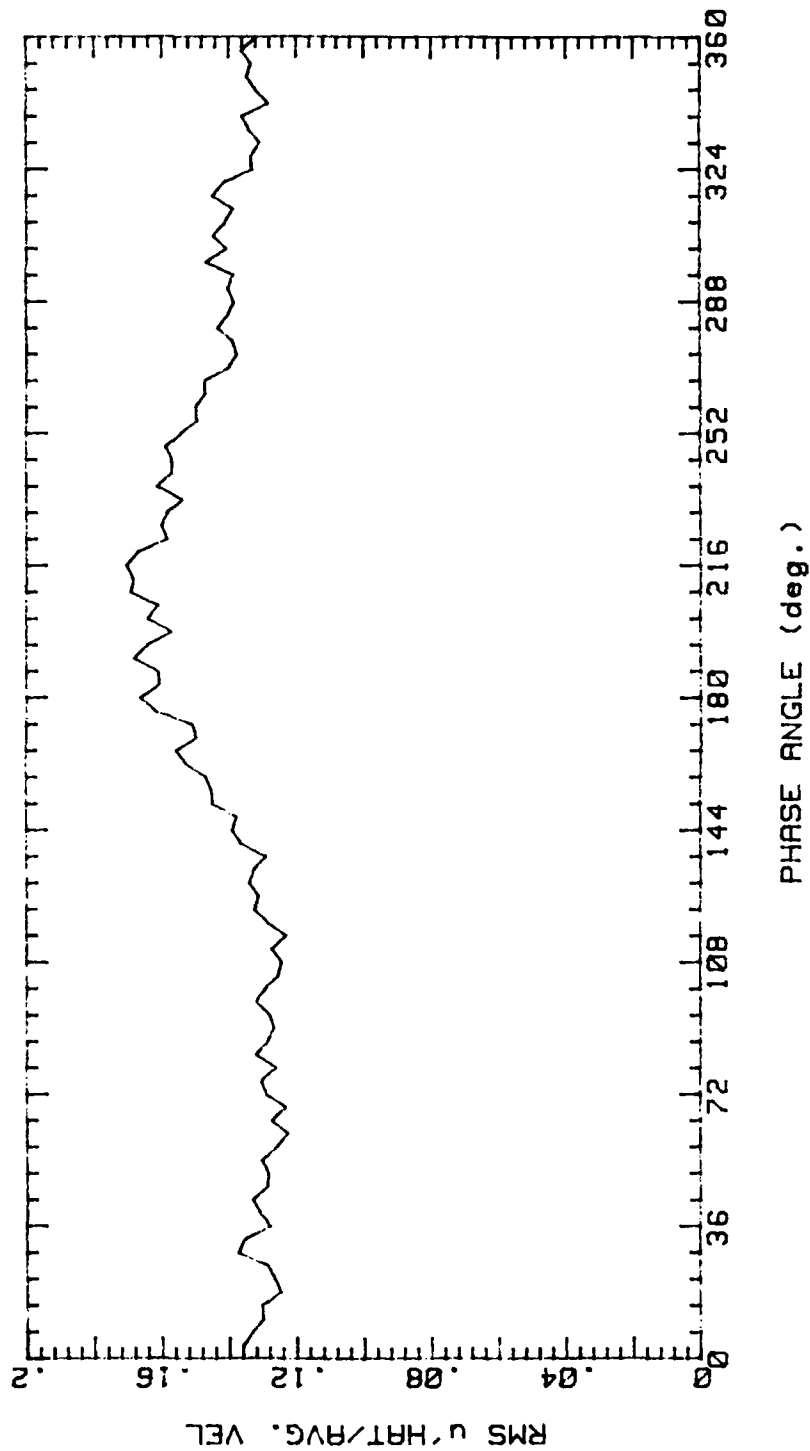


Figure 81.

Peak to Peak Magnitude of 2 Hz Phase  
Averaged Velocity as a Function of  $y/d$

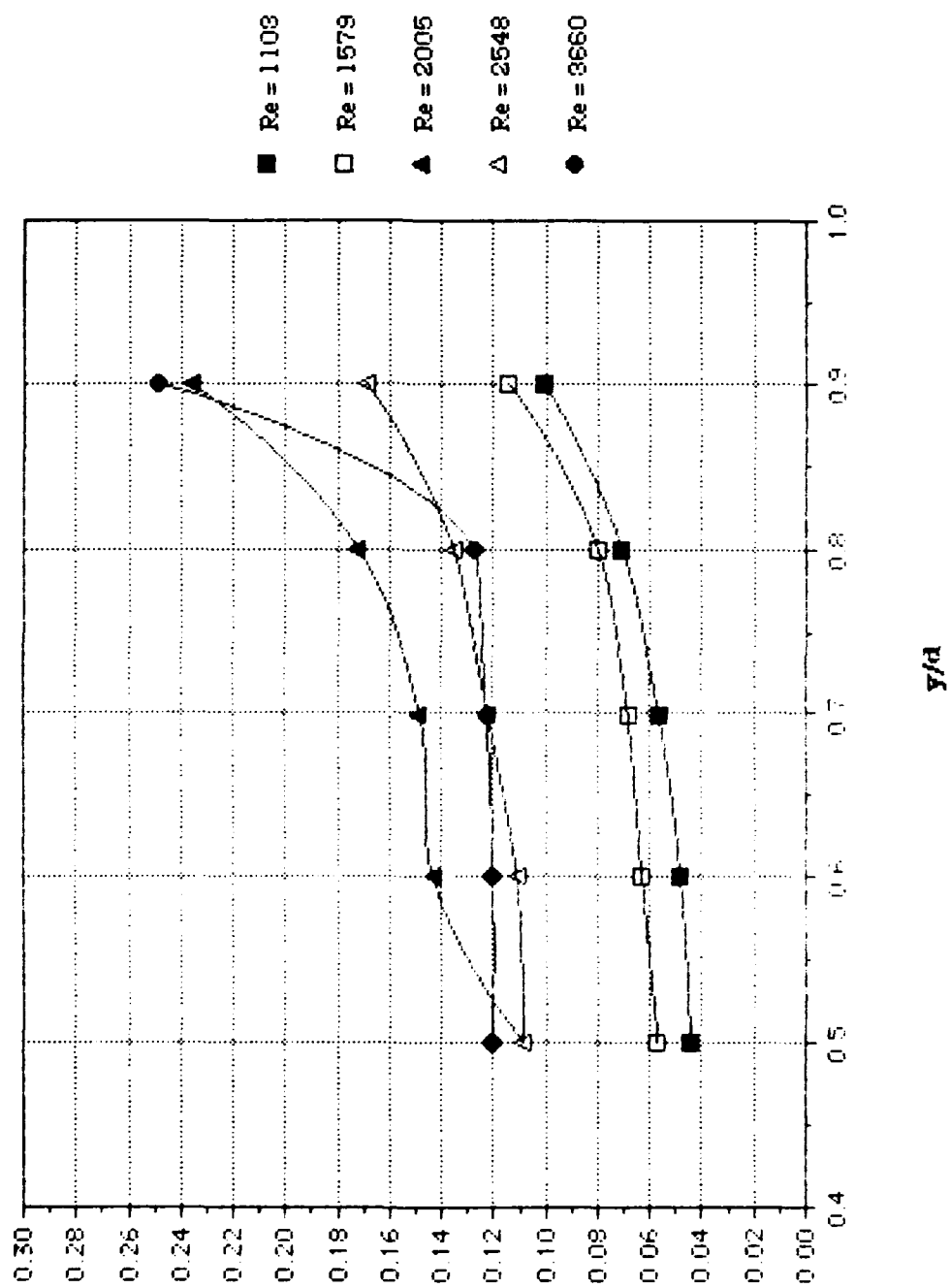


Figure 82.

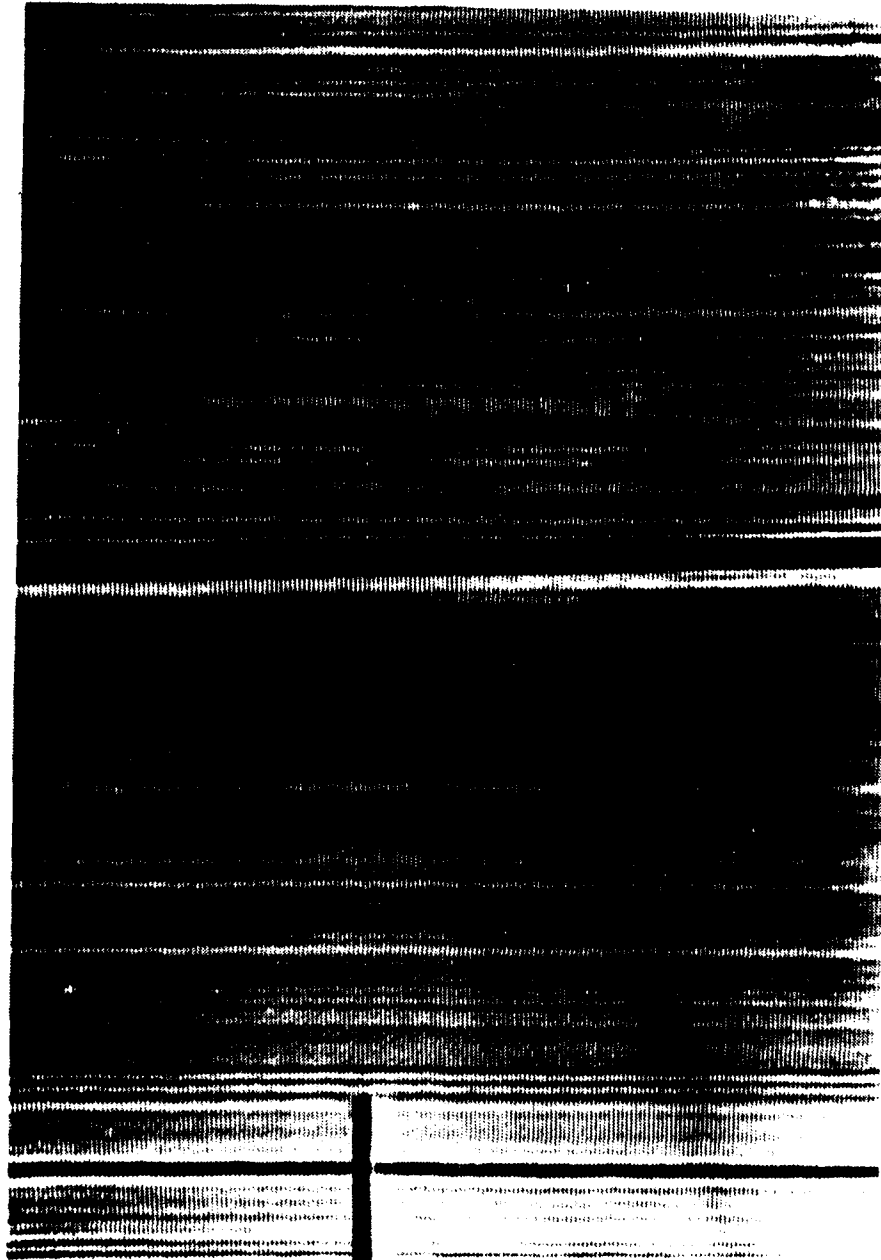


Figure 83. Re = 1136



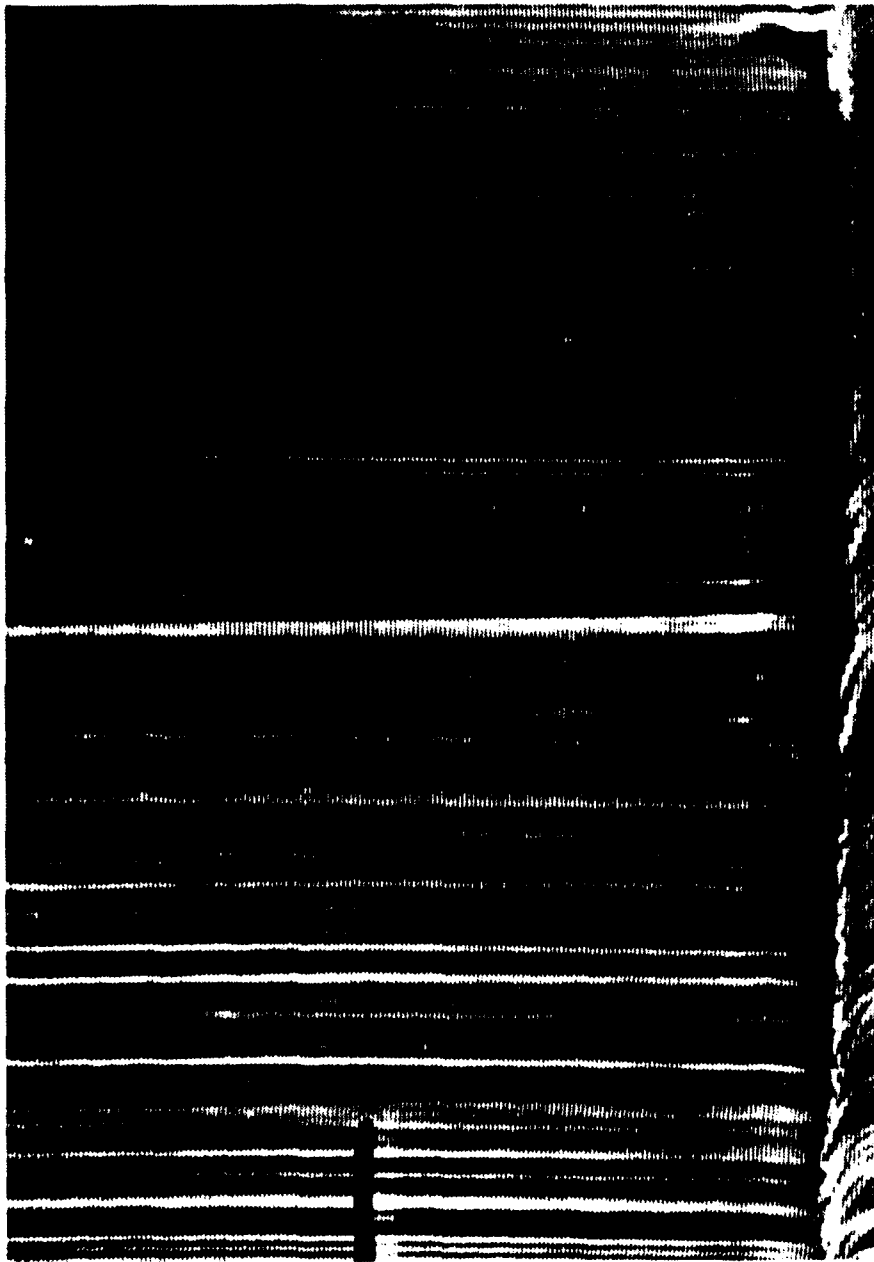


Figure 84.  $Re = 1328$



Figure 85.  $Re = 1377$

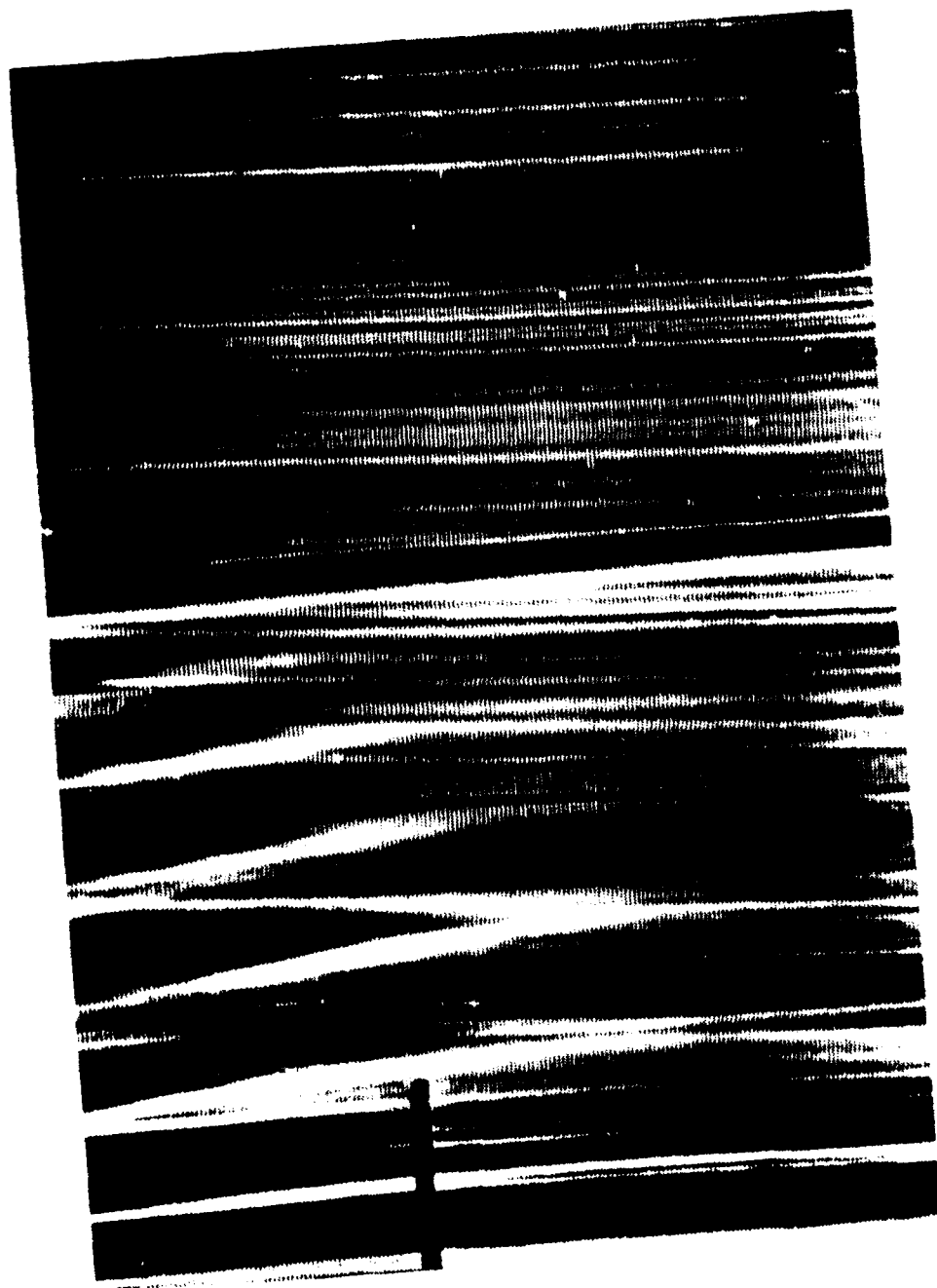


Figure 86. Re = 1395

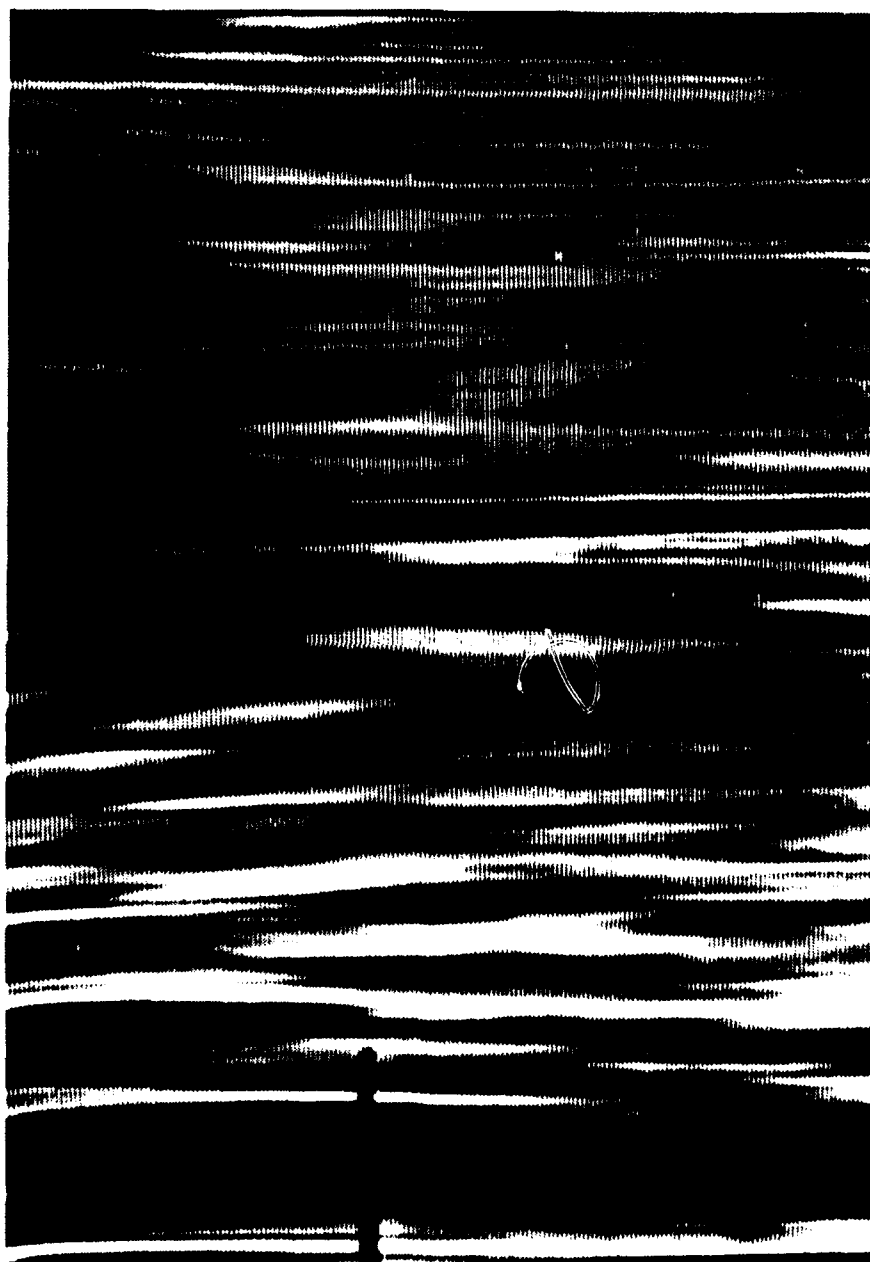


Figure 87.  $Re = 1496$

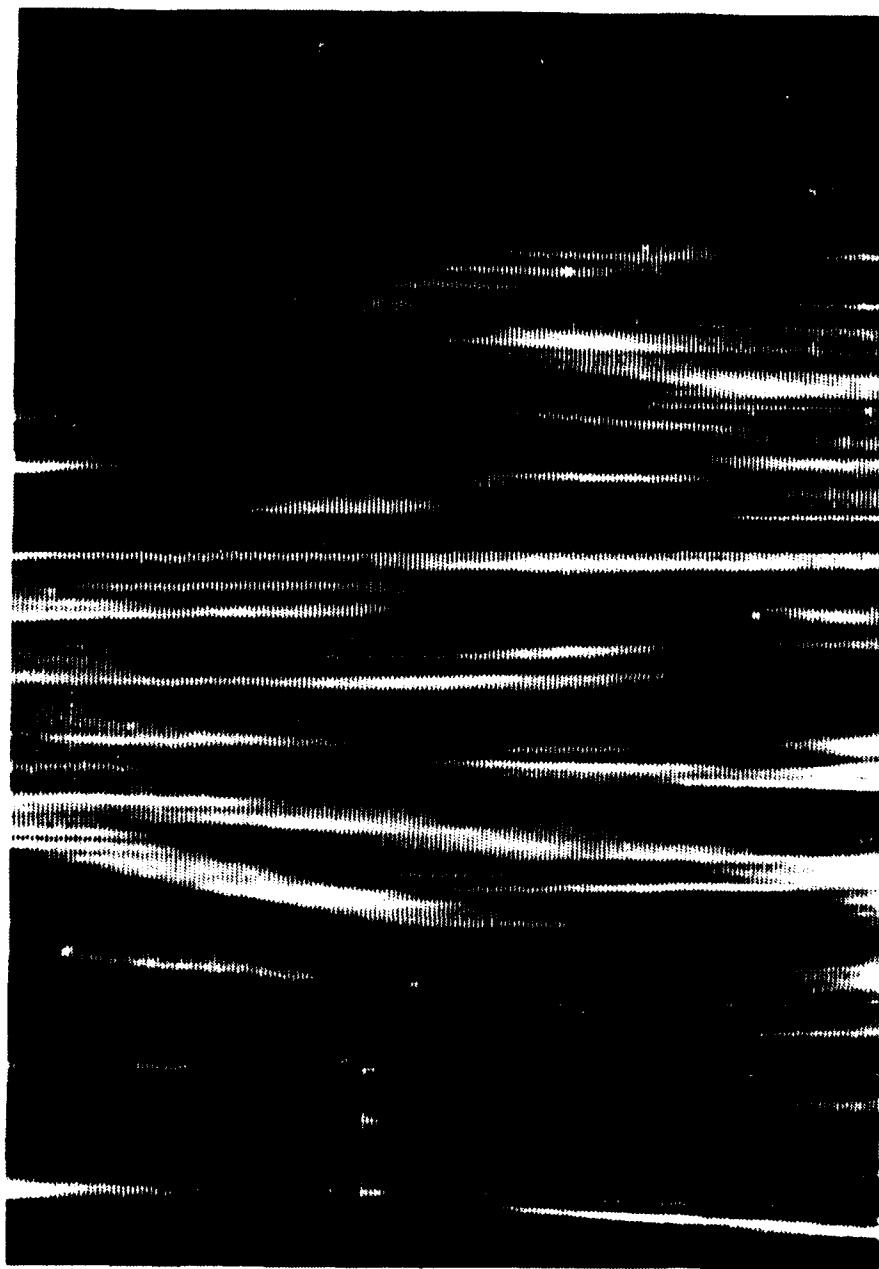


Figure 88.  $Re = 1529$

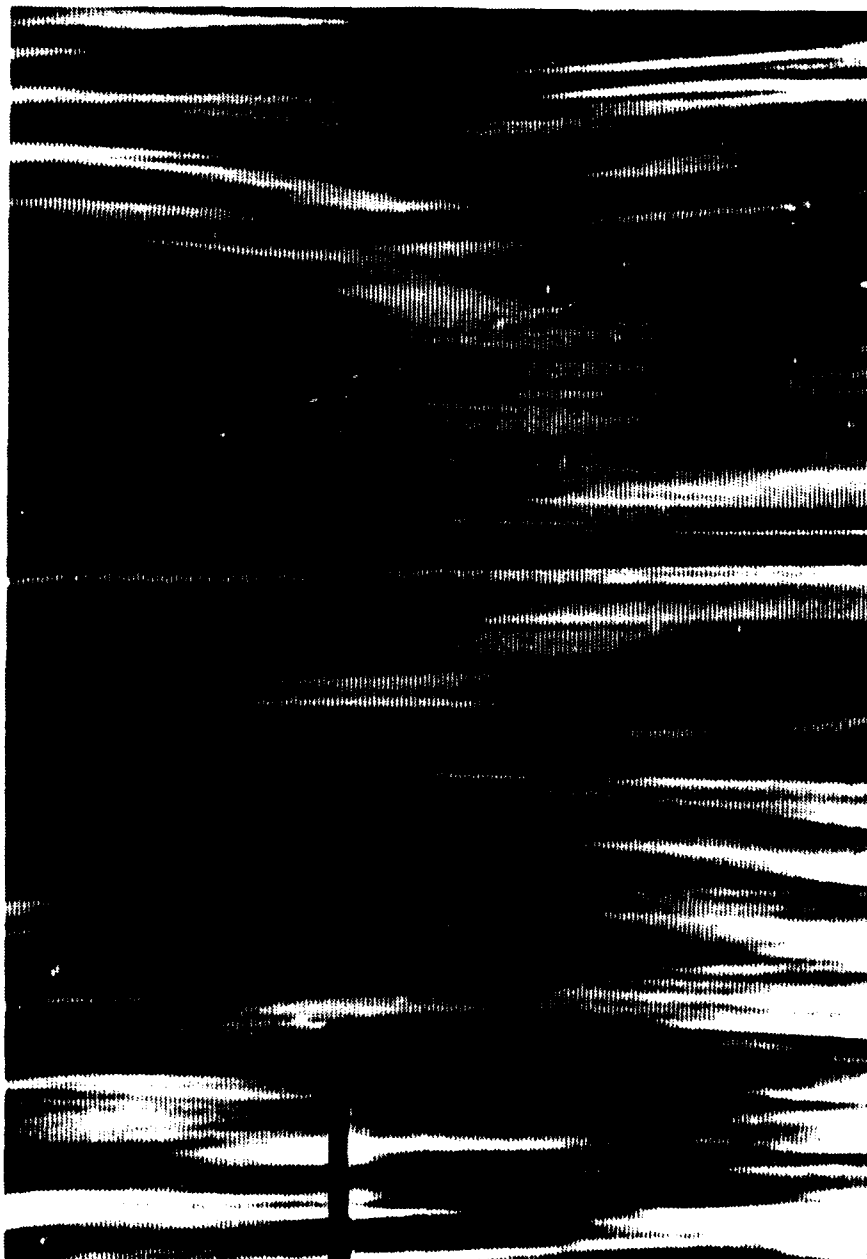


Figure 89. Re = 1713

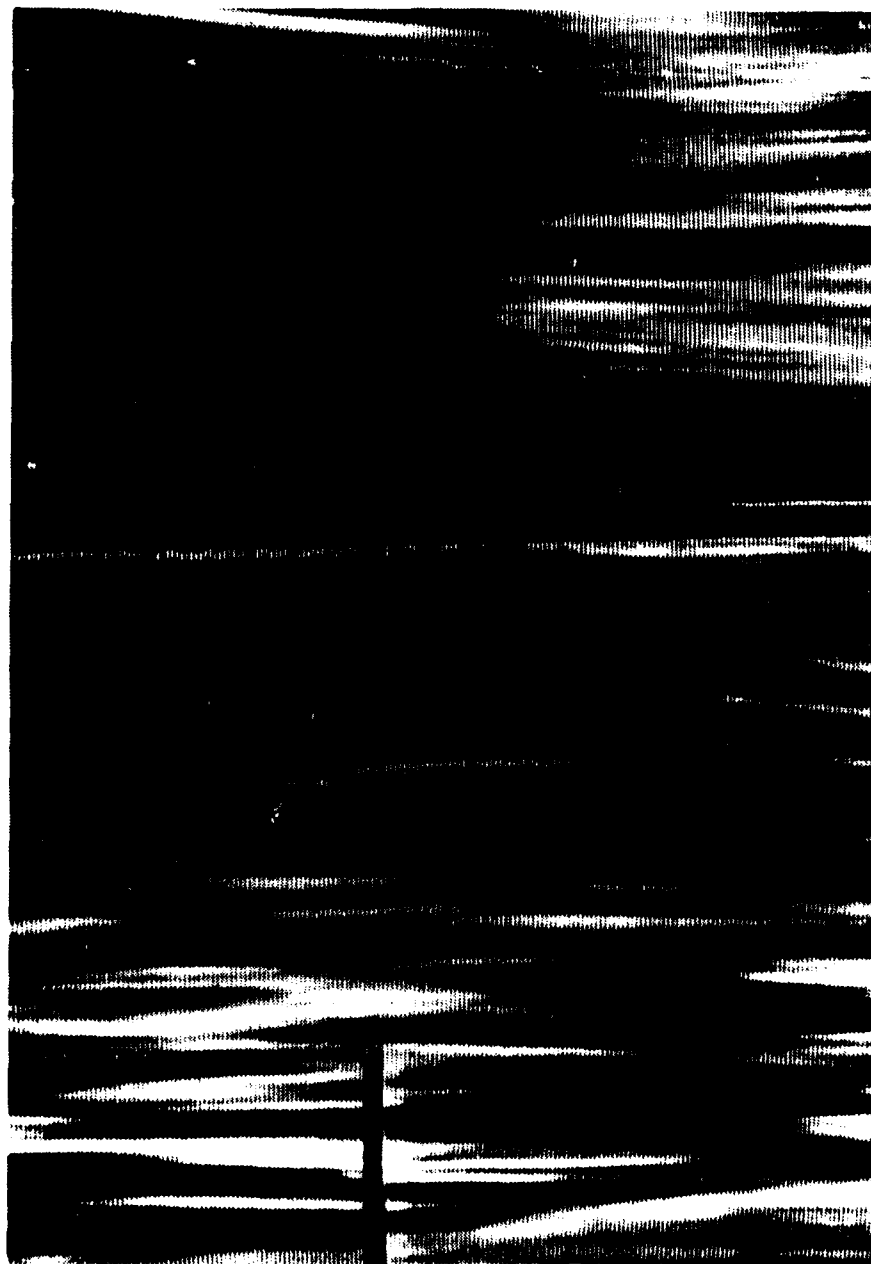


Figure 90. Re = 1713

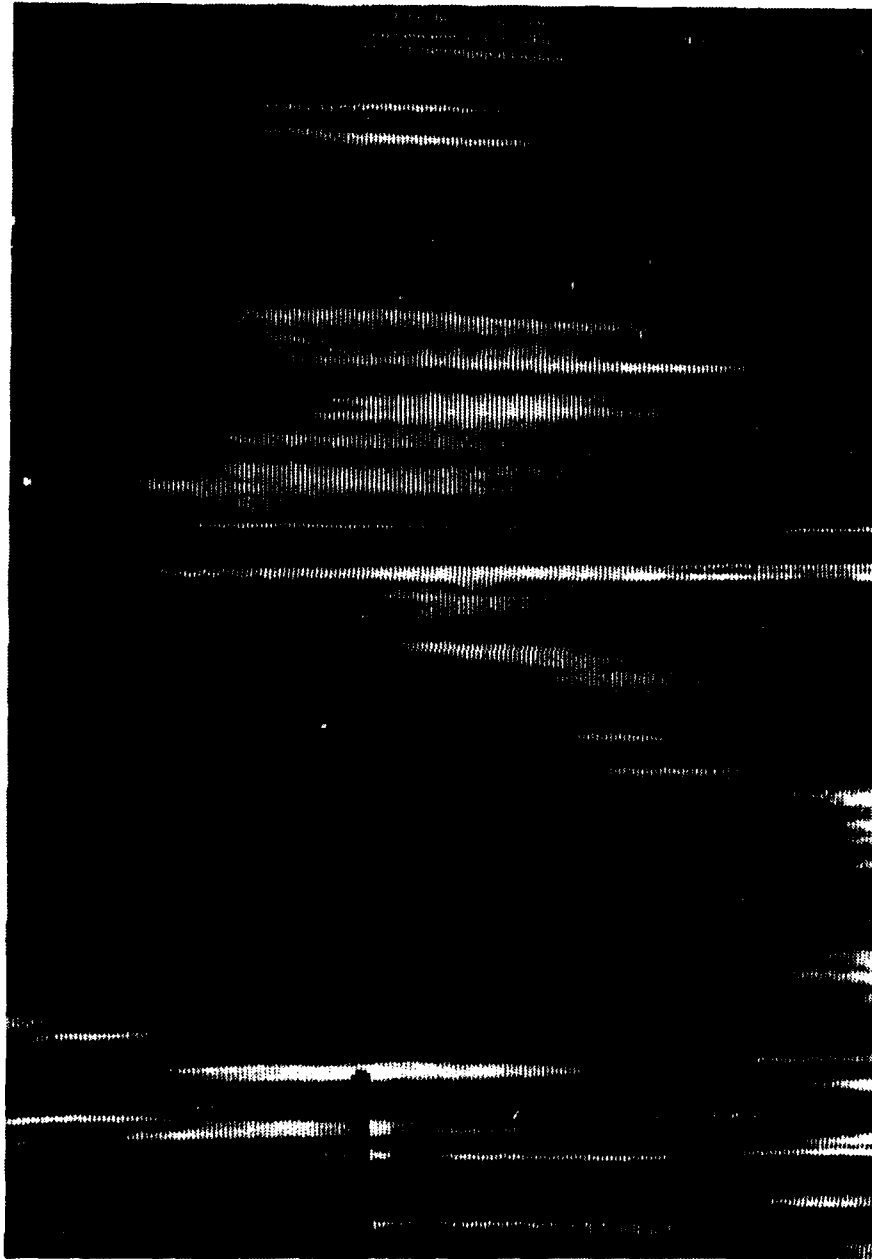


Figure 91. Re = 1854



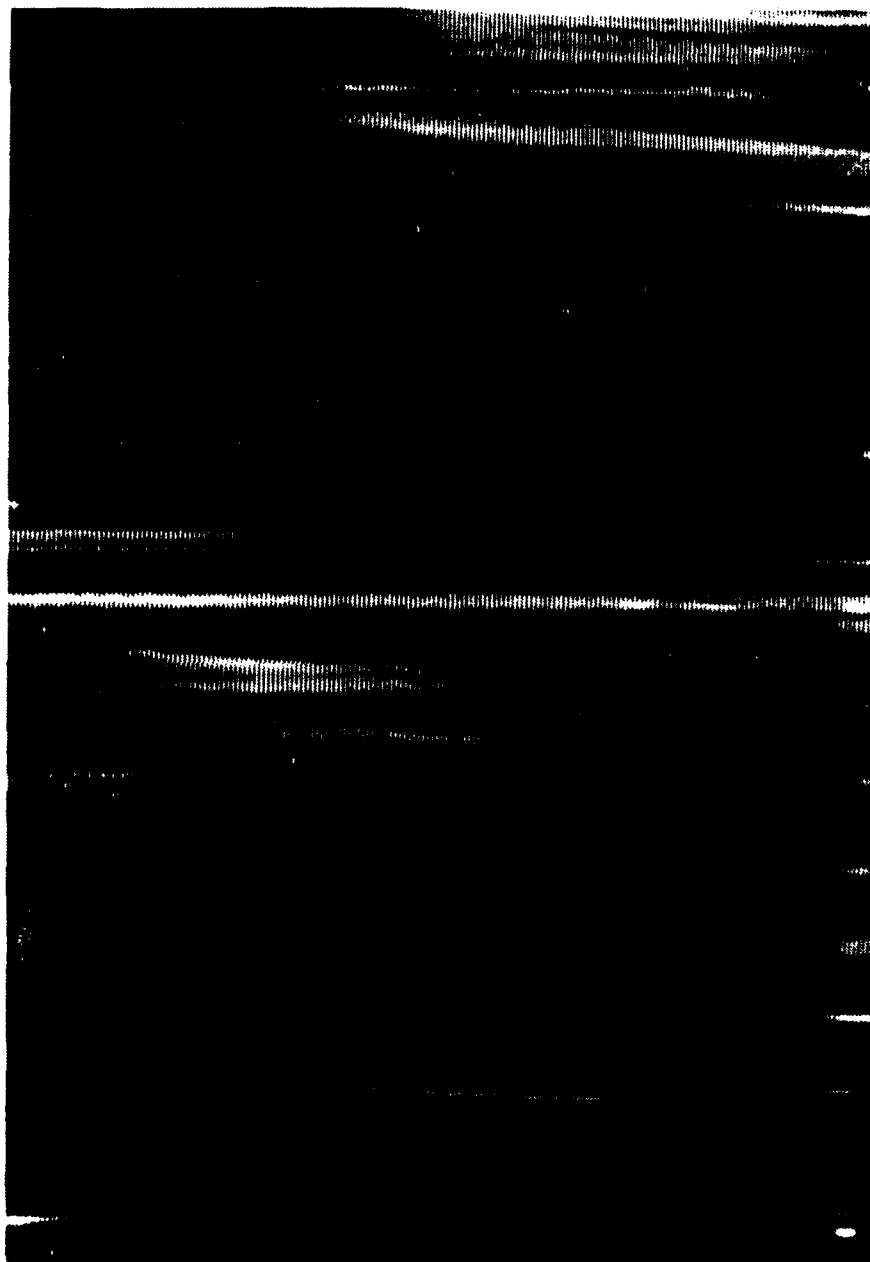


Figure 92. Re = 2239

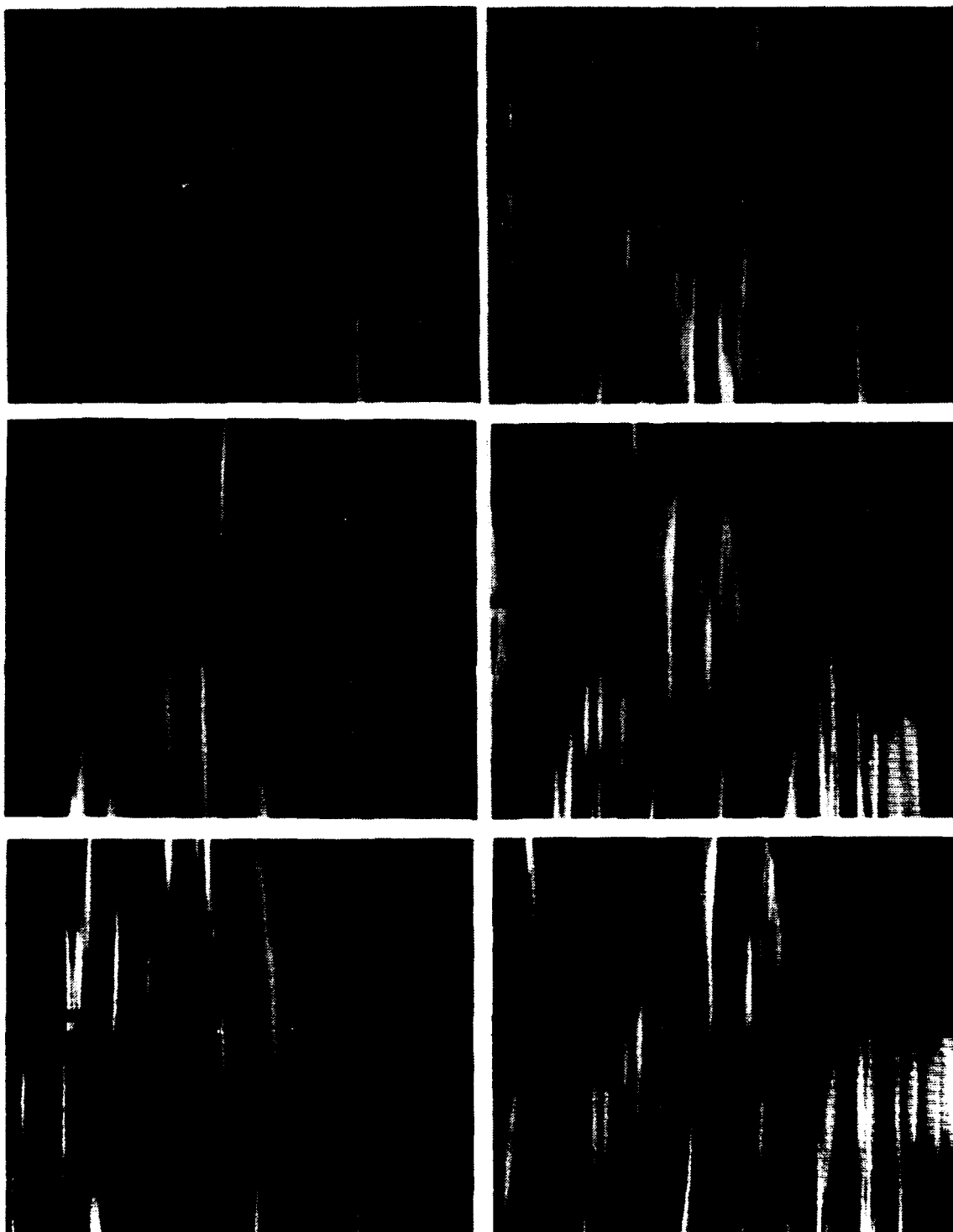


Figure 93. Time Sequence at  $Re = 1412$

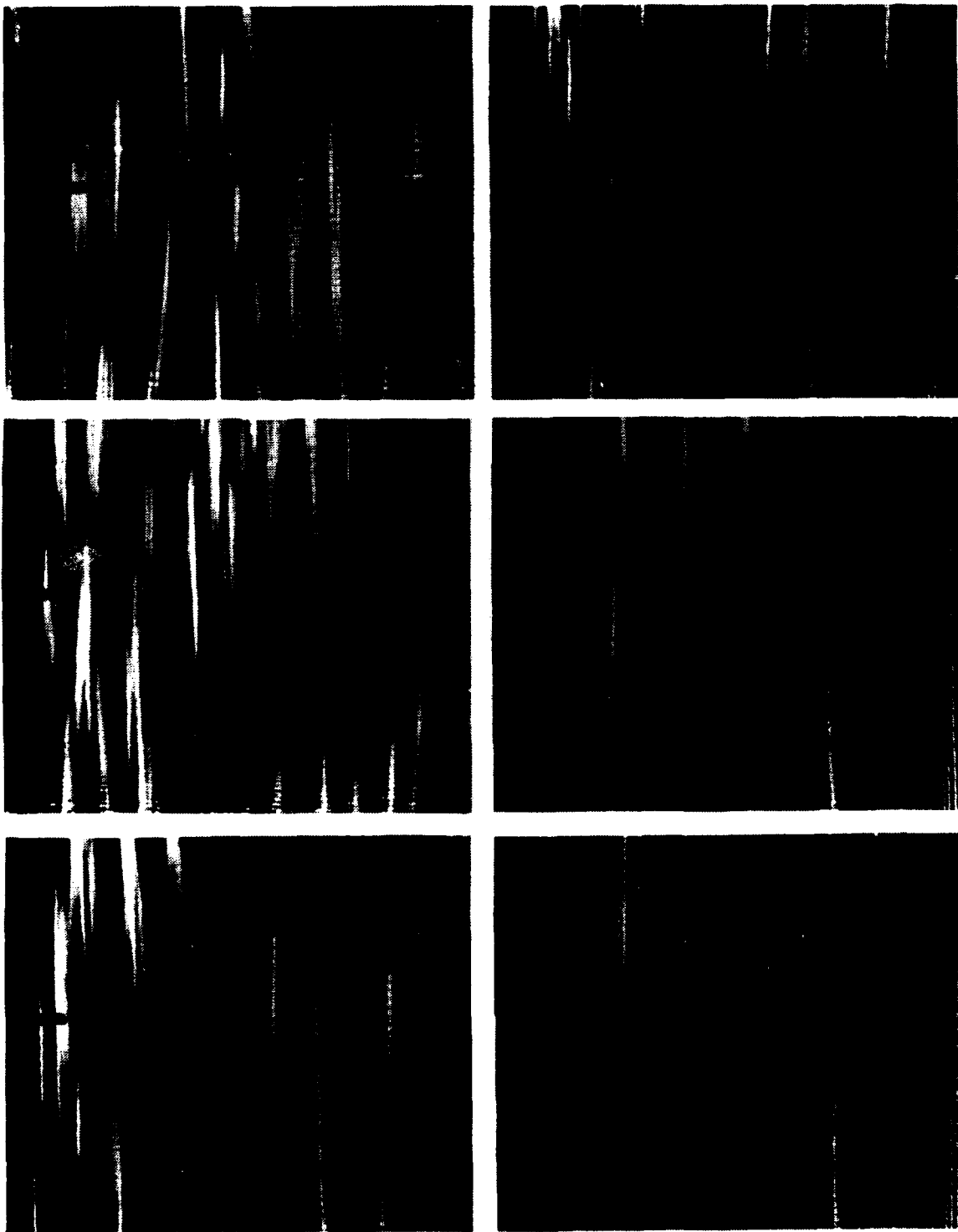


Figure 94. Time Sequence at  $Re = 1412$ , continued.

## LIST OF REFERENCES

1. Thermoscience Division, Department of Mechanical Engineering, Stanford University Report TF-31, *Numerical Simulation Studies of Laminar-Turbulent Transition in the Plane Channel*, by B. Singer, J. H. Ferziger, and H. Reed, May 1987.
2. Thermoscience Division, Department of Mechanical Engineering, Stanford University Report HMT-31, *Turbulent Boundary Layer on a Convex Curved Surface*, by J. C. Gillis, J. P. Johnston, W. M. Kays and R. J. Moffat, 1980.
3. Ligrani, P. M., Moffat, R. J. and Kays, W. M., "Artificially Thickened Turbulent Boundary Layers for Studying Heat Transfer and Skin Friction on Rough Surfaces", *ASME Transactions - Journal of Fluids Engineering*, 105, No. 2, pp. 146-153, 1983.
4. Herbert, T., "Modes of Secondary Instability in Plane Poiseuille Flow", *IUTAM Symposium on Turbulence and Chaotic Phenomena in Fluids*, 1983.
5. Herbert, T., "Subharmonic Three-dimensional Disturbances in Unstable Plane Shear Flows", *AIAA Paper 83-1759*, 1983.
6. Nishioka, M., Asai, M., and Iida, S., "An experimental Investigation of the Secondary Instability in Laminar-Turbulent Transition", *Laminar-Turbulent Transition*, R. Eppler and H. Fasell, eds. Springer-Verlag, pp. 37-46, 1985.
7. Nishioka, M., Asai, M., "Three Dimensional Wave Disturbances in Plane Poiseuille Flow", *Laminar-Turbulent Transition*, V. V. Kozlov, ed. Springer-Verlag, pp. 173-182, 1985.

8. Kozlov, V. V. and Ramazanov, M. P., "Development of Finite Amplitude Perturbations in Poiseuille Flow", *Journal of Fluid Mechanics*, 147, pp. 149-157, 1984.
9. Longest, J., *Flow Visualization Studies in (1) a Curved Rectangular Channel With 40 to 1 Aspect Ratio and (2) a Straight Channel With Bulk Flow Unsteadiness*, Master's Thesis, Naval Postgraduate School, Monterey, California, June 1989.
10. Ligrani, P. M. and Subramanian, C. S., "Effects of Unsteadiness on Laminar-Turbulent Transition in Straight Channel Flow", Naval Postgraduate School Project Progress Report, Department of Mechanical Engineering, Naval Postgraduate School, Monterey, California, March 1989.
11. Schlichting, H., *Boundary Layer Theory*, McGraw-Hill, Inc, 1979.
12. Miller, J. A. and Fejer, A. A., "Transition Phenomena in Oscillating Boundary-Layer Flows", *Journal of Fluid Mechanics*, vol. 18, pp. 438-448, 1964.

### INITIAL DISTRIBUTION LIST

- |  |   |
|--|---|
| 1. Defense Technical Information Center<br>Cameron Station<br>Alexandria, Virginia 22304-6145  | 2 |
| 2. Library, Code 0142<br>Naval Postgraduate School<br>Monterey, California 93943-5002  | 2 |
| 3. Professor P. M. Ligrani, Code 69Li<br>Department of Mechanical Engineering<br>Naval Postgraduate School<br>Monterey, California 93943-5000            | 6 |
| 4. Department Chairman, Code 69<br>Department of Mechanical Engineering<br>Naval Postgraduate School<br>Monterey, California 93943-5000                  | 1 |
| 5. Naval Engineering Curricular Officer, Code 34<br>Department of Mechanical Engineering<br>Naval Postgraduate School<br>Monterey, California 93943-5000 | 1 |
| 6. Professor C. S. Subramanian, Code 69Su<br>Department of Mechanical Engineering<br>Naval Postgraduate School<br>Monterey, California 93943-5000        | 2 |
| 7. LCDR Francis J. Greco<br>323 Kentucky Avenue<br>Pasadena, Maryland 21122  | 2 |